Dissertation for the attainment of

the academic title

doctor rerum naturalium

Characterization of the physiological and pathophysiological role of the proteasome in glomerular cells

Presented by

Wiebke Sachs

Department of Chemistry

University of Hamburg

Hamburg, 2019

The presented work was conducted from July 2016 until December 2019 externally in the Department of Physiology in the Institute of Cellular and Integrative Physiology at the University Medical Center Hamburg-Eppendorf under the supervision of Prof. Dr. Catherine Meyer-Schwesinger. Prof. Dr. Wolfram Brune supervised this work in the Department of Chemistry at the University of Hamburg.

1. Reviewer: Prof. Dr. Wolfram Brune

2. Reviewer: Prof. Dr. Catherine Meyer-Schwesinger

Date of the Disputation: 28.02.2020

Table of Content

Abbreviations 1

Zusammenfassung 6

Abstract 8

1. Introduction 10

1.1 The Kidney and the Glomerulus 10

1.1.1 The Podocyte 12

1.1.2 Mesangial cells 13

1.1.3 Glomerular endothelial cells 14

1.2 Membranous nephropathy 15

1.3 Animal models for the study of membranous nephropathy 16

1.3.1 Passive Heymann nephritis 16

1.3.2 Anti-podocyte nephritis 16

1.3.3 Anti-THSD7A membranous nephropathy 17

1.4 Protein degradation 18

1.4.1 The Ubiquitin-Proteasome System 18

1.4.2 The Autophagosome-lysosomal system 20

1.5 Mucolipidosis type II and III 21

2. Aim 23

3. Material and Methods 24

3.1 Material 24

3.1.1 Appliances 24

3.1.2 Consumable material 26

3.1.3 Chemicals, enzymes and kits 27

3.1.4 Kits 34

3.1.5 Antibodies 34

Immunofluorescence 34

Western Blot 35

FACS 36

3.1.6 Primer 37

3.1.7 Software 38

3.2 Methods 38

3.2.1 Animal experiments 38
3.2.2 Genotyping of animals 40
3.2.3 Immunofluorescence 40
3.2.4 Glomeruli Isolation 41
3.2.5 Isolation of glomerular cells 42
3.2.6 RNA Isolation, DNase digest and reverse transcription 44
3.2.7 Western Blot analysis 45
3.2.8 Immunohistochemistry 46
3.2.9 Determination of serum parameters 48
3.2.10 Electron microscopy 48
3.2.11 Urine analysis 48
3.2.12 Lysosomal activity assay 50
3.2.13 Proteasomal activity assay 51
3.2.14 Statistical analysis 51
4. Results 52
4.1 Podocyte proteostasis depends on the proteasomal degradation system 52
4.1.1 Podocytes preferentially express players of the UPS 52
4.1.2 Proteasomal impairment compromises the glomerular filtration barrier under homeostatic conditions 55
4.1.3 Crosstalk of degradative systems 58
4.2 Balancing glomerular proteostasis in lysosomal dysfunction 63
4.2.1 Glomerular cells of ML II and ML III mice exhibit lysosomal dysfunction 63
4.2.2 Renal and glomerular function is intact in ML II and ML III mice 67
4.2.3 Mucolipidosis type II but not type III patients exhibit microalbuminuria 70
4.2.4 Lysosomal dysfunction is differentially compensated for by the UPS in ML II and ML III mice 71
4.2.5 Pathways regulating protein translation are differentially regulated in ML II and ML III mice 73
4.3 Differential effect of proteasomal inhibitors on the progression of experimental MN 77
4.3.1 Preventive Bortezomib treatment of experimental MN aggravates disease progression 77
4.3.2 Preventive treatment of experimental MN with the immunoproteasome inhibitor ONX-0914 alleviates disease progression 82
4.4 Podocyte-specific Lmp7 knockouts are protected during experimental MN 84
4.4.1 Podocyte-specific Lmp7 knockouts show decreased glomerular Lmp7 levels 84

4.4.2 Lmp7Δpod mice are protected during anti-podocyte nephritis 87

4.4.3 Protection of Lmp7Δpod due to the upregulation of the standard proteasomal degradation system 88

5. Discussion 90

5.1 Podocyte proteostasis depends on the proteasomal degradation machinery 90

5.2 Mouse models of mucolipidosis type II and III show no renal involvement due to differential compensatory mechanisms 93

5.3 Proteasomal inhibitors have opposing effects on the progression of experimental membranous nephropathy 98

5.4 Podocyte-specific immunoproteasome deficiency alleviates progression of immune-complex mediated membranous nephropathy 103

6. Literature 105

7. Appendix 111

7.1 Hazard Statements 111

7.2 Precautionary statements 112

8. Acknowledgements 115

9. Eidestattliche Versicherung 116

Abbreviations

αACTN4	α-actinine 4
ACR	albumin to creatinine ratio
ALS	autophagosomal-lysosomal system
AMRF	myoclonus-renal failure syndrome
APN	anti-podocyte nephritis
ATG5	autophagy-related 5
Bort	Bortezomib
BSA	Bovine serum albumin
BUN	blood-urea-nitrogen
Col4	Collagen 4
CtsD	Cathepsin D
DMF	Dimethylformamide
DMSO	Dimethyl sulfoxide
DNA	Deoxyribonucleic acid
dNTP	Deoxyribonucleosidtriphosphate
DTT	Dithiothreitol
ec	endothelial cell
ECL	enhanced chemiluminescence
EDTA	Ethylenediaminetetraacetic acid
ELISA	Enzyme-linked Immunosorbent Assay
EM	Electron-microscopy

Epox	Epoxomicin
ER	endoplasmic reticulum
ERY	erythrocyte
EtOH	Ethanol
FACS	fluorescence-activated cell sorting
FIB	tubulointerstitial fibroblast
GBM	glomerular basement membrane
GFR	glomerular filtration rate
GlcNAc	N-Acetylglucosamine
HBSS	Hank's Balanced salt solution
HCl	Hydrochloric acid
HEPES	4-(2-hydroxyethyl)-1-piperazineethanesulfonic acid
ISR	Integrated stress response
K48pUb	lysine-48 polyubiquitine
Kim1	kidney injury molecule-1
KO	knock-out
Lamp1	lysosomal-associated membrane protein 1
Lamp2	lysosomal-associated membrane protein 2
LC3	microtubule-associated protein 1A/1B-light chain 3
Leup	Leupeptin A
Limp2	lysosomal integral membrane protein-2
M6P	mannose-6-phosphate
mc	mesangial cell

MeOH	Methanol
MHC	major histocompatibility complex
ML	Mucolipidosis
MN	membranous nephropathy
MPC	Magnetic particle collector
ms	mouse
msIgG	mouse immunoglobulin
mTORC1	mammalian target of rapamycin complex 1
MVB	Multivesicular bodies
NaCl	Sodium chloride
NaF	Sodium fluoride
NaOH	Sodium hydroxide solution
NaV	Sodium vanadate
NF	nuclear factor
P	Pipette
p57	Cyclin-dependent kinase inhibitor 1 C
PAS	Periodic acid Schiff
PBS	Phosphate buffered saline
pc	podocyte
PCR	polymerase chain reaction
PEC	Parietal endothelial cells
Pen/Strep	Penicillin-Streptomycin
PFA	Paraformaldehyde

PI	pre-immune
PLA_2R1	M-type phospholipase A2 receptor
PP	Pasteur pipette
PTC	Proximal tubular cells
pUb	Ubiquitin
qPCR	quantitative polymerase chain reaction
rb	rabbit
rbIgG	rabbit immunoglobulin
RNA	Ribonucleic acid
rpm	rounds per minute
S	Shear
SDS	Sodium dodecyl sulfate
SIAD	syndrome of inappropriate antidiuresis secretion
SMA	Smooth muscle actin
Suc-LLVY-AMC	Succinyl-Leucin-Leucin-Valin-Tyrosin-7-Amino-4-Methylcoumarin
TBS	Tris buffered saline
THSD7A	Thrombospondin type 1 domain containing 7A
TMB	3,3′,5,5′-Tetramethylbenzidine
TNT	Tris-NaCl-Tween
UCH-L1	Ubiquitin carboxy-terminal hydrolase L1
UPR	untranslated protein response
UPS	ubiquitin-proteasome system
V	Vortex

Veh	Vehicle
WGA	wheat germ agglutinin

Zusammenfassung

Die Filtration von Urin findet im renalen Glomerulum statt, welcher sich aus drei verschiedenen residenten Zelltypen zusammensetzt. Die tatsächliche Filtrationsbarriere wird von Podozyten, der glomerulären Basalmembran und Endothelzellen gebildet, während Mesangialzellen die Größe der Filtrationsfläche bestimmen. Zum heutigen Zeitpunkt ist wenig darüber bekannt, wie glomeruläre Zellen ihre Protein-Homöostase unter physiologischen und pathophysiologischen Bedingungen regulieren. Protein-Homöostase wird unter anderem durch zwei interagierende Protein-Abbausysteme reguliert: dem Autophagosom-lysosomalen System (ALS) und dem Ubiquitin-Proteasom-System (UPS). Glomeruläre Zellen werden von diesen beiden Systemen unterschiedlich stark beeinflusst. Podozyten und Endothelzellen exprimieren verstärkt Komponenten des UPS während Mesangialzellen vermehrt Komponenten des ALS exprimieren. Globale Inhibition des UPS in der naiven Niere führt überwiegend zu Schäden in Podozyten und Endothelzellen, welche Durchlässigkeit des glomerulären Filters und subepithelialen Immunkomplex Ablagerungenen nach sich ziehen, die sich nicht durch eine Hochregulation des ALS kompensieren lassen. Dahingegen wird eine Dysfunktion des ALS in Glomeruli durch spezifische Mechanismen kompensiert, welche vom Ausmaß der Dysfunktion abhängen und dadurch glomerulären Schäden zuvorkommen. Beispielsweise wurde in einem Mausmodell der Mucolipidose Typ III (moderate lysosomale Dysfunktion) das UPS hochreguliert, während in einem Mausmodell der Mucolipidose Typ II die Proteinbiosynthese herunterfahren wurde und somit ihre glomeruläre Protein-Homöostase regulierten.

Unter Pathologischen Bedingungen werden sowohl UPS als auch ALS hochreguliert. Fehlerhafter Proteinabbau führt zur Akkumulation von Proteinen, vor allem in Podozyten und wird mit glomerulären Erkrankungen, wie Membranöser Nephropathie (MN), assoziier. Bei MN handelt es sich um eine Autoimmunerkrankung, bei der Fußprozess Proteine des Podozyten wie THSD7A, von Autoantikörpern angegriffen werden. In einem Maus-Modell der anti-THSD7A MN führte globale Proteasom-Inhibition zu einer Verschlechterung des Krankheitsverlaufs, welche sich in erhöhter

Proteinurie und abnormalen Proteinablagerungen äußerte. Dahingegen führte die Subtypen-spezifische Inhibition des Immunoproteasoms (eine spezifische Form des Proteasoms) zu einer Verbesserung im Krankheitsverlauf mit verringerter Proteinurie. Um Effekte der Inhibition auf das Immunsystem auszuschließen, wurden Mäuse mit podozyten-spezifischem Lmp7-*knockout* generiert und eine ant-podozyten Nephritis, durch Gabe von anti-podozyten-Serum, induziert. Die *knockout*-Mäuse waren vor dem, durch anti-podozyten Antikörper verursachten, Schaden geschützt. Diese Ergebnisse lassen darauf schließen, dass der Effekt des Immunsystem-Inhibitors auch auf einen Effekt der residenten glomerulären Zellen zurückzuführen ist.

Die feinen Interaktionen und Abhängigkeiten der verschiedenen Zelltypen von den unterschiedlichen Protein-Degradationswegen ist noch wenig verstanden. Diese neuen Erkenntnisse geben Anlass spezifische Untereinheiten des proteasomalen Degradationsweges pharmakologisch anzugreifen.

Abstract

Urine is filtered within the renal glomerulus, which comprises three resident cell types. The ultimate filtration barrier is formed by podocytes, the glomerular basement membrane and endothelial cells, while mesangial cells regulate the size of the filtration area. Current knowledge about the governing mechanisms that maintain glomerular cell protein homeostasis in the physiological and pathophysiologic context is very limited. Protein homeostasis depends on two interacting degradation systems, the autophagosomal-lysosomal system (ALS) and the ubiquitin-proteasome system (UPS). Glomerular cells differentially depend on these degradation systems. While podocytes and endothelial cells strongly express players of the UPS, mesangial cells strongly depend on the ALS. In the naïve kidney, global proteasome inhibition predominantly disrupts podocyte and endothelial integrity and thereby leads to a disruption of the glomerular filter function and to subepithelial protein accumulations that cannot be compensated by the ALS. Lysosomal dysfunction in glomerular cells, on the other hand, is compensated for by upregulation of distinct protective mechanisms, depending on the clinical and biochemical severity of the impairment, thereby precluding glomerular dysfunction. While mucolipidosis type III mice (moderate lysosomal dysfunction) upregulate the UPS, mucolipidosis type II mice (severe lysosomal dysfunction) balance glomerular protein homeostasis by reducing overall protein synthesis.

Under pathophysiological conditions the UPS and ALS are upregulated in glomerular cells. Defective protein turnover has been associated with glomerular diseases, such as membranous nephropathy (MN), resulting in abnormal protein accumulations especially in podocytes. MN is an autoimmune disease, in which autoantibodies target podocyte foot process proteins such as THSD7A. In a mouse model of α-THSD7A MN global proteasome inhibition aggravates disease progression with increased proteinuria and enhanced abnormal protein accumulations, while subunit-specific inhibition of a specialized form of the proteasome, the immunoproteasome, leads to attenuated disease progression with decreased proteinuria. To exclude effects on the immune response as the origin of the disease attenuating effect of subunit-specific immunoproteasome inhibition, podocyte-specific immunoproteasome knock-out mice

were generated, and anti-podocyte nephritis induced. In this setting, podocyte-specific immunoproteasome knock-out mice were protected from anti-podocyte antibody mediated injury, suggesting that the protective effects observed by application of subunit-specific immunoproteasome inhibitors in α-THSD7A MN were also attributable to an effect on the resident glomerular cells.

The intricate interplay and dependence of distinct cell types on different degradation systems has, so far, been little understood. These novel insights lead to a new necessity of targeting specific players of the proteasomal degradation system pharmacologically.

1. Introduction

1.1 The Kidney and the Glomerulus

The kidney is the organ in which blood is filtered, and solutes are reabsorbed to be returned to the circulation. Therefore, the kidneys receive approximately 25 percent of the cardiac output and are well vascularized. The kidney is divided into multiple parts, an outer region, the renal cortex, and an inner region, the medulla. Connective tissue that spreads from the cortex through the medulla is called the renal columns, the renal columns sperate the renal pyramids and the renal papillae, they also divide the kidney into lobes and thereby provide a framework for vessels that enter and exit the renal cortex. The renal papillae are a collection of collecting ducts that transport urine to the calyces of the kidneys for excretion. Blood flow through the kidney is ensured by a system of arteries. The renal artery is divided into segmental arteries which branch out further to form interlobar arteries that pass through the renal columns to reach the cortex. The interlobar arteries also branch out further into arcuate arteries, cortical radiate arteries and finally into afferent arterioles which service the nephrons.
The nephron is the smallest functional unit of the kidney but one of the most important, as filtration and urine production takes place there. The site of filtration is located at the beginning of the nephron, in the renal corpuscule. The renal corpuscule contains the glomerulus, which contains a network of capillaries (glomerular tuft) that is surrounded by the parietal epithelial cells of the Bowman's capsule and by this is separated from the tubular system (Figure 1). Blood enters the glomerulus through the afferent arterioles at the vascular pole and is drained into efferent arterioles. The resistance of these arterioles generates high pressure within the capillary convolute of the glomerulus, which drives the ultrafiltration of primary urine through the glomerular filtration barrier into Bowman space (Figure 1). The filtration barrier is size and charge dependent and favors the filtration of positively charged solutes (1, 2). Further processing of the primary urine after exiting the renal corpuscule at the urinary pole takes place in the downstream tubular system. Small molecules and water can freely pass the glomerular filtration barrier, while bigger molecules such as albumin cannot freely pass into the primary urine. Therefore, the existence of albumin in the urine is a strong indicator for a disturbance of the glomerular filtration barrier. The impermeability

of the glomerular filtration barrier to large particles is achieved by the interplay of two types of highly specialized glomerular cell types, the visceral epithelial cells, also known as podocytes, and glomerular endothelial cells (3).

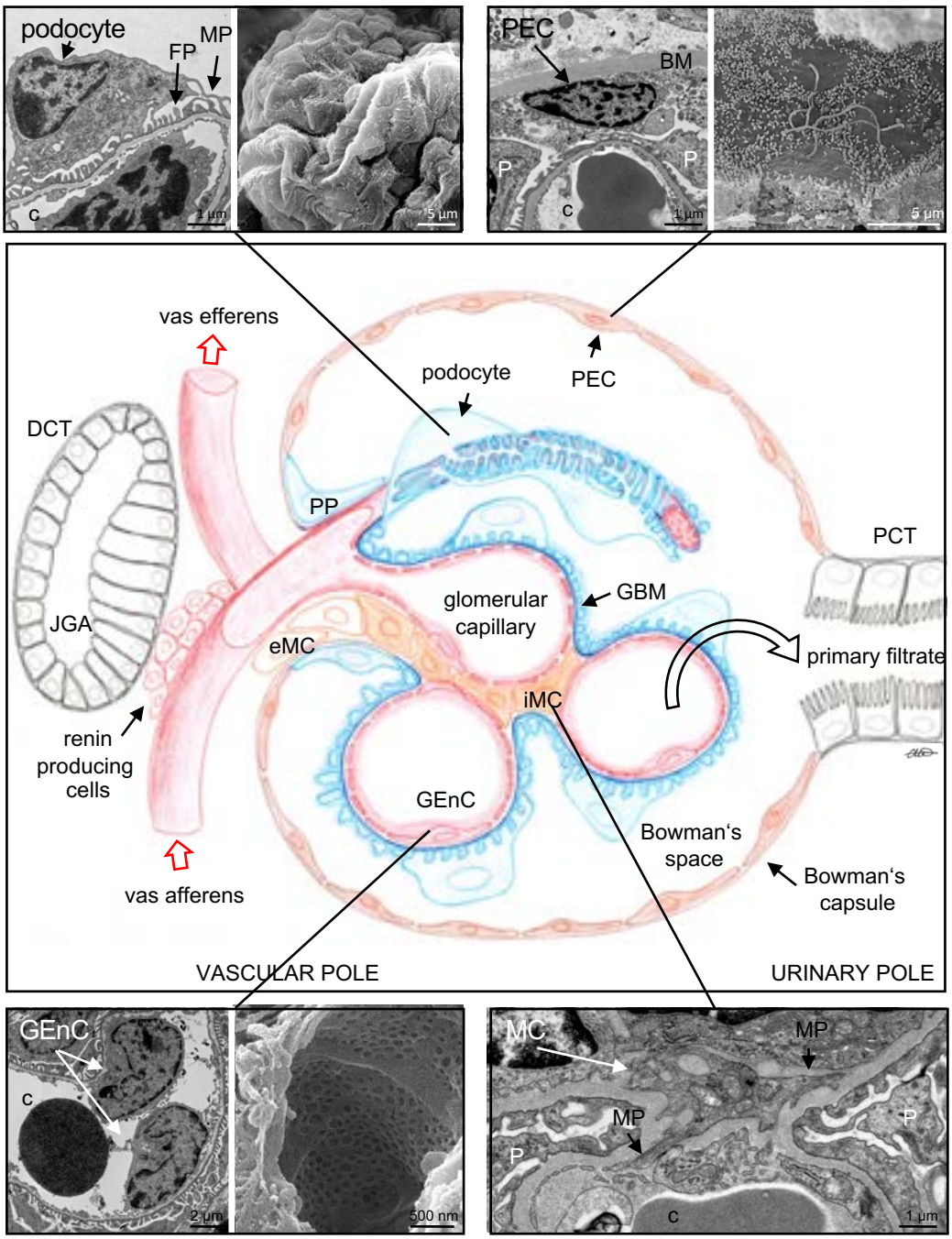

Scheme 1: The Glomerulus
Schematic depiction of a glomerulus. Blood is filtered through the glomerulus, more specifically through the glomerular filtration barrier consisting of the glomerular basement membrane (GBM), glomerular endothelial cells (GEnC) and podocytes (Brenner and Rector's: The kidney, Chapter 4, Figure 1)

These two cell types together with the glomerular basement membrane (GBM) ultimately compose the three-layered glomerular filtration barrier. The GBM is composed of multiple extracellular matrix proteins such as laminin, collagen type IV, the heparan sulfate proteoglycans agrin and nidogen, which form a network to impart charge and size selective properties (4). To provide structural support, intraglomerular mesangial cells occupy the space between the glomerular filtration barrier. The mesangial cells are specialized pericytes and indirectly participate in filtration by reducing the glomerular surface area by contraction (3).

1.1.1 The Podocyte

Podocytes are highly differentiated, mesenchymal-derived cells (5). Podocytes are able to orient between the urinary space and the glomerular basement membrane (GBM) due to an apico-basal polarity axis (6). Podocytes occupy the urinary space and embrace the glomerular capillaries with their flat cell body from which they extend long processes that branch out again to form the podocyte foot processes. The podocyte foot processes interdigitate in a zipper like fashion with the podocyte foot processes of neighboring podocytes (3). The podocyte foot processes attach podocytes to the extracellular matrix of the GBM with the help of specific adhesion receptors such as integrins, syndecans, vinculin, talin and dystroglycan (7). The podocyte foot processes are interconnected by slit-diaphragms, which are highly-sophisticated cell-cell-contacts that form an adjustable barrier through which filtration occurs. The core component of the slit diaphragm is formed by nephrin and neph1, with neph1 spanning the lower part of the slit close to the GBM, and nephrin located on the apical side (8). Podocin, a member of the stomatin protein family, helps anchor nephrin to the plasma membrane, where it generates a signaling hub in the lipid rich membrane compartments that can translate mechanical tension to ion channel action and cytoskeletal regulation (9). Nephrin and neph1 are associated with multiple signaling adaptor and scaffold proteins on their intracellular C-terminal parts, which link the slit-diaphragm to the actin cytoskeleton (8, 10). Podocyte foot processes contain elaborate cytoskeletal structures, where actin, α-actinin-4, and myosin form a contractile system in foot processes, which is regulated by the interplay of the actin binding protein synaptopodin and α-actinin-4 with rho GTPases (11). This actin- and microtubule-cytoskeleton ensures a high plasticity of the podocyte foot process network. In order to keep the

adjacent foot processes separated and the glomerular filtration barrier open, the apical surfaces of podocytes are covered by podocalyxin, which is highly negatively charged (12, 13).

Podocytes are responsible for the building, maintenance and regulation of the glomerular filtration barrier; therefore, they are constantly required to respond and adapt to various physiologic and pathophysiologic stressors. If stress overwhelms podocytes, complex changes ensue, resulting in the typical histopathologic sequence of foot process effacement, podocyte hypertrophy, podocyte detachment from the GBM with loss into the urine (3). Podocyte dysfunction eventually results in clinical proteinuria and a variety of glomerular responses, such as disruption of podocyte-endothelial crosstalk and activation of podocyte-parietal cell interaction leading to glomerulosclerosis (3).

1.1.2 Mesangial cells

Mesangial cells can be divided into intraglomerular and extraglomerular mesangial cells. They are derived from the metanephric mesenchyme (14) and migrate to the maturing glomerulus under the control of platelet-derived growth factor B and the survival factor VEGF (15). In the mature glomerulus, mesangial cells are in continuity with the extraglomerular mesangium and the juxtaglomerular apparatus. Extraglomerular mesangial cells are closely connected to afferent and efferent arteriolar cells by gap junctions which allows for intercellular communication (16). Mesangial cells also form processes that contain bundles of microfilaments, microtubules and intermediate filaments (17). The major processes contain actin, myosin and α-actinin which connect mesangial cells by means of anchoring filaments to the GBM opposite podocyte foot processes and at paramesangial angles, giving them contractile properties (18). Furthermore, mesangial cells have additional processes in the form microvili which move out from the cell body and the processes. Glomerular endothelial cells and mesangial cells are in direct contact on the side of the capillary lumen, where the cell membranes of both cell types interdigitate (3).

Mesangial cells form a functional unit together with the glomerular endothelial cells and podocytes and they have various functions. They are responsible for the development and structural support of glomerular capillary loops, they regulate the glomerular capillary flow and the surface available for ultrafiltration, they are responsible for the

homeostasis of the mesangial matrix, they are also the source and target of growth factors, cytokines and vasoactive agents. Additionally, mesangial cells keep the mesangial space free from accumulating macromolecules by phagocytosis, they are also involved in the tubuloglomerular feedback by communicating with vascular smooth muscle cells over gap junctions. Lastly, mesangial cells maintain endothelial health and function by cross communication.(3)

So far, no primary diseases of mesangial cells have been described, but mesangial cells do react to changes of the intravascular milieu. Glomerular mesangial cell injury is observed in IgA nephropathy, lupus nephritis and IgA vasculitis and is mostly associated with mesangial immune deposit formation.(3)

1.1.3 Glomerular endothelial cells

Glomerular endothelial cells are highly specialized cells that form the inner layer of glomerular capillaries (3). They have an embryonic origin by vasculogenesis from mesenchymal precursors (19, 20). The nucleus of glomerular endothelial cells reaches into the capillary lumen in mature glomeruli. The cytoplasm of glomerular endothelial cells is punctuated by fenestrae, which represent circular pores that cover the glomerular endothelial surface (21). Glomerular endothelial cells are covered by a negatively charged glycocalyx that is made up of proteoglycans with their bound polysaccharide chains (3). The glycocalyx is associated with the glomerular endothelial cells by charge-charge interactions, which makes the glomerular endothelial cells very sensitive to hemodynamic factors (22). Glomerular endothelial cells also express their specific markers such as platelet endothelial cell adhesion molecule 1 (CD31), intercellular adhesion molecule 2 (ICAM2), vascular endothelial growth factor receptor 2 (VEGFR2), von Willebrand facor (vWF) and vascular endothelial (VE)-cadherin (CD144).(23)

Glomerular endothelial cells are, together with podocytes, responsible for the production of the glomerular basement membrane (GBM). They also contribute to the hydraulic conductivity of the glomerular filtration barrier, as well as to its size and charge selectivity. The glycocalyx of the glomerular endothelial cells additionally protects against protein leakage, inflammation and coagulation.(3)

Diseases that involve glomerular endothelial cells are also associated with mesangiolysis and proteinuria, for example hemolytic uremic syndrome, pre-eclampsia and various forms of vasculitis.(3)

1.2 Membranous nephropathy

Membranous nephropathy (MN) is the most common cause of nephrotic syndrome in Caucasian males. It is an autoimmune disease of renal podocytes, in which autoantibodies target podocyte foot process proteins such as the identified autoantigens M-type phospholipase A2 receptor (PLA_2R1) (24) and the thrombospondin type-1 domain-containing 7A (THSD7A) (25). About 70% of patients with membranous nephropathy are PLA_2R1-autoantibody positive (24), while only 3 – 5% of patients are THSD7A-autoantibody positive (25), which suggests that there are still unidentified podocyte foot process antigens involved in membranous nephropathy. MN is further characterized by immune deposits that form at the base of the foot processes of podocytes, which are in part responsible for the thickening of the glomerular basement membrane that becomes apparent as disease progresses (26). The autoantibody/antigen complexes are thought to lead to the activation of the complement system, and both of these characteristics are thought to ensue in podocyte injury, with alterations of the glomerular filtration barrier function and subsequent proteinuria (26). The clinical course of MN is slowly progressive, but leads in about 40% of patients to end-stage renal disease (27). MN can present as a primary glomerular disease (idiopathic), or as a secondary disease following for example systemic lupus erythematosus, or infections such as hepatitis B, the exposure to toxins, the use of certain drugs, as well as malignancy (27).

So far, MN is treated with general immunosuppressive therapies, but new therapies are being developed specifically targeting autoantibody producing B-cells as well as the complement system (28). A patient, who was initially diagnosed with IgA nephropathy and later was rediagnosed with MN, was treated in a clinical study with the proteasomal inhibitor bortezomib, which induced remission of MN in this patient (29). Therefore, the treatment of MN with proteasomal inhibitors is currently under consideration.

1.3 Animal models for the study of membranous nephropathy

1.3.1 Passive Heymann nephritis

Passive Heymann nephritis is the oldest model of membranous nephropathy and is induced in rats. The target antigen responsible for the deposition of immune complexes in this rat model was identified as megalin, which is an antigen that is not expressed in humans by podocytes (27). The rat model was a good model for membranous nephropathy because the histopathology and major clinical aspects closely resembled the human disease manifestations (27). Passive Heymann nephritis can be induced in different rat strains by the passive transfer of heterologous sheep or rabbit antibodies directed against Fx1A antigens isolated by ultracentrifugation procedures from rat proximal tubular brush border. This transfer induces the thickening of the glomerular basement membrane, podocyte abnormalities, subepithelial IgG, C3 and C5b9 deposits as well as proteinuria after 3 to 7 days following the transfer (27). The initial phase is the heterologous phase, where immune complexes are exclusively formed by heterologous IgG, the autologous phase follows after 2 – 4 weeks when the rats develop antibodies against the foreign rabbit or sheep IgG. The autologous phase is characterized by glomerular deposition of rat IgG, which increases proteinuria (27).

1.3.2 Anti-podocyte nephritis

Since the importance of antibodies against podocyte specific proteins has been established in the passive Heymann nephritis, it was postulated that the administration of anti-podocyte antibodies could also induce MN in mice (27). Therefore, sheep anti-podocyte antiserum was generated by immunizing a sheep with intact murine podocytes (30). The administration of anti-podocyte serum to C57Bl6 mice causes podocyte foot process effacement and formation of subepithelial immune complex deposits resulting in severe nephrotic syndrome (30). The development of anti-podocyte nephritis (APN) was shown to be independent of complement activity. Similarly to passive Heymann nephritis and human MN, APN does not lead to increased blood urea nitrogen (BUN) levels (30). Further, mice treated with APN develop the symptoms reminiscent of nephrotic syndrome such as severe edema, proteinuria, hypoalbuminemia, elevated serum cholesterol and triglycerides by day 9

post injection, which peaks at day 14 (27). Histologic changes include swollen podocytes, podocyte loss and thickening of the glomerular basement membrane. APN induction also results in the glomerular deposition of mouse IgG in a linear and granular pattern along the GBM and in the subepithelial space and some mesangial IgG deposition (27). This generated model of anti-podocyte nephritis exhibits all of the typical histomorphologic and clinical signs of human MN with the caveat of presenting with additional mesangial IgG deposition, which is not found in human MN. Nonetheless, the advantage of the APN model is that it can be induced in a variety of mouse strains including Balb/C and C57Bl6 mice.

1.3.3 Anti-THSD7A membranous nephropathy

Before the discovery of THSD7A as a podocyte antigen, PLA_2R1 was the only antigen identified for membranous nephropathy. The development of a mouse model targeting PLA_2R1 proved difficult, because PLA_2R1 is not expressed on mouse podocytes. THSD7A proved more practical after its discovery, since it is expressed in mouse podocytes. To develop a mouse model of membranous nephropathy specifically targeting mouse THSD7A, anti-THSD7A antibodies were generated in rabbits (31). For this purpose, two expression constructs encoding full-length mouse THSD7A and human THSD7A were conjugated to gold particles and ballistically injected into three rabbits (31). Four months after immunization the animals were euthanized, and the serum collected. Rabbit IgG was purified, and the antigen binding characteristics to THSD7A evaluated. Thereby, the purified rabbit IgG recognized THSD7A in both human and mouse glomerular extracts (31). After injection of anti-THSD7A IgG into Balb/c mice, mice gradually developed proteinuria over the course of 14 days as well as ascites. Serum BUN levels were not elevated, suggesting that no acute kidney failure developed, on the other hand serum cholesterol and triglycerides were elevated in these mice (31). Histologic investigations revealed podocyte swelling and thickening of the glomerular basement membrane as well as linear and granular deposition of rbIgG along the glomerular filtration barrier (31). Ultrastructural analysis revealed podocyte foot process effacement and electron-dense deposits in a subepithelial location. However, THSD7A MN was only inducible in Balb/C mice, C57Bl6 mice exhibiting subepithelial immune deposit formation in the absence of proteinuria and

nephrotic syndrome. This generated model of anti-THSD7A membranous nephropathy in Balb/C mice exhibits the typical histomorphologic signs of human MN (31).

1.4 Protein degradation

A hallmark of membranous nephropathy is the formation of immune-complex deposits in the subepithelial space. Under homeostatic conditions two protein degradation systems are involved in the degradation of the majority of cellular proteins, the ubiquitin-proteasome system and the autophagosome-lysosomal system (32). It has been shown that in patients with membranous nephropathy, as well as in the rat model of passive Heymann nephritis, and in the mouse model of anti-podocyte nephritis, players of the ubiquitin-proteasome system are upregulated (33). So far this upregulation of the UPS has been observed but not published by our group in the mouse model of anti-THSD7A nephritis.

1.4.1 The Ubiquitin-Proteasome System

The ubiquitin-proteasome system (UPS) plays an important role in the regulation of multiple cellular functions by degrading mostly short-lived and regulatory proteins as well as damaged or misfolded proteins. Among others the UPS is involved in the regulation of the cell cycle, gene transcription and translation, cell survival, apoptosis, cell metabolism, protein quality control and inflammation (32).
The UPS is an intricate system consisting of an enzyme cascade, which regulates the ubiquitination of substrate proteins, marking them for degradation by the proteasome system. The 26S standard proteasome consists of a 20S catalytic core particle and a 19S cap. The 19S cap recognizes ubiquitinated substrates, removes the ubiquitin chain and unfolds the substrates. Subsequently, the substrates are degraded by the 20S catalytic core. The catalytic core houses three proteolytic subunits, the β1, β2 and β5 subunits, which harbor distinct proteolytic activities. β1 preferentially cleaves after acidic amino acids (caspase-like), β2 preferentially cleaves after basic amino acids (trypsin-like) and β5 preferentially cleaves after hydrophobic amino acids (chymotrypsin-like).

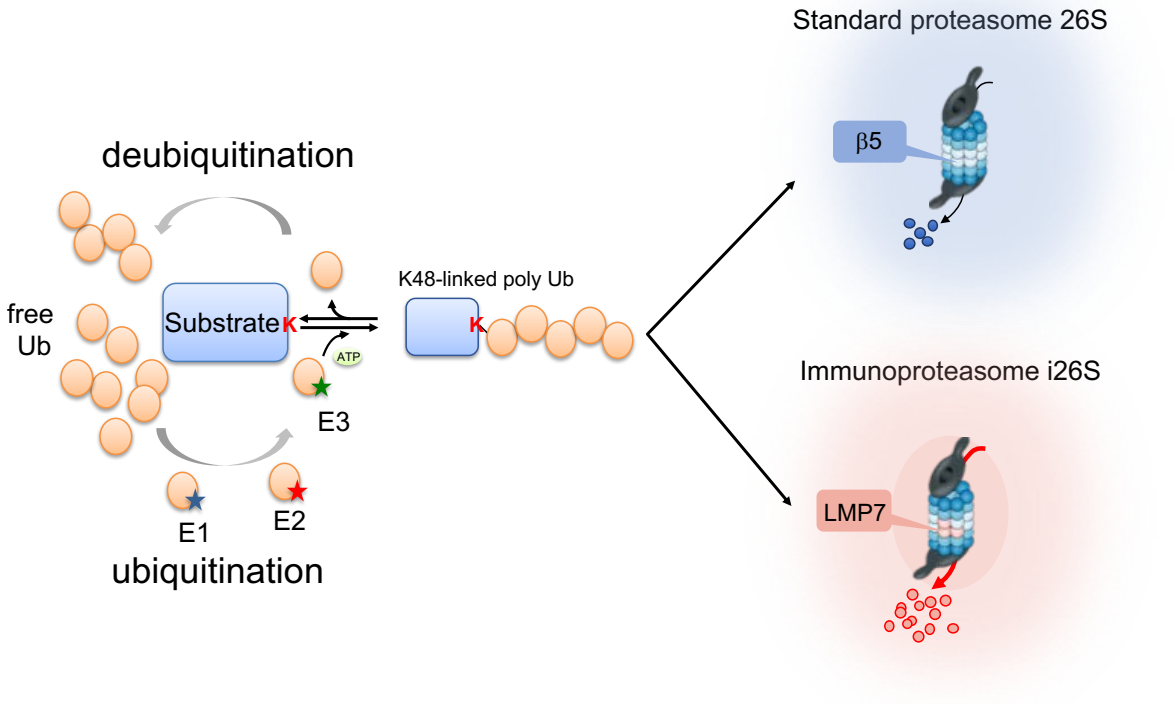

Scheme 2: The Ubiquitin-proteasome System.

Substrate proteins are recognized and ubiquitinated at their lysine 48 residue by an enzyme cascade. The lysine 48 ubiquitinated substrates are then degraded by either the standard proteasome or the immunoproteasome.

These favored cleavage specificities are enabled by size and substrate specific binding pockets (34). The proteasome is a convertible structure and therefore exists in different constitutions, which differ in the efficiency of proteolysis, ubiquitin and ATP dependence, as well as in the kind of peptides generated. One of these proteasome forms is the immunoproteasome, which differs from the standard proteasome by its catalytic subunits within the 20S core particle. The immunoproteasome is constitutively expressed by hematopoietic cells, and structural differences between the standard

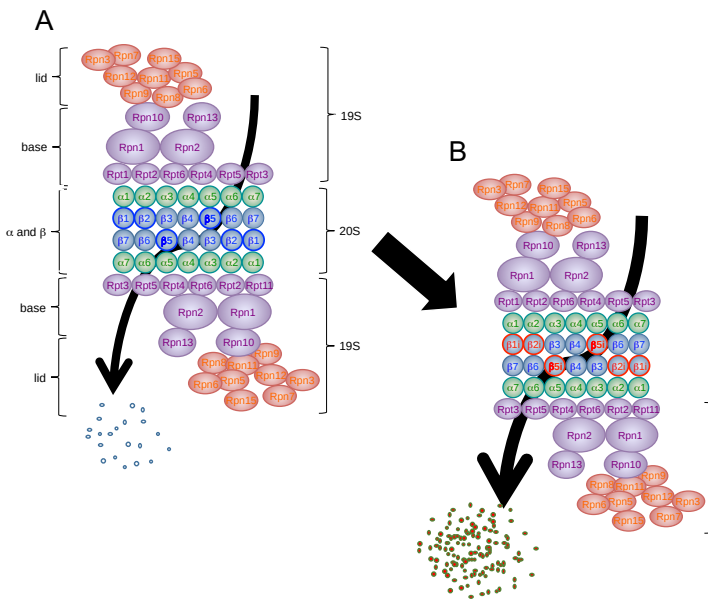

Scheme 3: Subunit organization of the standard (26S) and immunoproteasome (i26S).

Depiction of (A) the standard proteasome with 19S cap and 20S catalytic core with the proteolytic subunits (highlighted in blue) and the (B) immunoproteasome with its proteolytic subunits (highlighted in red).

subunits β1, β2 and β5 and the proteolytic subunits of the immunoproteasome β1i (Lmp2), β2i (Mecl1) and β5i (Lmp7) change the substrate specificity pockets and therefore result in different cleavage preferences (32). The immunoproteasome generates antigenic peptides that are suitable for presentation in the cleft of MHC class I molecules (32). Recently, it was described that the immunoproteasome also holds other functions besides antigen processing (35).

Since the proteasome has come into pharmaceutical focus, several proteasomal inhibitors have been developed for therapeutic and research use. So far broad proteasomal inhibitors have been approved for the treatment of multiple myeloma, such as bortezomib (with high affinity for β5, β5i, β1i and lower affinity for β1, β2, β2i) and carfilzomib (with high affinity for β5, β5i and lower affinity for β1, β1i, β2, β2i). Currently, there are multiple subtype/subunit specific inhibitors in clinical development such as ONX-0914 (with high affinity for β5i and lower affinity for β5 and β1i) or UK-101 (with high affinity for β1i and lower affinity for β5i) (32).

1.4.2 The Autophagosome-lysosomal system

The autophagosome-lysosomal degradation system (ALS) is primarily responsible for the degradation of proteins, polysaccharides and complex lipids, so mostly bulk materials, into respective molecules (36). Lysosomes contain more than 60 different types of hydrolases, among them lipases, proteases and glycosidases. Lysosomes can receive their cargo in different ways: They receive extracellular and cell surface cargos through endocytosis and intracellular substrates through autophagy. Increases in the endocytotic and autophagic flux increases lysosomal degradation, while the

accumulation of catabolites in the lysosomes downregulates lysosomal degradation (36). Lysosomal enzymes are delivered to lysosomes after being tagged with mannose-6-phosphate in the *cis*-Golgi, which then bind to mannose-6-phosphate receptors in the *trans*-Golgi network. The bound enzymes are then delivered to endosomes, where they separate from the mannose-6-phosphate receptors and the enzymes continue on to the lysosomes (37). The degradation of cytoplasmic components is done *via* autophagy. In autophagy, autophagosomes (double-membrane vesicles) sequester part of the cytoplasm and the fuse with lysosomes to from autolysosomes (37) which then degrade the material stored in autophagosomes.

1.5 Mucolipidosis type II and III

Renal involvement is a usually rare occurrence in lysosomal storage diseases. However, renal involvement is common and contributes to the morbidity and mortality in patients with Fabry disease, a lysosomal storage disorder caused by mutations in the GLA gene encoding α-galactosidase A (38). Furthermore, renal dysfunction has been observed in patients with nephrosialidosis (39), infantile sialic acid storage disease (40), cystinosis (41) as well as in mucopolysacharidosis (42). In patients with mucolipidosis type II or type III (another lysosomal storage disease) only few cases of renal involvement have been reported (43, 44).

Mucolipidosis type II and type III are rare lysosomal storage disorders, whose classification is based on the age of onset, clinical symptoms, and severity. The disease is caused by mutations in *GNPTAB* (MLII) which encodes the α and β subunit of the GlcNac-1-phosphotransferase, resulting in inactive GlcNac-1-phosphotransferase activity, or by mutations in *GNPTG* (MLIII alpha/beta or MLIII gamma) which encodes the γ subunit of the GlcNac-1-phosphotransferase, resulting in residual phosphotransferase activity (45). In cells from patients with MLII and MLIII, the tagging of mannose-6-phosphate to lysosomal enzymes is impaired, which leads to their missorting and hypersecretion into the extracellular compartment (46). The resulting deficiencies of lysosomal enzymes that end up in lysosomes results in the accumulation of various non-degradable macromolecules in dysfunctional lysosomes, leading to the impairment of cellular homeostasis. MLII patients present with progressive neurodegeneration, severe skeletal abnormalities, organomegaly, and death in the first decade of life (45). The manifestations of MLIII alpha/beta and MLIII

gamma are less severe compared to MLII and mainly affect skeletal and joint tissues (45). Renal involvement has only been described in very few cases of mucolipidosis. Two autopsy reports of patients with MLIII alpha/beta described a foamy appearance of podocytes in a 45-year-old woman (44) and in a man with normal renal function up to his death (43). Furthermore, in a large kindred family with MLIII alpha/beta two affected children exhibited nephrotic range proteinuria with focal segmental glomerulosclerosis and podocytes also displaying a foamy appearance, presumably due to lysosomal storage accumulation (47).

2. Aim

The objectives of this thesis are to 1) dissect the distribution and physiological significance of proteasomal and lysosomal degradation in glomerular cell types, 2) to investigate the mechanisms balancing proteostasis is glomerular cells in the setting of lysosomal impairment in mouse models of mucolipidosis type II and type III, and 3) to dissect the role of proteasome subtypes in the progression of podocyte injury in experimental THSD7A associated membranous nephropathy and to evaluate the potential of proteasome targeting as a new treatment strategy in membranous nephropathy.

3. Material and Methods

3.1 Material

3.1.1 Appliances

Analytic scale:		Sartorius AG, Göttingen
Autoanalyzer	Hitachi 717	Hoffmann-La Roche, Basel
Centrifuges:	Centrifuge 5417R	Eppendorf AG, Hamburg
	Heraeus Multifuge 1S-R Centrifuge	Thermo Fisher Scientific Inc. Waltham, MA, USA
Confocal Microscope:	LSM 800 with airyscan	Carl Zeiss AG, Oberkochen
Electron – transmission microscope	TEM 910	Carl Zeiss AG, Oberkochen
FACS sorter:	Aria IIIu	Becton Dickinson GmbH, Heidelberg
Fluorescent spectro-photometer:	Mithras LB940	Berthold Technologies, Bad Wildbad
Gel electrophoresis chamber:	MiniProtean Tetra Cell	BioRad Laboratories, Inc. Hercules, CA, USA
Imager:	Amersham Imager 600	GE Healthcare, Chicago, IL, USA
Light microscopes:	Axio Scope. A1 AxioCam MRc Axiovert 25	Carl Zeiss AG, Oberkochen

	StemiDV4	
Magnetic particle collector:	DynaMag™-2	Invitrogen AG, Carlsbad, CA, USA
Microplate spectro-photometer:	EL808 Ultra Microplate Reader	BIO-TEK Instruments, Inc. Winooski, VT, USA
Photometer:	DS-11 Spectro-photometer	DeNovix Inc., Wilmington, DE, USA
qPCR Thermocycler:	QuantStudio 3	Applied Biosystems, Foster City, CA, USA
Steam cooker:	FS10	Braun GmbH, Kronberg im Taunus
Thermomix:	Thermomixer comfort 1.5 ml	Eppendorf AG, Hamburg
Thermocycler:	Thermocycler	Biometra GmbH, Göttingen
TissueLyser:	TissueLyserII	QIAGEN GmbH, Hilden
Trans Blot sytem:	Trans-Blot Turbo Transfer system	BioRad Laboratories, Inc. Hercules, CA, USA
Transferpipette	S 8	Brand GmbH & Co KG, Wertheim
Transformer:	PowerPac Universal	BioRad Laboratories, Inc. Hercules, CA, USA
Ultramicrotome	UC6	Leica
Vortex:	VortexGenie2	Scientific Industries, Inc. Bohemia, NY, USA
Waterbath:	Waterbath	GFL, Gesellschaft für Labortechnik mbH, Burgwedel

3.1.2 Consumable material

96 well Plates	Sarstedt Aktiengesellschaft & Co. KG, Nümbrecht
High-bind 96 well Plates	Sarstedt Aktiengesellschaft & Co. KG, Nümbrecht
96 well plates fluorescence	Greiner Bio-One, Kremsmünster, Austria
Aluminium Foil	Cofresco Frischhalteprodukte GmbH & Co. KG, Minden
Centrifuge tubes 15 ml, 50 ml	Greiner Bio-One, Kremsmünster, Austria
Combitips	Eppendorf AG, Hamburg
Cotton buds	Meditrade GmbH, Kieferfelden
Cover Slips	Marienfeld Laboratory Glassware, Lauda-Königshofen
Dako Pen	Dako
Facial Tissues	GVS-Grossverbraucherspezialisten eG, Friedewald
FACS tubes	Corning Science Mexico S.A. de C.V.
Filter 100 µM	Sarstedt Aktiengesellschaft & Co. KG, Nümbrecht
Gloves (Nitrile)	Remesco Handelsges.m.b.H., Wien, Asutria
Gradient gels	BioRad Laboratories, Inc. Hercules, CA, USA
Hypodermic needle	B. Braun Melsungen AG, Melsungen
Microslides	Glasswarenfabrik Karl Hecht GmbH & Co. KG, Sondheim vor der Rhön
Parafilm©	Merck KGaA, Darmstadt
Petri dishes	Sarstedt Aktiengesellschaft & Co. KG, Nümbrecht
Pipette tips	Sarstedt Aktiengesellschaft & Co. KG, Nümbrecht

Pipette filter tips	Sarstedt Aktiengesellschaft & Co. KG, Nümbrecht
PVDF membrane	Merck Millipore Ltd., Cork, Ireland
Reaction tubes 0.2 ml, 0.5 ml 1.5 ml, 2 ml	Sarstedt Aktiengesellschaft & Co. KG, Nümbrecht
RTqPCR plates	Sarstedt Aktiengesellschaft & Co. KG, Nümbrecht
Scalpels	B. Braun Melsungen AG, Melsungen
Serological Pipettes	Sarstedt Aktiengesellschaft & Co. KG, Nümbrecht
Surgical Tape	3M Deutschland GmbH, Neuss
Syringe 1 ml	B. Braun Melsungen AG, Melsungen
Syringe 2 ml	Becton Dickinson GmbH, Heidelberg
Tungsten Carbide Beads	QIAGEN GmbH, Hilden
U-Stix	Siemens Healthcare Diagnostics, Inc., Tarrytown, NY, USA
Whatman paper	BioRad Laboratories, Inc. Hercules, CA, USA

3.1.3 Chemicals, enzymes and kits

All Chemicals and solvents were of analytical grade and were purchased from B. Braun (B.Braun, Melsungen, Germany), Sigma-Aldrich (St. Louis, MO, USA), Chemsolute (Th. Geyer GmbH & Co. KG, Renningen, Germany), J.T. Baker (Fisher Scientific, Hampton, NH, USA), Roche (Basel, Switzerland), Roth (Carl Roth GmbH & Co. KG, Karlsruhe, Germany) or Merck (Merck KGaA, Darmstadt, Germany)

100 bp ladder	Invitrogen	
4-nitrophenyl N-acetyl-β-D-glucosaminide	Sigma-Aldrich	
Acetic acid	Merck	H226, H290, H314

		P210, P280, P301+P330+P331, P305+P351+P338, P308+P310
Albumin	Sigma-Aldrich	
Aqua injectibilia	B. Braun	
Bortezomib	UbpBio	
Bovine serum albumin	Sigma-Aldrich	
Bromphenol blue	Chemsolute	
Calyculin A	Enzo	
Carbonate – bicarbonate buffered saline	Sigma-Aldrich	H319 P305+P351+P338
Chloroform	J.T. Baker	H302, H331, H315, H319, H351, H361d, H372 P302+P352, P304+P340, P305+P351+P338, P308+P310
Coomassie Brilliant Blue G-250 Dye	Thermo Scientific	
Cozy XL Prestained Protein Standard	highQu	
Collagenase from Clostridium histolyticum	Sigma-Aldrich	H334
Citric acid	Sigma-Aldrich	H319 P305+P351+P338
Creatinine	Sigma-Aldrich	
Dimethylformamide	Sigma-Aldrich	H226, H312+H332, H319, H360D P201, P280, P305+P351+P338, P308+P313

Dithiothreitol	Sigma-Aldrich	H302, H315, H319, H335 P261, P305+P351+P338
DMSO	Pierce	
DNase I from bovine pancreas grade II	Roche	
dNTP Set, 100 mM	Invitrogen	
Dulbecco's Phosphate Buffered Saline	Gibco	
Durcupan epoxy resin	Sigma-Aldrich	H302, H315, H317, H319, H360Df, H410 P201, P273, P280, P301+P312+P330, P302+P352, P308+P313
Dynabeads M-450 Tosylactivated	Invitrogen	
ECL reagent Super Signal	Thermo Fischer Scientific	
EDTA	Roth	H303, H332, H373 P260, P271, P304+P340, P312, P501
Epoxomicin	Selleckchem	
Ethanol	Chemsolute	H225, H319 P210, P240, P305+P351+P338, P403+P233
Eukitt	O. Kindler ORSAtec GmbH	H226, H312, H315, H319, H335, H373 P210, P241, P260, P280, P303+P361+P353, P305+P351+P338, P405, P501

Glycerol	Sigma-Aldrich	
Glycine	Roth	
Gum Arabic	Sigma-Aldrich	
Hank's Balanced salt solution	Gibco	
HCl, 1 N	Roth	H290, H314 P260, P280, P303+361+353, P305+351+338, P390, P501
Hematoxylin	Serva	H302, H315, H319, H335 P261, P305+P351+P338
HEPES Buffer Solution	Gibco	
Hoechst trihydrochloride trihydrate	Invitrogen	
Isopropanol	Chemsolute	H225, H319, H336 P210, P233, P240, P305+P351+P338, P403+P235
ITS Solution II	Pan Biotech	
Leupeptin A	Sigma-Aldrich	
Liberase TL	Roche	
β-Mercaptoethanol	Roth	H227, H301+H331, H310, H317, H318 P262, P280, P301+P310, P302+P352, P305+P351+P338, P361, P370+P378, P403+P233
Methanol	J. T. Backer	H225, H301, H311, H331, H370 P210, P233, P280, P302+P352, P304+P340, P308+P310, P403+P235
NaH_2PO_4 x H_2O	Merck	

Na_2HPO_4 x 2 H_2O	Merck	
Naphthol-As-Bisphosphate	Serva	H315, H319, H335 P261, P264, P304+P340, P305+P351+P338, P337+P313
New fuchsin	Sigma-Aldrich	H315, H319, H335, H351, H410 P201, P273, P302+P352, P305+P351+P338, P308+P313
Normal horse serum	Vector Laboratories	
ONX-0914	UbpBio	
Ovalbumin	Sigma-Aldrich	
Paraformaldehyde	Electron Microscopy Sciences	H228, H302+H332, H315, H317, H318, H335, H350 P201, P210, P280, P302+P352, P305+P351+P338
Paraplast Plus	McCormack Scientific	
Penicillin-Streptomycin	Gibco	H317, H334, H360 P201, P202, P261, P280, P284, P272
Periodic Acid	Roth	H271 P210, P221, P280, P283, P306+P360, P370+P378, P371+P380+P375
Phosphoric acid	Sigma-Aldrich	H290, H314 P280, P305+P351+P338, P310
Picric acid	Hengler Analytik	H201, H301, H311, H331 P210, P280, P301+P310, P312
POLAP Polymer	Cymed	

Ponceau	Serva	H315, H319, H335 P261, P264, P302+P352, P304+P340, P305+P351+P338, P337+P313
Potassium alum	Merck	
Protein G Resin	Genscript	
Random Primers	Invitrogen	
RevertAid Reverse Transcriptase	Thermo Scientific	
RPMI Medium 1640	Gibco	
Schiff's reagent	Merck	
SDS	Roth	H228, H302+H332, H315, H318, H335 P210, P261, P280, P302+P352, P305+P351+P338, P370+P378, P403+P233, P501
SigmaFast Protease Inhibitor Cocktail Tablets, EDTA free	Sigma-Aldrich	H318 P280, P305+P351+P338+P310
Sodium chloride	Roth	H303, P312
Sodium fluoride	Merck	H301, H315, H319 P302+P352, P305+P351+P338, P308+P310
Sodium hydroxide solution	Hengler Analytik	H290, H314, P280, P305+P351+P338, P310
Sodium iodate	Merck	H272, P210
Sodium nitrite	Merck	H272, H301, H319, H400

		P273, P305+P351+P338, P308+P310
Sodium vanadate	Sigma-Aldrich	H302 P301+P312+P330
Suc-LLVY-AMC	Calbiochem	
TMB Elisa Peroxidase Substrate	Biozol	
T-Per Tissue Protein Extraction Reagent	Thermo Scientific	
Tris Buffered Saline with Tween20	Sigma-Aldrich	
Tris Buffered Saline with BSA	Sigma-Aldrich	
Tris-HCl	Merck	
Trisodium citrate	J.T. Backer	
TritonX-100	Sigma-Aldrich	H302, H315, H318, H410 P273, P280, P301+P312+P330, P302+P352, P305+P351+P338+P310
Trizma Base	Sigma-Aldrich	
Trizol	Ambion by Life Technologies	H301+H311+H331, H314, H335, H341, H373, H412 P201, P261, P264, P280, P273, P301+P310, P302+P352, P305+P351+P338, P304+P340, P403+P233, P501
Tween20	Bethyl	

Urea	Sigma-Aldrich	
Xylol	Chemsolulute	H226, H304, H312+H332, H315, H319, H335, H412 P261, P273, P280, P301+P310, P305+P351+P338, P331

3.1.4 Kits

NucleoSpin RNA Plus XS	Macherey-Nagel Ref: 740990.50
Human albumin ELISA system	Dunn Labortechnik GmbH

3.1.5 Antibodies

Immunofluorescence

pUb (rabbit)	Novus
Nephrin (guinea pig)	ProGene
Limp2 (rabbit)	Eurogentic
LC3B (rabbit)	Sigma-Aldrich
Lamp1 (mouse)	DSHB
p57 (rabbit)	Santa Cruz
WGA	Vector Laboratories
rbIgG (Cy2)	Jackson ImmunoResearch
msIgG (Cy5)	Jackson ImmunoResearch
collagen 4 (goat)	Southern Biotechnologies
Podocin (rabbit)	Sigma-Aldrich

Lmp7 (rabbit)	Abcam
SMA	Abcam
Kim1	R&D
Cleaved Caspase 3	Cell Signaling
β5	Xuejun Wang, University of South Dakota
ATF4	Bioss
NRF1	Cell Signaling
pNRF2	Bioss
peIF2α	Cell Signaling
pPERK	Invitrogen
TFEB	Abcam
THSD7A	Santa Cruz
Hoechst	Invitrogen

Western Blot

Primary antibodies (Species)	Dilution	Origin
α-actinine 4 (rabbit)	1:1000 in superblock	Immunoglobe
β5 (rabbit)	1:5000 in superblock	Xuejun Wang, University of South Dakota
β-Actin (mouse)	1:10000 in superblock	Sigma-Aldrich
Cathepsin D (goat)	1:100 in 5 % sm	Santa Cruz
eIF2α (rabbit)	1:1000 in superblock	Cell Signaling
K48pUb (rabbit)	1:1000 in superblock	Abcam

Lamp2 (rabbit)	1:1000 in superblock	Sigma-Aldrich
LC3 (rabbit)	1:5000 in 5 % sm	Sigma-Aldrich
Limp2 (rabbit)	1:2000 in superblock	P. Saftig, Kiel
Lmp7 (rabbit)	1:5000 in 5 % sm	E. Krüger, Greifswald
PA28α (rabbit)	1:1000 in superblock	Enzo Life Sciences, Inc.
p62 (rabbit)	1:2000 in superblock	Sigma-Aldrich
peIF2α (rabbit)	1:1000 in superblock	Cell Signaling
pS6 (rabbit)	1:1000 in superblock	Cell Signaling
pUb (mouse)	1:250 in superblock	Millipore
rbIgG	1:1000 in 5 % sm	Jackson ImmunoResearch
Rpt5 (mouse)	1:1000 in superblock	Enzo Life Sciences, Inc.
S6 (rabbit)	1:1000 in superblock	Cell Signaling
THSD7A (human)	1:100 in 0.05 % sm	Patient serum
THSD7A (rabbit)	1:1000 in 0.5 % sm	Atlas
UCH-L1 (rat)	1:250 in 5% sm	Self-made

FACS

CD31 (BV421)	1:800	BD OptiBuild
CD73 (AF647)	1:2000	BioLegend
Podoplanin (PE)	1:200	BioLegend
NIR	1:4000	BioLegend

All secondary antibodies were purchased from Jackson ImmunoResearch Laboratories Inc. (West Grove, PA, USA).

3.1.6 Primer

Primer for qPCR

Primer	Sequence 5' to 3'	Tm
ATF4 fw	CGGCAAGGAGGATGCCTT	60 °C
ATF4 rev	TGGTTTCCAGGTCATCCATT	60 °C
ATF6 fw	CCTGTGGCTTGTGGGTGTT	60 °C
ATF6 rev	TCTACTTGGTCCATCGTGGG	60 °C
CHOP fw	GAACCTGAGGAGAGAGTGTT	60 °C
CHOP rev	TATAGGTGCCCCCAATTTCA	60 °C
EIF2A fw	GCAAACAATGTCCCATCCTT	60 °C
EIF2A rev	GGACCACCACACTTCACAGA	60 °C
EIF2AK1 fw	CAGTACGATGCCAAGTCAGAT	60 °C
EIF2AK1 rev	TCTGTCCCGAATGGCTGAAA	60 °C
EIF2AK2 fw	ACAAATCGTGACCGGAGTGG	60 °C
EIF2AK2 rev	CAGGTCGGTCCTTGGGTTTC	60 °C
EIF2AK4 fw	TGCCCACCTACATACCCAGA	60 °C
EIF2AK4 rev	TCATCACCTCTCCACACTGC	60 °C
GADD34 fw	AGAGAAGCCAGAATCACCTT	60 °C
GADD34 rev	AGTGTACCTTCCGAGCTTTT	60 °C
IRE1α fw	CCAGGGTCGAGACAAACAAC	60 °C
IRE1α rev	GTGGCTGTTGCTCCTGCT	60 °C
NFE2L2 fw	AGATGACCATGAGTCGCTTGC	60 °C
NFE2L2 rev	CCTGATGAGGGGCAGTGAAG	60 °C
NRF1 fw	AATGACCCAGGCTCAGCTTC	60 °C
NRF1 rev	GCTTGCAGCTTTCTTTCCCC	60 °C
PERK fw	TGGAAGAGGTCTCCATCCAG	60 °C
PERK rev	GGGTCTGGTTCCTTGGTTTC	60 °C

3.1.7 Software

Adobe Illustrator	Adobe Systems Software Ireland Limited
Adobe Photoshop	Adobe Systems Software Ireland Limited
Fiji	Open Source program based on ImageJ
FlowJo	Becton Dickinson GmbH
GraphPad Prism 5	GraphPad Software Inc. San Diego, CA
LSM	Carl Zeiss AG, Oberkochen
ZENblue	Carl Zeiss AG, Oberkochen

3.2 Methods

3.2.1 Animal experiments

Mice were housed in a pathogen-free animal facility at the University Medical Center Hamburg-Eppendorf, and experimental procedures were performed according to the institutional guidelines. Mice had free access to water and were fed with standard mouse chow.

MLII and MLIII

MLII and MLIII mice have kindly been provided by Sandra Pohl. The *Gnptg*^{ko} (ML III have been described elsewhere (48). A *Gnptab* targeting vector (49) used for generation of MLII mice contained a neomycin resistance cassette between exons 16 and 17, allowing selection for recombination in targeted embryonic stem cells, and two loxP sites located in introns 13 and 16. Targeted embryonic stem cells were injected into C57Bl6/J blastocysts and subsequently implanted into the uterine horns of C57Bl6/JxCBA foster female mice according to standard protocols. Offspring chimeric males from three clones were further crossed with Cre-expressing mice, resulting in

mice, which carry the *Gnptab*$\Delta^{ex14\text{-}16}$ (MLII) allele lacking the floxed region (exons 14, 15 and 16, and the neomycin cassette). Heterozygous MLII mice were then inbred to generate homozygous MLII animals. Experiments were performed with mice of a mixed C57Bl/6-129/SvJ genetic background with littermates used as controls. MLII and MLIII mice were older than 15 weeks and predominantly analyzed at 30 - 40 and 60 - 90 weeks of age, respectively.

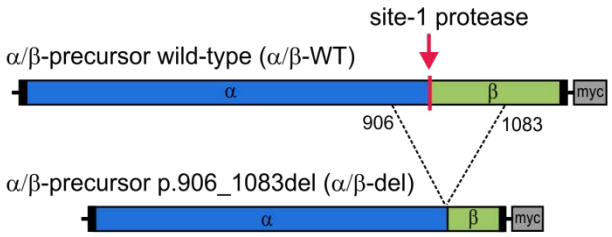

Scheme 4: The non-cleavable mutant p.906_1083del α/β-precursor

Schematic representation of myc-tagged wild-type (WT) and p.906_1083del mutant α/β-precursors. The position of the deletion (amino acid 906 to 1083) is indicated by a dotted line.

BALB/cAnNCrl

Wildtype BALB/cAnNCrl were purchased from Charles River. They were predominantly analyzed at 12 - 20 weeks of age.

Lmp7Δpod mice

Lmp7$^{fl/fl}$ mice were kindly provided by Elke Krüger. The Lmp7$^{fl/fl}$ mice contain two loxP sites around exon 3. To produce a podocyte-specific Lmp7 knockout, the Lmp7$^{fl/fl}$ mice were crossed with mice expressing the Cre recombinase in dependence of the podocin promoter, which have been described elsewhere (50). This crossing resulted in Lmp7Δpod mice lacking the floxed regions specifically in podocytes. Heterozygous Lmp7Δpod mice were then inbred to generate homozygous Lmp7Δpod animals. Experiments were performed with mice of a C57Bl/6 genetic background with

littermates used as controls. Lmp7Δpod mice were predominantly analyzed between 10 – 20 weeks of age.

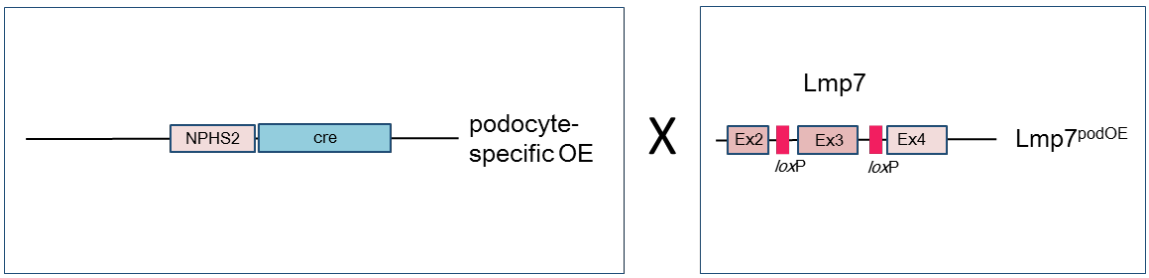

Scheme 5: The podocyte-specific Lmp7 knockout mouse

Schematic representation of the genetic targeting of the podocin-cre mouse with the genetic targeting of the $Lmp7^{fl/fl}$ mouse.

3.2.2 Genotyping of animals

DirectPCR Tail	200 µl DirectPCR - Tail lysis buffer
ProteinaseK	0.2 mg/ml proteinase K

MLII and MLIII mice were genotyped by extracting genomic DNA from tail biopsies using the KAPA Mouse Genotyping Hot Start Kit (VWR) and analyzed by multiplex PCR using primers F1 (5'-CAT CCC ACC GAC TCA GGA AG-3'), F2 (5'-GAA ATG TTG CAC CAA ACT GG-3') and R (5'-GCA GCA GTG CCC ATC TGA TA-3').

The Lmp7Δpod mice were genotyped by extracting genomic DNA with DirectPCR-Tail, whereby the tail pieces were lysed in lysis buffer with proteinase K for 16 h at 55°C. Proteinase K was inactivated for 45 min at 85°C. Centrifugation for 10 s at 13000 rpm was performed, the supernantant removed and the pellet solved in H_2O. The DNA was analyzed by PCR using primers Fwd (5'-GCTATAATGCCAGCTCTGTCTGAACTTCG-3') and Rev (5'-TGCCTCTTGCATCTCTTAGCCCACC-3').

3.2.3 Immunofluorescence

Blocking buffer:	5 % normal horse serum, 0,05 % Triton X-100 in PBS
Dako Target Retrieval Solution	10 x citrate buffer, pH 6.1

For immunofluorescent stainings, 2 µm paraffin sections were deparaffinized and antigen retrieval was performed by microwave boiling (10 mM citrate buffer, pH 6.1) or by protease XXIV (Sigma-Aldrich, 5 µg/ml) digestion. Unspecific binding was blocked with blocking buffer for 30 minutes. Primary antibody incubations (blocking buffer, over-night, 4°C) were followed by incubation with biotinylated or AF488- or Cy3-coupled secondary antibodies (1:400, 30 minutes). Stainings were evaluated with an LSM510 meta microscope for conventional microscopy or with an LSM800 with airyscan for high-resolution confocal microscopy using the LSM or ZENblue software (all Zeiss).

3.2.4 Glomeruli Isolation

Collagenase-solution:	3 ml HBSS per mouse, 1.2 mg/ml collagenase 1A, 100 U/ml DNaseI
Dynabead-solution:	50 ml HBSS, 150 µl Dynabeads (Invitrogen)
HBSS + BSA:	HBSS, 0,05% BSA

The kidneys were removed from the mouse with the aorta still attached. The kidneys were perfused with 5 ml Dynabead solution per kidney through the renal artery. After perfusion, the kidney capsule was removed and the kidneys were chopped up with a scalpel. The kidney pieces were separated into two Eppis and 1.5 ml collagenase solution was added. Digestion was performed for 15 min, 37°C, 1300 rpm in a thermomix. The content of 1 reaction tube was strained over a 100 µM filter, which was placed atop a 50 ml Falcon tube, with the help of a 2 ml syringe pestle, rinsing the filter with 10 ml HBSS. The content of the second reaction tube was strained over a new 100 µM filter into the same Falcon tube and also rinsed with 10 ml HBSS. A new 100 µM filter was set atop a new 50 µl Falcon tube and the content of the first falcon was strained into the second tube. The filter was rinsed with 10 ml HBSS. Centrifugation was performed for 5 min, 1700 rpm, at 4°C. The supernatant was decanted and the pellet solved in 6 ml HBSS, which was separated into four 2 ml reaction tubes. The tubes were hung on the magnetic particle concentrator (MPC) and incubated on ice for 5 min. The supernatant was removed, the pellet resuspended in 1.5 ml HBSS + BSA, and incubated for 5 min on the MPC. This step was repeated 2 times. After the third wash the glomeruli of all four tubes were collected in one tube. 1 ml of HBSS was

added to one tube, the glomeruli were resuspended and moved to the next tube until all the glomeruli were collected in the last tube. The glomeruli were counted in 10 µl under a light microscope. The glomeruli were centrifuged for 10 min, 4000 rpm, 4°C, the supernatant discarded and the glomeruli pellet was shock frozen in liquid nitrogen and stored at -80°C.

3.2.5 Isolation of glomerular cells

Liberase digestion solution 1 ml per mouse:	1000 µg/ml Liberase TL, 100 U/ml DNaseI, In Cell culture media
Cell Culture media:	10% FCS, 1% ITS, 1% Pen/Strep, 25 mM HEPES, RPMI Media 1640
MACS buffer:	PBS, 0.5% BSA, 2 mM EDTA

Isolation of the different glomerular cells followed the protocol of glomeruli isolation until the digested solution was centrifuged. After the supernatant was decanted the pellet was solved in 3 ml HBSS and split into two 2 ml reaction tubes. The tubes were hung on the MPC for 1 min, 1 ml supernatant was removed. 1 ml HBSS was added per tube and directly removed again. This step was repeated twice. 1 ml HBSS + BSA was added and the reaction tube removed from the MPC, the glomeruli were resuspended with a pipette and vortexed. The tubes were hung on the MPC, after 1 min 1 ml supernatant was removed, then 1 ml HBSS was added and directly removed again. This step was repeated twice, after the second time all the supernatant was removed. The pellet was resuspended with 1.5 ml HBSS + BSA with a pipette. The tubes were hung on the MPC, after 1 min 1 ml supernatant was removed, then 1 ml HBSS was added and directly removed again. This step was repeated twice, after the second time all the supernatant was removed. The pellet was resuspended with 1.5 ml HBSS + BSA with a pipette. The reaction tubes were placed back on the magnet and incubated for 5 min. The glomeruli were combined from one individual into one reaction tube by incubating the reaction tubes on the MPC for 5 min. The supernatant was removed and the glomeruli of one reaction tube resuspended with 1 ml HBSS, then the glomeruli of the second reaction tube were resuspended with the solution of the first reaction tube. Counting of the glomeruli and tubuli contamination was performed

by looking at 5 µl of glomeruli solution under the phase contrast microscope at a 25-fold magnification. 50 µl of the glomeruli solution were set aside as a positive control, pelleted by centrifuging for 5 min, 1000 x g, 4°C. The supernatant was removed and the glomeruli shock frozen in liquid nitrogen, and stored at – 80°C. The remaining glomeruli were centrifuged for 5 min, 1000 x g, 4°C and the supernatant discarded. The glomeruli were resuspended in 1 ml Liberase digest solution, the solution moved into a 2 ml reaction tube and incubated for 2 h, 37°C, 1400 rpm in a thermomix. The glomerular cell types were removed from the glomerular scaffold following a precise time thread of mechanical treatment (Table XX), whereby “V” signifies vortexing and “S” shear stress through a Pasteur pipett.

Time	Treatment	Incubation time
2:00		30 min
1:30	Vortex (V), shear (S),V	20 min
1:10	V, S, V, pipette up and down with a pasteur pipette (PP),V	20 min
0:50	V, S, V, PP, V	10 min
0:40	V, S, V, PP, V	10 min
0:30	V, PP, V	10 min
0:20	V, S, V, pipette up and down 1x with a 200 µl pipette tip on a 1000 µl pipette tip (P), V	5 min
0:15	V, P, V	5 min
0:10	V, P, V	5 min
0:05	V, P, V	5 min
0:00	3 x V	

Following mechanical disruption, the reaction tubes were placed on the MPC for 5 min and the supernatant (which contains the cells) moved into 1,5 ml reaction tubes. The reaction tube was filled with MACS buffer to a final volume of 1.5 ml and the cells pelleted for 10 min, 1000 x g, 4°C, the supernatant was removed. The cells were resuspended in 100 µl MACS buffer and the FACS antibodies added and incubated for 30 min at 4°C in the dark. The cells were washed with 1 ml MACS buffer and pelleted by centrifugation for 10 min, 1000 x g, 4°C, the supernatant was removed. The cells were resuspended in 300 µl MACS buffer and filtered through a 40 µM filter into FACS tubes. The collecting tubes were filled with 100 µl MACS buffer each. The cells

were sorted in the FACS core unit at the Aria IIIu. After the sort the cells were pelleted by centrifugation for 10 min, 1500 x g, 4°C, the supernatant was removed. In case the cells were used for Western blot analysis the pellets were shock frozen in liquid nitrogen and stored at -80°C.

3.2.6 RNA Isolation, DNase digest and reverse transcription

Master Mix 1:	21 µl H_2O, 2 µl random hexamer primer, 2 µl dNTPs
Master Mix 2:	8 µl reverse transcriptase buffer, 1 µl RNase Out, 2 µl reverse transcriptase

RNA isolation with phenol/chloroform. The Trizol was warmed up to room temperature. One Tungsten Carbide Bead was added to each sample, then 500 µl Trizol were added to each kidney sample and the samples were lysed in the tissue lyser for 1 min at 30 Hz. The samples incubated at room temperature for 5 min. 1/6 volume of chloroform was added to each sample, the reaction tubes were shaken well and incubated at room temperature for 3 min. The samples were centrifuged for 15 min, 12000 rpm, 4°C and the upper phase, containing the RNA, was moved to a new reaction tube. 200 µl cold (-20°C) isopropanol were added to each sample and shaken well. The samples incubated on ice for 30 min, centrifuged for 10 min, 10000 rpm, 4°C. The supernatant was decarded. The pellets were washed with 500 µl 80% EtOH, centrifuged for 10 min, 13000 rpm, 4°C and the supernatant discarded. The wash step was repeated once more. The supernatant was removed completely and the pellet dried for 10 min at room temperature. The RNA was resuspended in 40 µl RNase free water. The RNA concentration was determined at a DeNovix Spectrophotometer. Store the RNA at -80°C. If RNA is isolated from glomeruli only half of the solutions was used.

200 ng RNA were DNase digested with rapid DNase for 10 min at 37°C.

4 µl digested RNA were added to 25 µl Master Mix 1 and incubated for 5 min at 65°C. Meanwhile Master Mix 2 was put together, and 11 µl Master Mix 2 were added to the reaction and the RNA was reverse transcribed in a thermocycler (Biometra). 10 min at 25°C, 1 h at 42°C, 10 min at 70°C, 4°C forever. The transcribed cDNA was stored at –20°C.

3.2.7 Western Blot analysis

Lysis buffer:	1 mM NaF, 1 mM NaV, 1 x Complete, 1 mM Calyculin A, T-Per
Lysis buffer for the pellet:	8 M Urea
5 x Laemmli buffer:	20% (v/v) 1.5 M Tris-HCl pH 6.8, 50% (v/V) Glycerol, 25 % (v/v) β-mercaptoethanol (reducing) or H_2O (non-reducing), 2 g SDS, 0.05 % (v/v) bromphenol blue
10 x Migration buffer:	0.25 M Tris, 1.92 M Glycin, 1% (w/v) SDS, in dest. H_2O, pH 8.3
10 x Transfer buffer:	1.92 M Glycin, 0.25 M Tris, in dest. H_2O
10 X TBS:	200 ml 5 M NaCl, 100 ml 1 M Tris, ad to 1 L with dest. H_2O

The amount of lysis buffer to solve the glomeruli was adapted to the number of isolated glomeruli, 5000 glomeruli were lysed in 150 µl lysis buffer. The glomeruli were solved by adding 50 µl lysis buffer to the pellet and then the pellets were crushed with a pestle after which the rest of the lysis buffer was added. The samples incubated on ice for 30 min, while ratcheting the reaction tubes over a reaction tube holder every once in a while. The samples were centrifuged for 30 min, 13000 rpm, 4°C. The supernatant containing the solved proteins were transferred to a new reaction tube. If the unsoluble glomeruli pellet was also analyzed the pellet was solved in 30 µl 8 M Urea the same way as the glomeruli were lysed. The proteins were denatured by mixing the lysates with 5 x laemmli buffer so that the end concentration is 1 x, the samples were incubated for 10 min at 95°C. The samples were loaded on a gel and the gel was ran in migration buffer for 10 min at 80 V then at 120 V. Meanwhile 4 filter papers were soaked in 1 x transfer buffer and stored in the fridge. Membranes were activated for 2 min in MeOH and washed with dest. H_2O. After the gel run the blotting chamber was prepared by putting first a filter, then a membrane, then the gel and lastly a filter and all possible air bubbles were removed. The gel was blotted for 30 min, 25 V, maximum 2.5 A. after the blot the membrane was incubated with ponceau red for 10 min to visualize all the proteins. The ponceau red stain was documented on the imager. The membrane was washed for 5 min with 1 x TBST, the membrane was blocked for 1 h at room temperature with 5% skimmed milk. The membrane was washed 3 x 5 min each with

1 x TBST, the membranes were cut and incubated with primary antibody overnight at 4°C. The membranes were washed 4 x 5 min each with 1 x TBST and incubated with secondary antibody for 1 h at room temperature, the membranes were washed 4 x 5 min each and the blots were developed with ECL reagents and the protein signal was documented on the Imager. The membranes were washed 3 x 5 min each. The membranes were stored dry. Densitometric analysis was performed with Fiji (Open Source software) and consolidated in Adobe Illustrator. Western blot results were normalized to the home keeper.

rbIgG Pulldown

In order to pull rbIgG from glomeruli for Western blot analysis, the glomeruli were lysed as has been described earlier. The glomeruli lysates were transferred to an appropriate amount of protein G resin (static binding capacity of 20 mg IgG per ml) and incubated over night at 4°C. The samples were centrifuged for 10 min, 14000 x g, °C, the supernatant was discarded. The rbIgG was released from the protein G resin by denaturing it with an equal amount of laemmli buffer. The Western blot was conducted the same as has been described earlier.

3.2.8 Immunohistochemistry

HCl alcohol:	0.25 % HCl in EtOH
Citrate buffer:	8 mM Trisodium citrate, 1.5 mM citric acid, dest. H_2O, pH 6
Blocking buffer:	PBS, 0.05 % Tx-100, 5% horse serum
TNT-buffer:	0.05 M TrizmaBase, 0.15 M NaCl, 2.4 % 1 N HCl, 0.1 % Tween 20, dest. H_2O, pH 8.31
New-fuchsin solution:	0.14 M New fuchsin in 2 N HCl
Naphtol As-Bi Phosphat:	0.06 M Naphthol As-Bi Phosphate in DMF
Haematoxylin solution 1:	0.1 M potassium aluminium sulfate, 2.5 mM sodium iodate in dest. H_2O
Haematoxylin solution 2:	0.017 M Haematoxylin in EtOH

Kidney cortex was embedded in paraffin for light or high-resolution confocal microscopy. One µm thick sections were cut on a rotation microtome to evaluate kidney morphology and stained with periodic-acid-Schiff reagent (Sigma-Aldrich) for light microscopic evaluation according to the manufacturer's instructions. The Schiff reagent was warmed up to room temperature and the paraffin sections were deparaffinized in the descending alcohol sequence (3 x xylene, 3 x 100% EtOH, 2 x 96% EtOH, 2 x 70% EtOH, 5 min each) and the sections were washed 2 x in dest. H_2O for 5 min each. The sections incubated for 15 min in 1% periodic acid at room temperature, the sections were washed for 3 min under running tap water, then washed with dest. H_2O. The slices were incubated for 40 min in Schiff reagent, then washed for 7 min under running tap water and then washed with dest. H_2O. The cell nucleus was stained with hematoxylin after Böhmer for 1 min at room temperature, the slices were washed for 3 min with running tap water and the staining was differentiated shortly in HCl alcohol. The slices were run through the ascending alcohol sequence (1 x 70% EtOH 2 min, 3 x 96% EtOH 2 min, 1 x 100% EtOH 2 min, 1 x 100% EtOH 5 min, 1 x 100% EtOH 10 min, 3 y xylene 5 min) and the slices were covered with Eukitt. Pictures of the PAS staining were taken with a light microscope with camera (Zeiss) with a 40 x ocular.

To determine podocyte loss and swelling of glomerular tufts, 3 µM thick sections were cut on a rotation microtome. The kidney sections were deparaffinized in the descending alcohol sequence (3 x xylene, 3 x 100% EtOH, 2 x 96% EtOH, 2 x 70% EtOH, 5 min each) and the sections were washed 3 x 5 min each with dest. H_2O. 1 x citrate buffer (pH 6.1) was pre-warmed for 40 min in a steam cooker, the kidney sections were incubated for 30 min in the warm citrate buffer at 95°C in the steam cooker. The sections were cooling for 15 min at room temperature, and the sections were washed 3 x, 5 min each with tap water. The kidney sections were circled with a hydrophobic Dako pen and PBS was added to each slide. The unspecific binding places were blocked with blocking buffer for 30 min at room temperature. The kidney slices were incubated over night with primary antibody against p57 1:400 at 4°C. The kidney slices were washed 3 x, 5 min each with PBS and incubated with POLAP-AP polymer for 30 min at room temperature. The kidney slices were washed 3 x with PBS, 5 min each and incubated in new-fuchsin staining solution until the podocytes were visibly red. The

reaction was stopped in dest. H_2O. The slides were covered with gum arabic. Podocytes were counted under a light microscope and pictures were taken under a 40 x ocular to determine the glomerular tuft area. The podocytes of 20 glomeruli were counted per animal.

3.2.9 Determination of serum parameters

Patient urine and mouse serum and urine were analyzed by standard methods using an autoanalyzer (Hitachi 717; Roche) in the Department of Clinical Chemistry at the University Hospital Hamburg.

3.2.10 Electron microscopy

For electron-microscopical analyses, small cortical samples that were perfusion-fixed in 4% buffered paraformaldehyde with 1% glutaraldehyde. Tissue was post-fixed with 1% osmium in 0.1 M phosphate buffer for 1 h at room temperature, stained with 1% uranylacetate for 1 h at room temperature in 70% EtOH, dehydrated and embedded in epoxy-resin (Durcupan, Sigma-Aldrich). Ultrathin sections were cut (Ultramicrotome UC6; Leica) and contrasted with lead citrate. Micrographs were generated with a transmission – electron microscope (TEM 910; Zeiss, Oberkochen, Germany). The electron microscopy was performed by PD Dr. Oliver Kretz.

3.2.11 Urine analysis

Wash buffer:	1 pack Tris-Tween solved in 1 l dest. H_2O
Postcoat solution:	1 pack Tris with BSA solved in 1 l dest. H_2O
Coating buffer:	solve 1 capsule carbonate-bicarbonate buffer in 100 ml dest. H_2O
Conjugate diluent:	0.5 ml 10% Tween 20 in 100 ml postcoat solution
Primary antibody:	1:100 in coating buffer
Secondary antibody:	1:40000 in conjugate diluent
Creatinine reagent:	10 ml alkaline buffer + 2 ml picric acid

Coomassie staining solution: 0.025 % (w/v) Coomassie Brilliant Blue, 10 % (v/v) acetic acid

Mouse urine was collected in metabolic cages for 3 h. Urine albumin content was quantified using a commercially available ELISA system (Bethyl) according to the manufacturers' instructions.

A high-bind ELISA plate was coated with 100 µl primary antibody per well, and incubated overnight at 4°C. The urine samples were diluted in conjugate diluent. The primary antibody solution was discarded, and the plate was washed 3 x with wash buffer. 200 µl postcoat solution were added per well and the plates were incubated for 30 min at room temperature. Meanwhile, the standard was prepared in conjugate diluent:

S0	10000 ng/ml
S1	1000 ng/ml
S2	500 ng/ml
S3	250 ng/ml
S4	125 ng/ml
S5	62.5 ng/ml
S6	31.25 ng/ml
S7	15.625 ng/ml

The post-coat solution was discarded, and the plate was washed 3 x with wash buffer. 100 µl standard or sample were added per well and the plate was incubated at room temperature for 1 h. The supernatant was discarded, and the plate was washed 5 x with wash buffer. 100 µl secondary antibody were added per well and the plate incubated at room temperature for 1 h. The supernatant was discarded, and the plate was washed 5 x with wash buffer. 100 µl TMB substrate solution were added per well and incubated for 5 min in the dark. The reaction was stopped by adding 100 µl H_3PO_4 per well, the readout of the results was done using an ELISA plate reader (BioTek) at 450 nm. Measurements in were conducted in duplicates.

The albumin content of patient urine was quantified using a commercially available kit by Dunn Labortechnik GmbH, according to the manufacturers instructions.

Urinary albumin values were standardized against urinary creatinine values of the same individuals. Urine creatinine values were determined according to Jaffe using a commercially available kit (hengler analytik). Creatinine values were determined in duplicates. 10 µl standard or urine were added to each well as well as 50 µl creatinine reagent. The plate was incubated for 1 min at room temperature. The readout of the results was done using an ELISA plate reader at 490 nm.

S1	0.5 g/l
S2	0.4 g/l
S3	0.3 g/l
S4	0.2 g/l
S5	0.1 g/l
S6	0.05 g/l
S7	0.02 g/l

Further urine analysis *via* urine Coomassie staining was done. Urine was plotted on a gel creatinine adapted with the gel running as described for the Westen blot analysis. The gel was incubated over-night in Coomassie staining solution and slowly decolorized with dest. H_2O until clear bands were distinguishable. The Coomassie stain was documented at the imager.

3.2.12 Lysosomal activity assay

Lysis buffer:	T-Per with protease complete inhibitor cocktail without EDTA
Substrate buffer:	10 mM 4-nitrophenyl N-acetyl-β-D-glucosaminide, 0.1 M Na-citrate, 0.2% BSA, pH 4.6
Stop solution:	0.4 M glycine, pH 10.4

For photometric measurement of β-hexosaminidase activity in glomeruli, samples were lysed in lysis buffer, 150 µl lysis buffer per 5000 glomeruli. Protein concentration was determined by spectrophotometry (DeNovix DS-11), and 6 µl of samples were incubated with 24 µl H_2O and 30 µl substrate buffer per well for 1 hour at 37°C in the dark. The reaction was stopped with 240 µl stop solution per well. Activity was measured in duplicates using a microplate spectrophotometer (BioTek, EL 808) at

405 nm.

3.2.13 Proteasomal activity assay

Lysis buffer:	T-Per with protease complete inhibitor cocktail without EDTA
Incubation buffer:	20 mM HEPES, 0.5 mM EDTA, 5 mM DTT, 0.1 mg/ml ovalbumin, pH7.8 in H_2O
Substrate solution:	60 µM Suc-LLVY-AMC in incubation buffer

For measurement of the main proteolytic activity of the proteasome, isolated glomeruli were lysed in lysis buffer, 150 µl lysis buffer per 5000 glomeruli. Protein concentration was determined by Spectrophotometry (DeNovix DS-11). For the measurement of proteasomal (chymotrypsin-like) activity, 10 mg total protein were diluted in incubation buffer to a final volume of 50 µl. Samples were pre-incubated in incubation buffer for 2 hours at 4°C. Following pre-incubation, the substrate Suc-LLVY-AMC (Calbiochem) was added to the samples at a final concentration of 60 µM and to an end volume of 100 µl. Proteasomal activity was measured in triplicate at 355 and 460 nm in a fluorescent spectrophotometer after incubation at 37°C for 2 hours in the dark.

3.2.14 Statistical analysis

Statistical analysis was performed using GraphPad Prism 5 (GraphPad Software Inc. San Diego, CA). Results were expressed as mean ± SEM, and significance was set at $p < 0.05$. The means were compared using either the two-tailed nonparametric Mann-Whitney U test or an ANOVA, depending on group number. Replicates used were biological replicates, which were measured using different samples from distinct mice. All animals (in their respective group) were littermates and were blindly assigned to the experimental groups.

4. Results

4.1 Podocyte proteostasis depends on the proteasomal degradation system

4.1.1 Podocytes preferentially express players of the UPS

In the investigation of the role of the ubiquitin proteasome system (UPS) on the progression of membranous nephropathy (MN), a disease of glomerular podocyte foot processes, it became clear that very little is known about the dependence of cells, that make up the filtration barrier in kidney glomeruli, on the different degradation systems under homeostatic conditions. Therefore, it first had to be determined whether the different glomerular cell species (podocytes, glomerular endothelial cells, and mesangial cells) exhibit the same expression pattern of UPS and ALS players. First, we evaluated high-resolution confocal immunofluorescence images from kidney samples derived from both healthy mice (Figure 1 A) and from the healthy part of tumornephrectomy samples from human (Figure 1 B). Endothelial cells and podocytes predominantly showed high levels of polyubiquitinated (pUb) proteins, which are proteins targeted for degradation by the proteasomal system, as well as the microtubule-associated protein 1A/1B-light chain (LC3), which is a marker for autophagy. Podocytes additionally showed high levels of β5, which is the main proteolytic subunit of the standard proteasome. Mesangial cells on the other hand predominantly showed high levels of the lysosomal-associated membrane protein 1 (Lamp1) and the lysosomal integral membrane protein-2 (Limp2). To investigate this observation further, a novel technique, which allows the separation and subsequent isolation of the different glomerular cell types into podocytes, glomerular endothelial cells and mesangial cells *via* FACS sorting from mouse kidneys was developed. This technique allows later analysis of the isolated cells *via* qPCR and Western blot (Figure 2). Interestingly, it became clear that under homeostatic conditions there is a difference between glomerular cell types not only in respect to which degradation system is predominantly expressed but, also in the subtype of proteasome expressed in the different cell types.

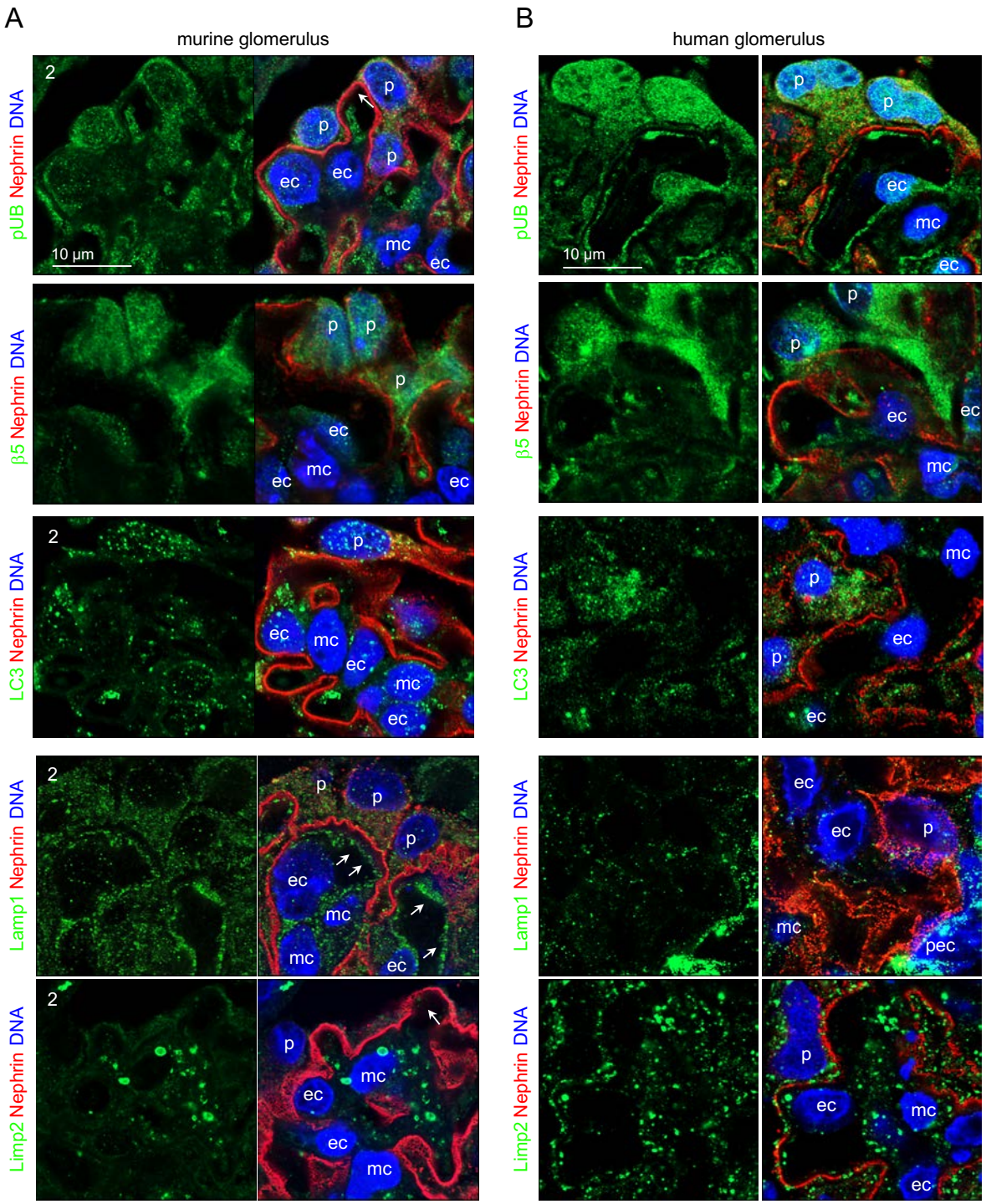

Figure 1: Glomerular cell-specific distribution of proteasomal and lysosomal proteins. Representative high-resolution confocal images of immunofluorescent stainings of polyubiquitin (pUB) and the proteasomal subunit β5 as UPS players and of microtubule-associated protein 1A/1B-light chain 3 (LC3), lysosomal-associated membrane protein 1 (Lamp1) and lysosomal integral membrane protein-2 (Limp2) as autophagosomal-lysosomal players in (A) mouse and (B) human glomeruli. The target protein is depicted in green, nephrin, a slit membrane protein to visualize the glomerular filtration barrier, in red and the DNA *via* Hoechst staining in blue, p = podocyte nucleus, ec = endothelial cell nucleus, mc = mesangial cell nucleus.

RTqPCR analysis of the different cell types showed that podocytes strongly expressed the main proteolytic subunit of the standard proteasome, the β5 subunit (*Psmb5*), whereas endothelial cells strongly expressed the main proteolytic subunit of the immunoproteasome, the β5i (Lmp7, *Psmb8*) subunit (Figure 2 A). This differential expression pattern of β5 and Lmp7 proteasome subtypes was validated at the protein level by Western blot (Figure 2 B). Additionally, Western blot analysis showed that podocytes exhibited elevated levels of the 19S cap protein Rpt5, whereas the alternative immunoproteasome cap protein Pa28α was predominantly found in endothelial cells (Figure 2 B). In contrast to podocytes and glomerular endothelial cells strongly expressing UPS players, mesangial cells, mainly expressed the lysosomal associated proteins Lamp2 and Limp2 (Figure 2 B). Of note, glomerular endothelial cells again differed from mesangial cells and podocytes as they showed high levels of Lamp2 but not Limp2. Of all glomerular cell types, podocytes showed lowest expression levels of Limp2 and Lamp2.

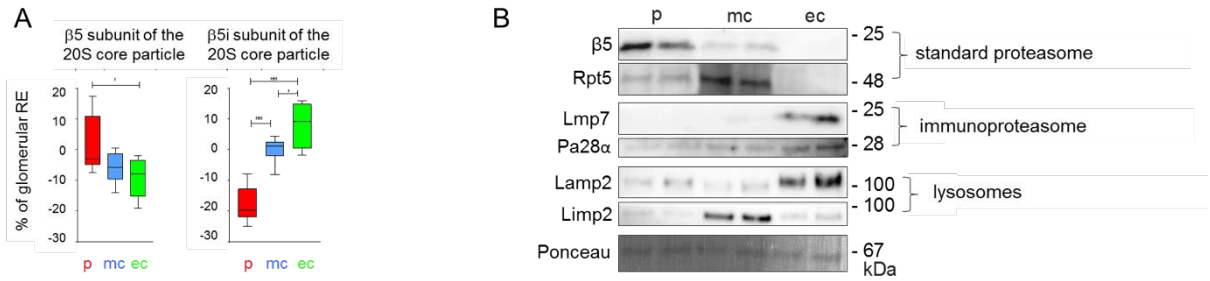

Figure 2: Podocytes preferentially express UPS players.

(A) Expression pattern of *Psmb5*, encoding for the β5 subunit of the standard proteasome, and *Psmb8*, encoding for the Lmp7 subunit of the immunoproteasome in glomerular cells quantified via qRT PCR. (B) Western blot analysis of standard proteasome subunit β5, 26S proteasome regulatory subunit 6A (Rpt5), immunoproteasome subunit β5i (Lmp7), and proteasome activator 28 subunit alpha (Pa28α) as proteasomal markers and Lamp2 and Limp2 as lysosomal markers from cell-number adapted FACS-sorted mouse podocytes (p), mesangial cells (mc) and endothelial cells (ec). Ponceau indicates equal loading. Statistical analysis (A): mean +/- SEM, $p^{*}<0.05$, $p^{**}<0.001$, $p^{***}<0.001$, Mann Whitney U-test

These results strongly suggest that under homeostatic conditions podocyte proteostasis strongly depends on the degradation of proteins through the proteasomal system and within the UPS on the standard proteasome. Glomerular endothelial cell proteostasis also depends on degradation *via* the proteasomal system but there mostly

on the immunoproteasome. While glomerular endothelial cells exhibit a specific dependence on the lysosomal system, the expression levels of UPS and ALS players strongly suggests that mesangial cell proteostasis mainly depends on the degradation through the lysosomal system.

4.1.2 Proteasomal impairment compromises the glomerular filtration barrier under homeostatic conditions

To investigate the dependence of podocyte proteostasis and therefore health on the proteasomal system, naïve Balb/c mice were treated with either vehicle, the lysosomal inhibitor leupeptin A, or the proteasomal inhibitor epoxomicin over the course of four days (Figure 3 A). To assess the general health of the mice the weight change from day one to day 4 was determined (Figure 3 B). No significant weight change between the three groups was to be observed. To assess general kidney function, blood-urea-nitrogen (BUN) levels were determined (Figure 3 C), as well as the albumin loss to the urine by measurement of the urine albumin to creatinine ratio (ACR) by ELISA (Figure 3 D). There was no significant difference between the three groups in the serum BUN levels, but an increase in albuminuria was observed in the animals treated with the proteasomal inhibitor epoxomicin after four days of treatment in comparison to vehicle treated controls and the lysosomal inhibitor leupeptin A treated mice. To asses general glomerular morphology, staining of kidney sections with periodic acid Schiff (PAS) was performed and the slices were assessed under the light microscope (Figure 3 E). Glomeruli derived from epoxomicin treated animals exhibit a slight change in morphology, especially podocytes show a decrease in structural integrity visible as cell swelling and enhanced cytoplasmic vacuolization and less defined cell borders. Animals treated with the lysosomal inhibitor leupeptin A exhibit a normal podocyte morphology. These results suggest that inhibition of the proteasomal degradation pathway but not of the lysosomal degradation pathway causes changes in podocyte morphology/integrity leading to a leakiness of the glomerular filtration barrier resulting in albuminuria. Further analysis of these mice showed, that the inhibition of the proteasomal system leads to swelling of the glomerular tufts causing relative podocytopenia as the absolute number of podocytes was not significantly changed (Figure 4 A). Western blot analysis of the known proteasomal substrate α-actinin-4

(32), a structural protein important for podocyte cytoskeletal integrity, shows a significant increase in protein levels after inhibition of the proteasomal system demonstrating successful proteasomal inhibition (Figure 5 A).

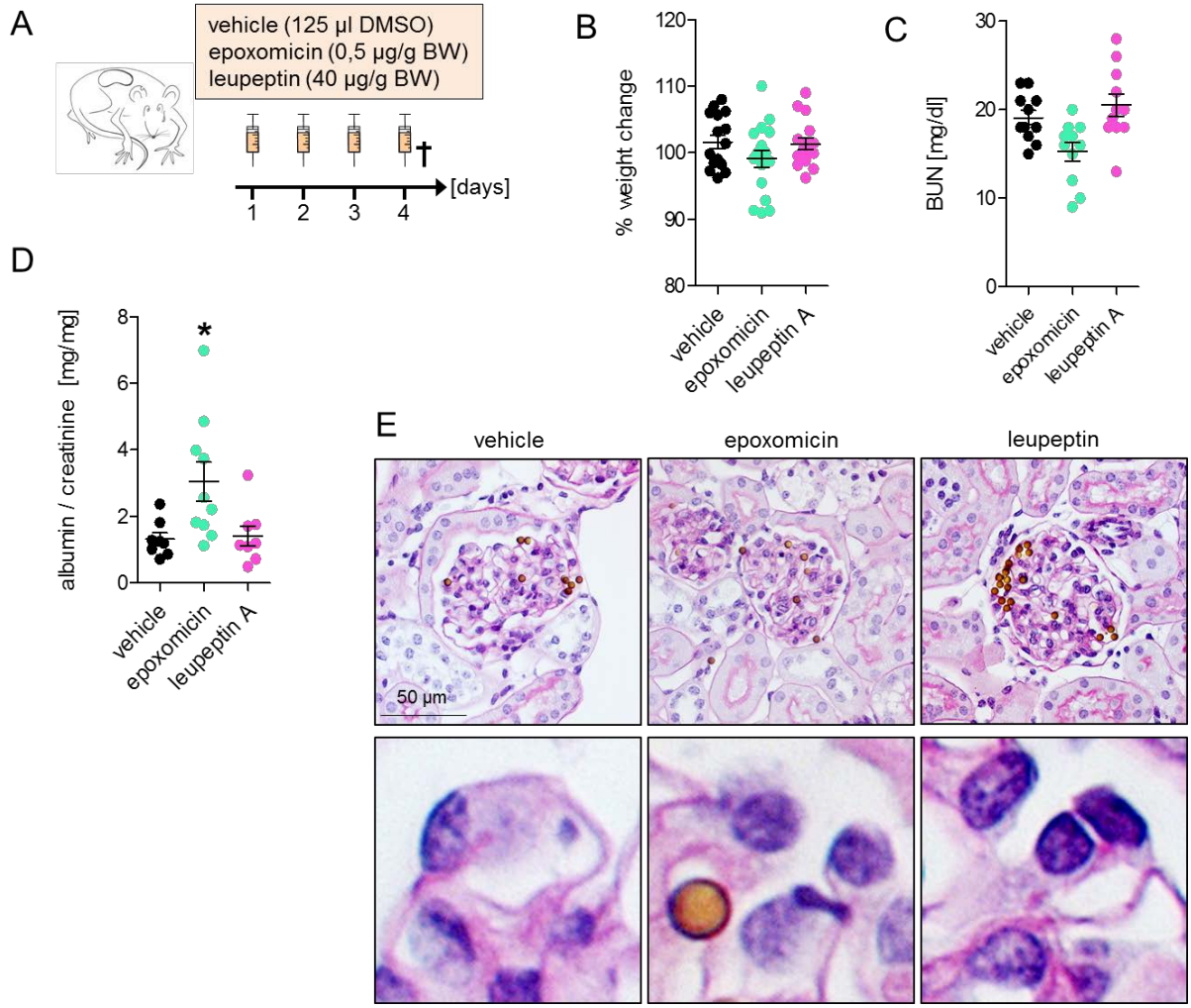

Figure 3: Global proteasome inhibition results in proteinuria.

(A) Scheme depicting the experimental setup. Renal health was assessed after treatment with either vehicle, the lysosomal inhibitor leupeptin A or the proteasomal inhibitor epoxomicin by measuring the weight change (B), serum blood-urea nitrogen (BUN) (C), and albuminuria by depicting the urinary albumin/creatinine ratio (D). (E) Representative micrographs exhibiting glomerular morphology by PAS staining after inhibitor treatment. Statistical analysis (B, C, D): mean ± SEM, *p ≤ 0.05, 1 way ANOVA with Dunn's multiple comparison test, n ≥ 11 per group.

To assess ultrastructural alterations in the inhibitor treated mice nephrin localization at the slit diaphragm (which represents a modified adherents junction that bridges the

interdigitating podocyte foot processes from neighboring podocytes) was analyzed by high-resolution microscopy (Figure 4 B).

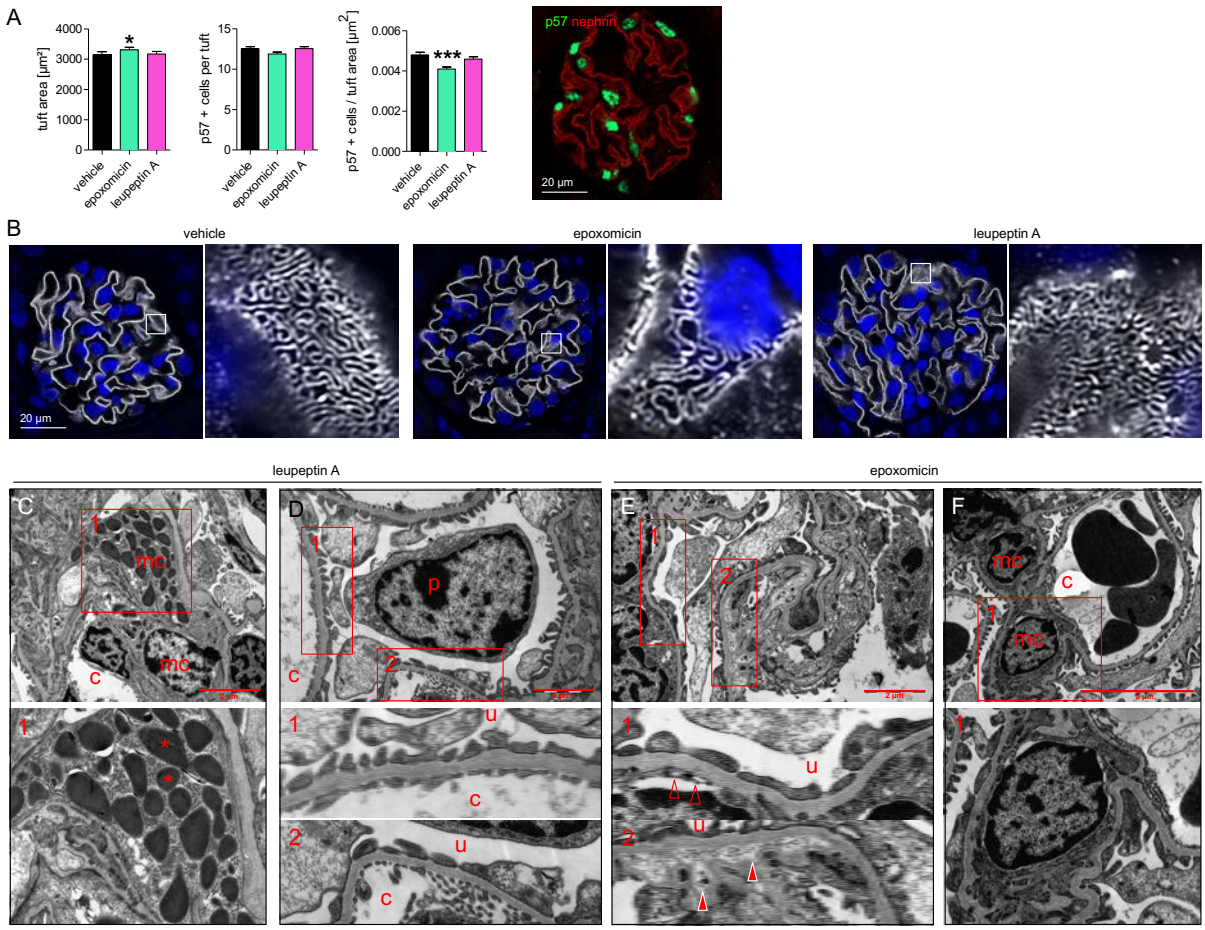

Figure 4: Proteasomal inhibition results in podocytopenia and focal ultrastructural alterations.

(A) Podocyte number and glomerular tuft area after inhibitor treatment were quantified by immunohistochemical staining of the podocyte marker p57 in kidney sections embedded in paraffin (n ≥ 16 per group), Podocyte foot process effacement and ultrastructural alterations were determined by (B) high-resolution confocal microscopy of immunofluorescent staining for the slit diaphragm protein nephrin (white) and DNA (blue, Hoechst), and by (C, D, E, F) electron microscopy. In leupeptin A treated mice mesangial cells (mc) show electron dense lysosomal storage (asterisk), podocytes (p) are normal, podocyte foot processes and endothelial fenestrations are normal. Mice treated with epoxomicin exhibit focal podocyte foot process effacement and broadened endothelial fenestrations (lucid arrows) as well as focal splitting of the glomerular basement membrane with accumulation of electron dense material (solid arrows). c = capillary, u = urine. Statistical analysis (A, B): mean ± SEM, *$p \leq 0.05$, ***$p < 0.0001$, 1 way ANOVA with Dunn's multiple comparison test.

Epoxomicin treated mice show broadening of the empty spaces between the meandering nephrin signal demonstrating podocyte foot process effacement in comparison to vehicle treated mice. The nephrin pattern of leupeptin A treated mice is normal. Ultrastructural analysis by electron microscopy showed that animals treated with the lysosomal inhibitor leupeptin A exhibit enlarged lysosomes with electron dense storage material in mesangial cells (Figure 4 C) while podocyte and podocyte foot processes and endothelial fenestrations appear normal (Figure 4 D). Mice treated with the proteasomal inhibitor epoxomicin on the other hand exhibit focal podocyte foot process effacement and loss of endothelial fenestrations (Figure 4 E 1), as well as focal splitting of the glomerular basement membrane with accumulation of electron dense material (Figure 4 E 2). Mesangial cells appear to be normal (Figure 4 F).

4.1.3 Crosstalk of degradative systems

To assess the extent of intracellular protein accumulations as well as to detect a possible compensatory regulation of the non-inhibited degradative system, Western blots detecting UPS (Figure 5 A, B) and ALS (Figure 6 B) associated proteins were performed as well as high-resolution confocal microscopy (Figure 5 C, Figure 6 A). Western blot analysis of the proteasomal substrate lysin-48 polyubiquitinated (K48pUb) proteins showed a significantly higher level of K48pUb proteins after proteasomal inhibition compared to vehicle treated controls, while the K48pUb levels of leupeptin A treated mice remained unchanged (Figure 5 B). This result was mirrored in the high-resolution immunofluorescence images of polyubiquitinated proteins, which accumulated in the podocyte cytoplasm of epoxomicin treated mice. Glomerular endothelial cells and mesangial cells did not show an accumulation of polyubiquitinated proteins by immunofluorescence (Figure 5 C). The glomerular protein levels of the main proteolytic subunit of the immunoproteasome (Lmp7) were unchanged in epoxomicin and in leupeptin A treated mice in comparison to vehicle treated controls (Figure 5 B). However, epoxomicin treated glomeruli exhibited a double band for Lmp7, the upper band relating to epoxomicin covalently bound to Lmp7 and the lower band relating to unbound Lmp7. In summary these results demonstrate a successful proteasomal inhibition in glomeruli of epoxomicin treated mice and no substantial compensatory induction of the proteasomal system in glomeruli of leupeptin A treated mice.

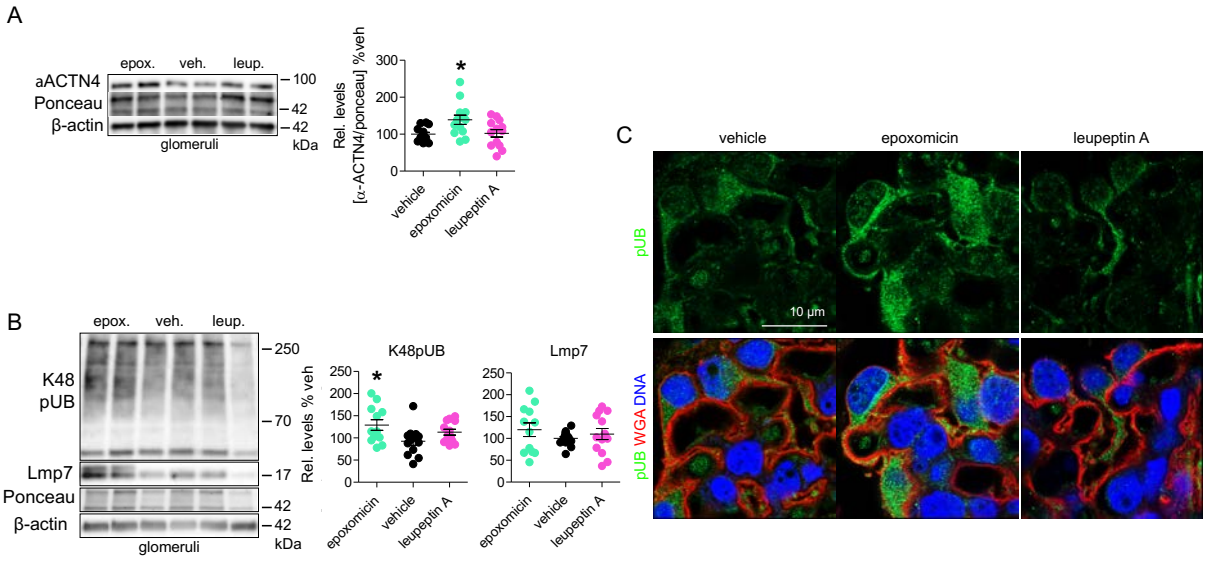

Figure 5: Proteasomal inhibition leads to intracellular protein accumulation.

(A) Levels of the structural podocyte foot process protein α-actinin 4 (αACTN4) after inhibitor treatment (vehicle = veh.; epoxomicin = epox.; leupeptin A = leup.) were determined by Western Blot analysis from isolated glomeruli. Graph exhibits densitometric quantification (n ≥ 8 per group). Western blot analysis of lysin 48 polyubiquitinated (K48pUb) proteins and the immunoproteasome subunit Lmp7 (B) and representative high-resolution confocal images of immunofluorescent stainings for ubiquitinated proteins (C) demonstrate covalent binding of epoxomicin to LMP7 and glomerular accumulation of K48pUB proteins in mice with proteasomal inhibition, especially in podocytes. Statistical analysis (A, B): mean ± SEM, *p ≤ 0.05, **p < 0.01, 1 way ANOVA with Bonferroni's multiple comparison test, n ≥ 8 per group.

We next evaluated, whether the lysosomal inhibition was successful in leupeptin A treated mice and whether the lysosomal system was induced in glomeruli of epoxomicin treated mice to compensate for proteasomal inhibition. High-resolution microscopic localization of the lysosomal integral membrane protein-2 (Limp2) showed an increase of Limp2 positive lysosomes in leupeptin A treated mice but also in epoxomicin treated mice compared to vehicle treated controls (Figure 6 A). Interestingly, Limp2 positive lysosomes were predominantly increased in size and amount in mesangial and glomerular endothelial cells and not in podocytes of inhibitor treated mice. Western blot analysis of Limp2 corroborated the immunofluorescent observations and exhibited significantly increased levels of Limp2 in epoxomicin treated mice and elevated Limp2 levels in glomeruli of leupeptin A treated mice. To

assess whether we had obtained lysosomal impairment in leupeptin A treated mice, we quantified glomerular levels of the autophagosome cargo protein, ubiquitin-binding protein p62 which should accumulate in the setting of lysosomal impairment. Indeed, Western blot analyses for p62 showed increased protein levels in glomeruli derived from leupeptin A treated mice in comparison to glomeruli derived from vehicle or epoxomicin treated mice. We next determined levels of the lysosomal enzyme cathepsin D to evaluate, whether we could detect a compensatory upregulation in glomeruli of leupeptin A treated mice as a sign of successful lysosomal inhibition. Indeed, Western blot analyses show significant higher cathepsin D protein levels in glomeruli derived from leupeptin A treated mice than in glomeruli derived from vehicle treated controls (Figure 6 B). Of note, also glomeruli from epoxomicin treated mice exhibited significantly higher levels of cathepsin D in glomeruli compared to vehicle treated controls (Figure 6 B).

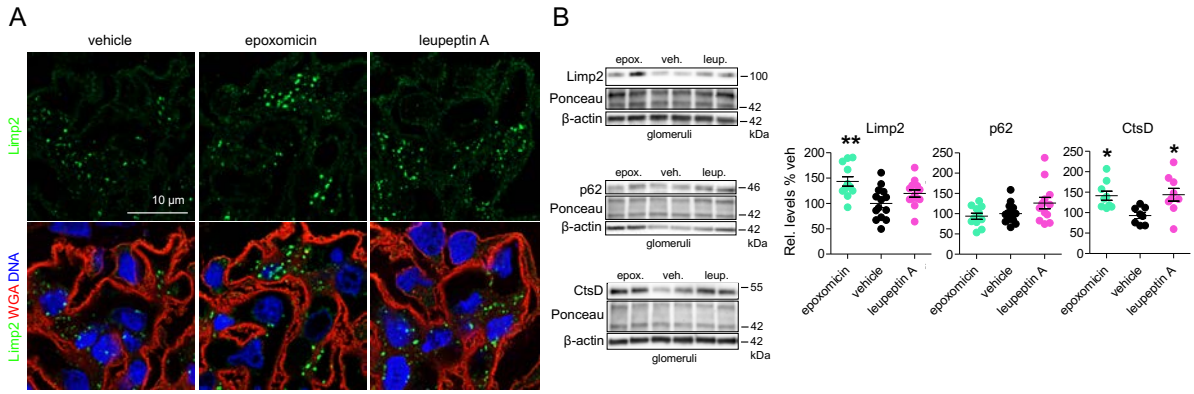

Figure 6: Proteasomal inhibition results in intracellular protein accumulations, which are not prevented by upregulation of the lysosomal system.

(A) Representative high-resolution confocal images of immunofluorescent stainings for the lysosomal integral membrane protein (limp) 2, (B) and Western blot analysis of Limp2, the autophagy associated protein p62 and the lysosomal enzyme Cathepsin D demonstrate a compensatory upregulation of the lysosomal system in epoxomicin treated mice, especially in endothelial and mesangial cells, and a compensatory induction of Cathepsin D in epoxomicin and leupeptin A treated glomeruli. The increased levels of p62 in leupeptin A treated mice reflect the defect in lysosomal degradation in leupeptin A treated glomeruli. For immunofluorescence, the target proteins are depicted in green, wheat germ agglutinin (WGA) in red was used to visualize general morphology by binding to N-acetyl-glucosamine and sialic acid and DNA is depicted in blue using Hoechst. Graphs exhibit the densitometric analysis of the Western blots. Statistical analysis: mean ± SEM, *$p \leq 0.05$, **$p < 0.01$, 1 way ANOVA with Bonferroni's multiple comparison test, $n \geq 8$ per group.

These results suggest that if the proteasomal degradation system is impaired in glomeruli the lysosomal degradation system is compensatory upregulated. Surprisingly, this compensatory upregulation does not appear to be sufficient to remove the accumulated polyubiquitinated proteins in glomeruli derived from epoxomicin treated mice, most likely because compensatory upregulation occurs mainly in endothelial and mesangial cells and not in podocytes as seen by immunofluorescence.

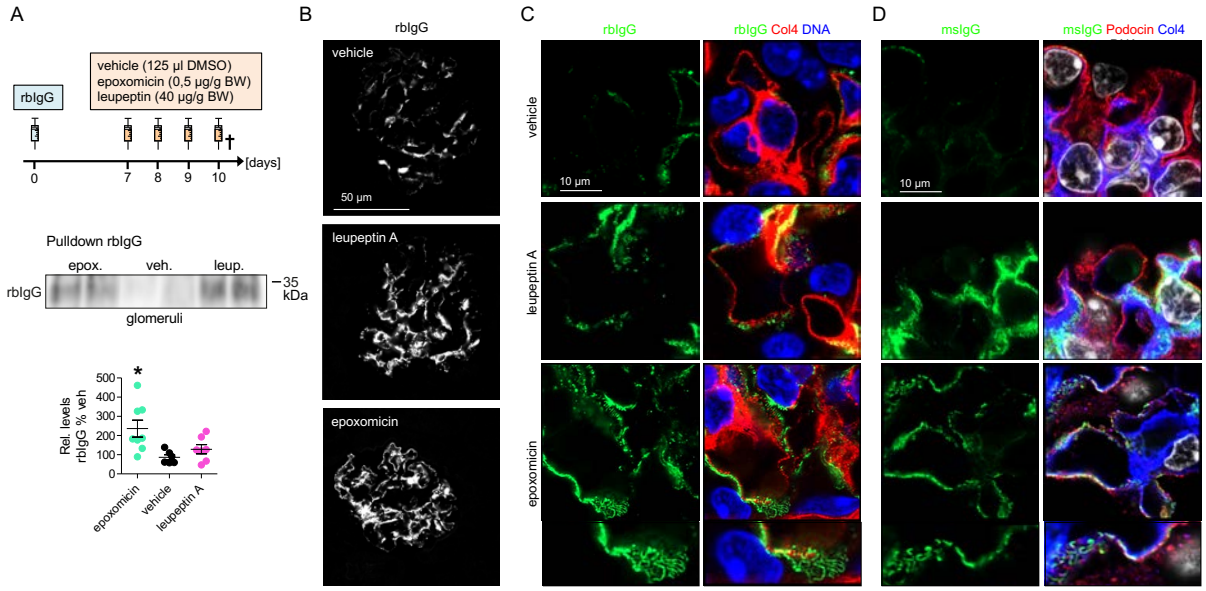

Figure 7: Proteasomal inhibition results in glomerular IgG accumulation in the subepithelial space.

(A) Scheme depicting the experimental setup and Western blot analysis of rbIgG pulled from isolated glomeruli after initial injection with rbIgG followed by the treatment with proteasomal or lysosomal inhibitor depicting rbIgG accumulation in glomeruli following proteasomal inhibition and lysosomal inhibition. (B) Representative confocal micrographs of immunofluorescence staining for rbIgG (white) in a mouse glomerulus. (C, D) High-resolution confocal micrographs depicting rbIgG (C) or msIgG (D) accumulation at the glomerular filtration barrier in the subepithelial space following proteasomal inhibition. RbIgG and msIgG are depicted in green, collagen type 4 as a structural protein of the glomerular basement membrane in red (C) or blue (D) and DNA using Hoechst in blue (C) or white (D). In (D) podocin in red is additionally used to demarcate podocyte foot processes. Statistical analysis (A): mean ± SEM, *p ≤ 0.05, 1-way ANOVA with Bonferroni's multiple comparison test, n ≥ 6 per group.

We observed glomerular tuft swelling and intracellular polyubiquitin accumulation in glomeruli of epoxomicin treated mice. In order to investigate whether extracellular protein accumulation, such as IgG deposition, a hallmark of membranous nephropathy,

contributed to the glomerular tuft swelling we assessed if foreign IgG could be removed from glomeruli and which degradation system is involved in this removal. For these investigations naïve Balb/c mice were injected with rbIgG, seven days later the mice were treated with either vehicle, epoxomicin or leupeptin A for four days (Figure 7 A). To assess the glomerular accumulation of rbIgG, glomeruli were perfused with PBS to remove the circulating rbIgG. Deposited rbIgG was pulled from number-adapted glomeruli and quantified *via* Western blot. Mice treated with epoxomicin exhibit significantly higher levels of rbIgG derived from glomeruli in comparison to vehicle treated controls. The levels of rbIgG in glomeruli derived from leupeptin A treated mice were increased to a lesser degree in comparison to glomeruli derived from vehicle treated mice (Figure 7 A). To assess the localization of accumulating rbIgG, high-resolution confocal immunofluorescence images were analyzed (Figure 7 B, C). In vehicle treated controls small amounts of rbIgG deposits could be detected within the glomerular mesangial space (Figure 7 B, C), while the inhibitor treated mice exhibited massive glomerular rbIgG accumulation. Interestingly, the accumulation pattern of rbIgG in glomeruli from epoxomicin and leupeptin A treated mice differed from each other. RbIgG in glomeruli derived from leupeptin A treated mice foremost accumulated in the mesangium, whereas rbIgG in glomeruli derived from epoxomicin treated mice additionally accumulated along the glomerular filtration barrier. (Figure 7 B). High-resolution confocal microscopy showed that in glomeruli of epoxomicin treated mice rbIgG deposited within the subepithelial space of the glomerular filtration barrier with an accentuated deposition in areas of the slit diaphragm (Figure 7 C).

The same inhibitor-dependent deposition pattern could be observed for inherent msIgG, where msIgG accumulated in the mesangium after leupeptin A treatment and accumulated along in the subepithelial space of the glomerular filtration barrier with accentuation at the slit diaphragm after epoxomicin treatment (Figure 7 D). These results emphasized our earlier findings that the glomerular cells differentially depend on the degradation systems, that glomerular protein accumulation partly depends on the degradation systems and that a compensatory upregulation of the lysosomal degradation system occurs in the setting of proteasomal inhibition. Interestingly, this lysosomal upregulation was not enough to actually compensate impairment of the UPS

under homeostatic conditions, as protein accumulations occurred and proteinuria was not prevented.

4.2 Balancing glomerular proteostasis in lysosomal dysfunction

4.2.1 Glomerular cells of ML II and ML III mice exhibit lysosomal dysfunction

Mucolipidosis (ML) is a rare lysosomal storage disorder, which is classified according to different mutations and disease severities.

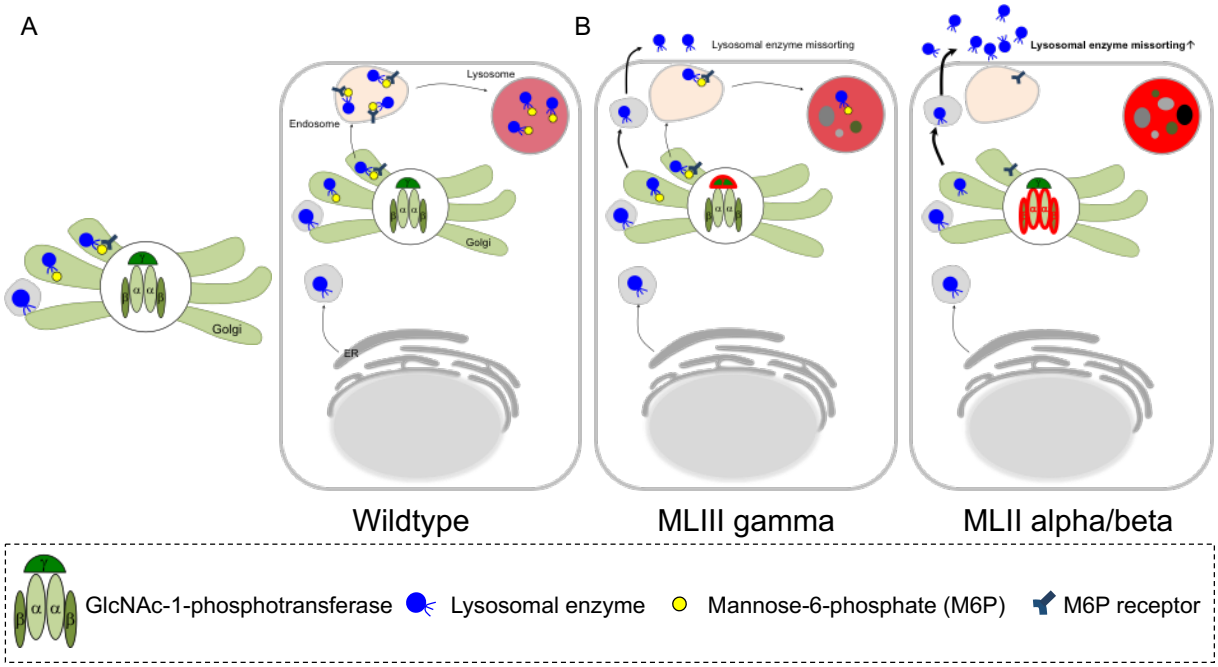

Figure 8: Schematic depiction of the alterations of the N-acetylglucosamine-1-phosphotransferase in Mucolipidosis.

(A) The N-acetylglucosamine (GlcNAc)-1-phosphotransferase is made up of two α subunits, two β subunits and one γ subunit and is located within the golgi apparatus. This phosphotransferase catalyzes the glycosylation of lysosomal enzymes with mannose-6-phosphate (M6P) residues. Enzymes tagged with M6P are transported to the lysosomes. (B) Mucolipidosis III γ (MLIII) is caused by a mutation of the γ subunit of the GlcNAc-1-phosphotransferase, which leads to less M6P glycosylated lysosomal enzymes. The enzymes without M6P glycosylation are miss sorted to the extracellular space and don't reach the lysosomes. (C) Mucolipidosis II α/β is caused by a mutation of the α and β subunit causing no enzymes to be glycosylated with M6P leading to a miss sorting of nearly all lysosomal enzymes.

To study the impact of lysosomal dysfunction on glomerular cell proteostasis, mouse models for ML type II and III were analyzed. MLIII gamma is caused by mutations in the *Gnptg* gene, affecting the gamma subunit of the GlcNAc-1 phosphotransferase, which leads to a residual GlcNac-1 phosphotransferase activity and causes the less severe MLIII gamma disease as only a subset of lysosomal enzymes is missorted to the extracellular space (Figure 8 B). MLII alpha/beta is caused by mutations in the *Gnptab* gene, the alpha and beta subunits of the GlcNac-1 phosphotransferase, leading to inactive GlcNac-1 phosphotransferase activity causing the severe ML II disease due to missorting of most of the lysosomal enzymes to the extracellular space (Figure 8 B).

First, we evaluated whether the glomerular cell types in MLII and MLIII mice exhibited lysosomal dysfunction (Figure 9). To evaluate lysosomal activity the activity of the lysosomal enzyme β-hexosaminidase was measured in glomeruli. In MLIII glomeruli the β-hexosaminidase activity was significantly reduced by about 25% and in MLII glomeruli it was also significantly reduced but by about 45% (Figure 9 A) demonstrating decreased β-hexosaminidase activity due to missorting of the enzyme. It is known that in lysosomal storage disorders the accumulation of nondegraded products in lysosomes leads to an increase in lysosomal size and number. Western blot analysis of lysosomal and autophagosomal markers in glomeruli derived from MLII (Figure 9 B) and MLIII (Figure 9 C) mice showed elevated amounts of these proteins. The strongest increase was noted in the levels of the lysosomal integral membrane protein 2 (Limp2) in MLII and MLIII glomeruli. Levels of the lysosomal associated membrane protein 2 (Lamp2) and the microtubule-associated proteins 1 A/1 B light chain 3 B (LC3) were less notably elevated. Not only did the total amount of LC3 increase in MLII and MLIII glomeruli but also the ratio of the lipidated autophagosomal membrane bound LC3-II form to the cytoplasmic LC3-I form, which is an indicator of enhanced autophagosome formation. High-resolution confocal images of kidney slices derived from wildtype, MLII and MLIII mice exhibited an increase of large Limp2 positive vesicles in glomerular cells in MLII and MLIII mice, which was in accordance with the Western blot results. Interestingly, Limp2 positive vesicles were most prominently increased and enlarged in mesangial cells and endothelial cells, in comparison to podocytes.

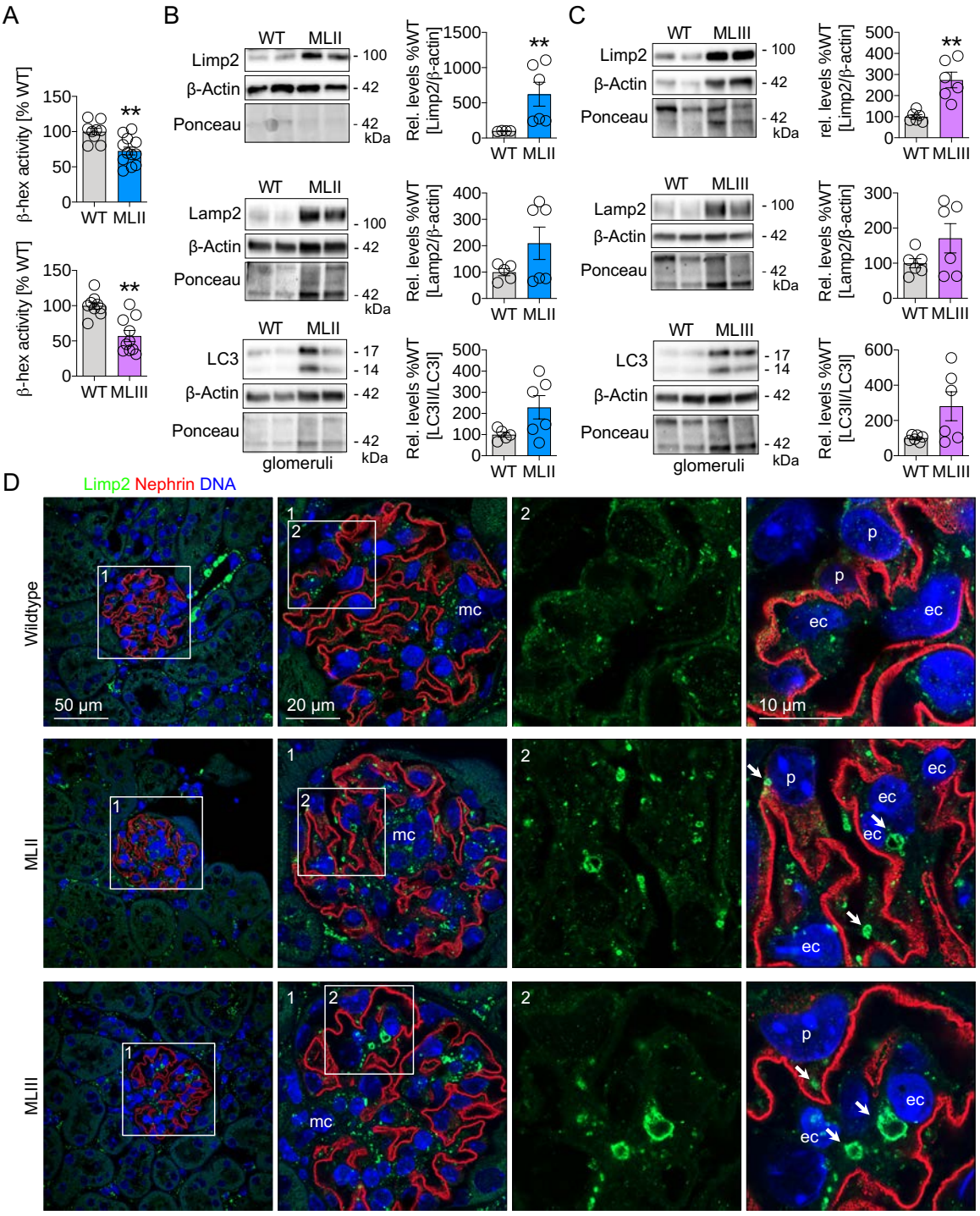

Figure 9: Upregulation of lysosomal proteins and enlarged lysosomes in glomeruli of MLII and MLIII mice.

(A) Lysosomal β-hexosaminidase activity was measured in isolated glomeruli (nmol/mg/h) from MLII and MLIII mice compared to littermate controls. Western blot analysis of lysosomal (Limp2, Lamp2) and autophagosomal proteins (LC3) in isolated glomeruli from MLII (B) and MLIII (C) compared to littermate controls. (D) Representative high-resolution confocal immunofluorescence images of Limp2 (green), nephrin (red) to visualize the podocyte slit membrane and DNA (blue) using Hoechst in kidney sections derived from MLII, MLIII and control littermates. Statistical analysis: mean ± SEM, **p ≤ 0.01, Mann Whitney U test, n ≥ 6 per group.

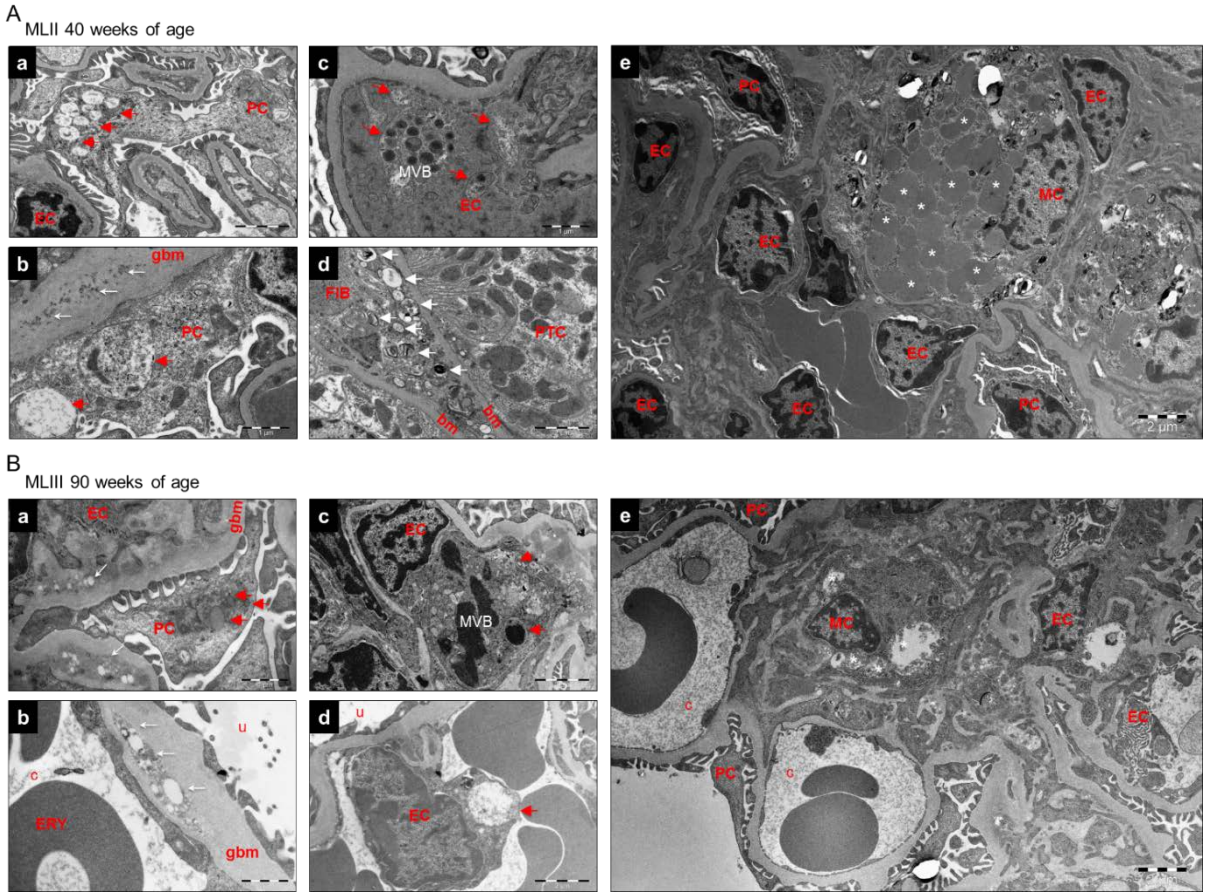

Figure 10: Glomerular cells and the glomerular basement membrane show lysosomal storage accumulations in MLII and MLIII mice.

Electron microscopic evaluation of MLII (A) and MLIII (B) mice show lysosomal enlargement with storage material (red arrows) of varying electron density depending on the glomerular cell type. Podocytes (PC), and parietal epithelial cells (PEC) contain electron-lucent storage vesicles (A, a, b; B, a); endothelial cells (A, c; B, c, d) display electron lucent storage material in lysosomes and prominent multivesicular bodies (MVB) full of lysosomes with electron dense storage material; mesangial cells (A, e; B, e) exhibit lysosomes filled with electron dense storage material (white asterisk) in MLII (A, e) and with less dense storage material in MLIII (B, e). White arrows point towards irregularities, splitting, electron-dense and vacuolar accumulations within the glomerular basement membrane (B, b; gbm) and the Bowman's capsule (A, b; B). FIB = tubulointerstitial fibroblast with prominent lysosomal accumulations (white arrows), bm = basement membrane, PTC = proximal tubular cell. MC = mesangial cell, ERY = erythrocyte. Endothelial fenestrations and podocyte foot processes are mostly intact.

Further, ultra-structural analyses of MLII (Figure 10 A) and MLIII (Figure 10 B) glomeruli were performed in comparison to wildtype littermates to assess lysosomal storage accumulations in renal cells, especially in glomeruli. Thereby, podocytes and endothelial cells showed accumulation of lysosomes with electron lucent material,

whereas mesangial cells showed accumulation of lysosomes with electron dense material in both MLII and MLIII models. Endothelial cells further contained multivesicular bodies filled with lysosomes, which could relate to the large Limp2 positive vesicles detected *via* high-resolution confocal microscopy. Podocyte foot processes and endothelial fenestrations were mostly intact in MLII and MLIII mice. The GBM exhibits focal irregularities and splitting in both MLII and MLIII mice with accumulation of electron-dense and vesicular material within the GBM. Together these results suggest that MLII and MLIII mice exhibit lysosomal dysfunction in glomerular cells.

4.2.2 Renal and glomerular function is intact in ML II and ML III mice

After determination that lysosomal function was impaired in glomerular cells, we wanted to assess the renal and glomerular function of MLII and MLIII mice. Since the glomerular cells of MLII and MLIII mice showed similar extents of lysosomal dysfunction we evaluated if we could determine alterations in renal/glomerular function in MLII (Figure 11) and MLIII (Figure 12) mice with an advanced general (skeletal and neurodegenerative) phenotype in comparison to wildtype littermate controls. To assess renal function serum creatinine and BUN were measured, MLII (Figure 11 A) mice exhibited elevated BUN levels whereas MLIII (Figure 12 A) mice showed no difference to wildtype littermate controls. Serum electrolytes (calcium, sodium, potassium, chloride) were normal in MLIII mice (Figure 12 A), whereas the potassium levels were elevated in MLII mice (Figure 11 A). Serum markers of nephrotic syndrome (cholesterol, triglycerides, albumin) were normal in MLIII mice (Figure 12 A), whereas MLII mice exhibited decreased serum albumin levels with normal serum lipids (Figure 11 A). The mostly normal serum parameters were emphasized by the inconspicuous glomerular, tubular and tubulointerstitial morphology in MLII and MLIII kidneys. Thereby, PAS staining of MLII (Figure 11 B) and MLIII (Figure 12 B) kidney sections compared to wildtype littermate controls exhibited normal glomerular and tubulointerstitial morphology. Further, staining for specific kidney injury markers, such as kidney injury molecule 1 (Kim1, a sensitive marker for tubular injury), smooth muscle actin (SMA, a marker for renal fibrosis), and cleaved caspase 3 (a marker for apoptotic cells) did not reveal any renal injury confocal microscopy in MLII (Figure 11 B) or MLIII (Figure 12 B) mice, that could have been missed in the PAS staining.

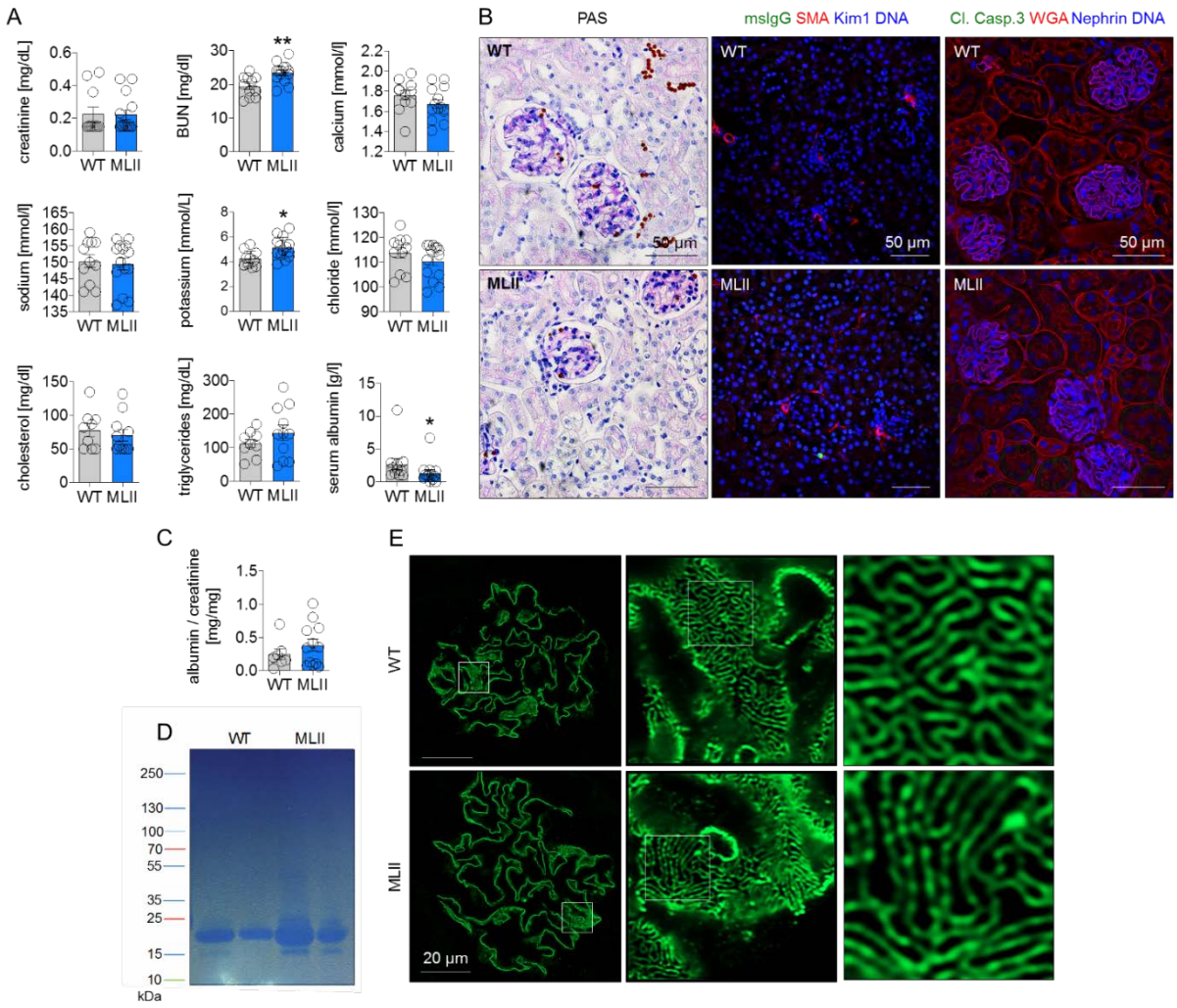

Figure 11: Glomerular filtration barrier of MLII mice is mostly normal.

(A) Serum parameters of MLII mice to determine kidney function. Serum BUN and potassium are increased in MLII mice compared to littermate controls, while serum albumin is decreased. (B) PAS staining show no structural changes in kidney morphology in MLII mice compared to littermate controls. Representative confocal immunofluorescence images of the kidney injury molecule-1 (Kim1, blue), a marker for acute renal tubular injury, shows no upregulation in MLII mice. There is no accumulation of msIgG (green). Smooth muscle actin (SMA), a marker for fibrosis shows no tubulointerstitial fibrosis. There is no induction of apoptosis visualized by cleaved caspase-3 (green), WGA visualizes membrane structures (red) and the glomerular slit membrane is visualized by nephrin staining (blue). DNA is visualized in blue using Hoechst. (C) Quantification of proteinuria by urinary albumin to creatinine ratio by ELISA in 30-40 weeks old MLII mice compared to littermate controls. (D) Representative coomassie blue staining of creatinine-adapted urine from MLII mice and littermate controls. (E) High-resolution confocal microscopy demonstrates normal localization of the slit membrane protein nephrin in MLII mice and wildtype littermate controls. The even meandering pattern of nephrin demonstrates normal podocyte foot processes. Statistical analysis: mean ± SEM, *p ≤ 0.05, **p ≤ 0.01, Mann Whitney U test, n ≥ 6 per group.

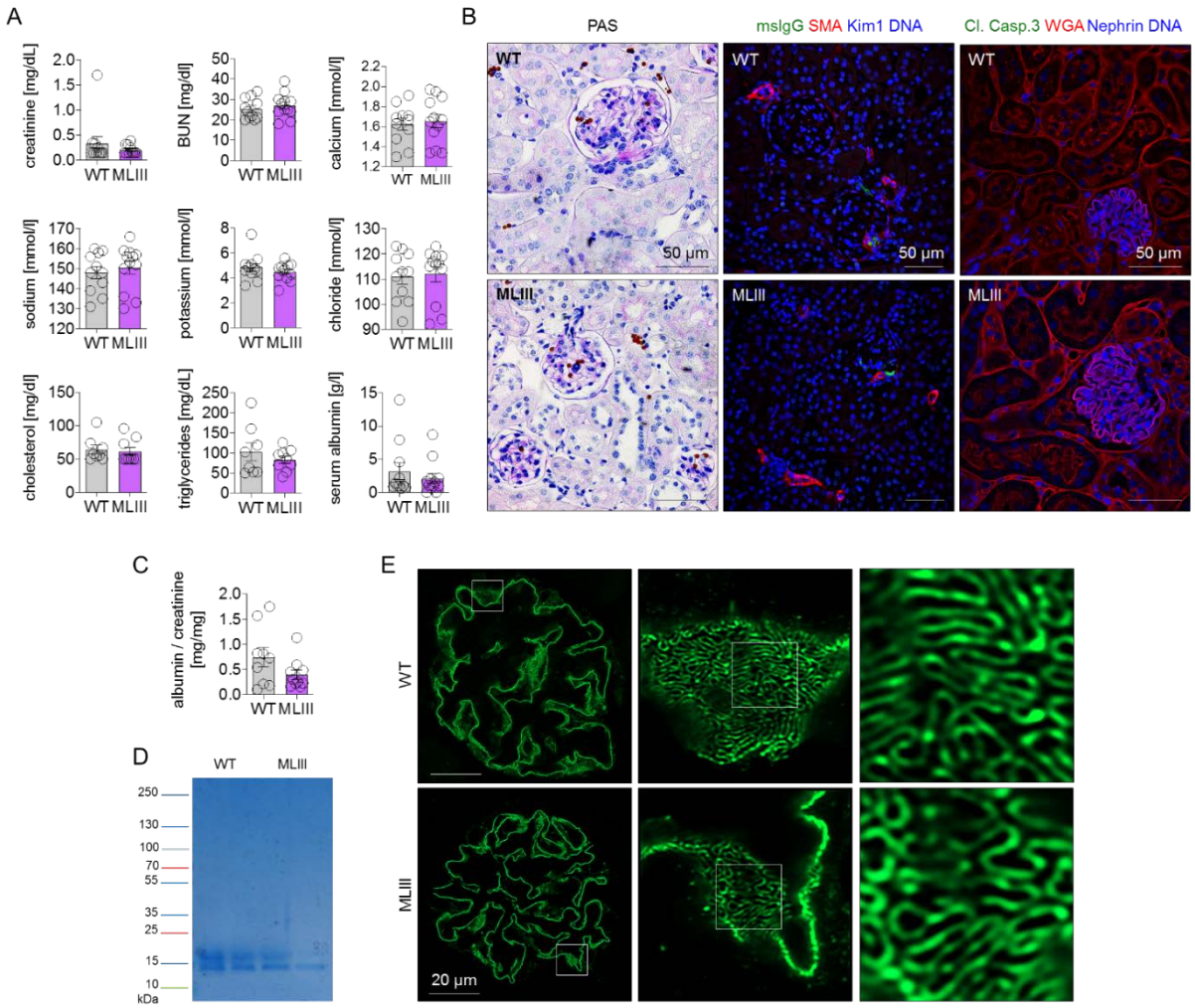

Figure 12: Glomerular filtration barrier of MLIII mice is normal.

(A) Serum parameters of MLIII mice to determine kidney function. Serum parameters are normal in MLIII mice. (B) PAS stainings show no structural changes in kidney morphology in MLIII mice compared to littermate controls. Representative confocal immunofluorescence images of the kidney injury molecule-1 (Kim1, blue), a marker for acute renal tubular injury, shows no upregulation in MLIII mice. There is no accumulation of msIgG (green). Smooth muscle actin (SMA), a marker for fibrosis shows no tubulointerstitial fibrosis. There is no induction of apoptosis visualized by cleaved caspase-3 (green), WGA visualizes membrane structures (red) and the glomerular slit membrane is visualized by nephrin staining (blue). DNA is visualized in blue using Hoechst. (C) Quantification of proteinuria by urinary albumin to creatinine ratio by ELISA in 60 - 90 weeks old MLIII mice compared to littermate controls. (D) Representative coomassie blue staining of creatinine-adapted urine from MLIII mice and littermate controls. (E) Localization of the slit membrane protein Nephrin in MLIII mice and wildtype littermate controls visualized by high-resolution confocal microscopy. The even meandering pattern demonstrates normal podocyte foot processes. Statistical analysis: mean ± SEM, *p ≤ 0.05, Mann Whitney U test, n ≥ 6 per group.

Next, the urine albumin/creatinine ratio of MLII (Figure 11 C) and MLIII (Figure 12 C) mice was measured in comparison to wildtype littermate controls to determine if the

glomerular filtration barrier was permeable to protein. No enhanced glomerular permeability to albumin was seen. In order to assess the presence of enhanced permeability to low and high molecular weight proteins, the urine was further analyzed by creatinine adapted Coomassie staining in MLII (Figure 11 D) and MLIII (Figure 12 D) mice which could indicate glomerular and proximal tubular damage. The results were normal and did not indicate glomerular or proximal tubular changes in MLII or MLIII mice. High-resolution microscopic analysis of nephrin localization did not show any podocyte foot process effacement in MLII (Figure 11 E) or MLIII (Figure 12 E) mice. Taken together these results suggest that the glomerular function of MLII and MLIII mice was not altered despite lysosomal dysfunction and that the observed elevated BUN and decreased serum albumin levels in MLII mice were not of renal but most likely of hepatic origin.

4.2.3 Mucolipidosis type II but not type III patients exhibit microalbuminuria

Since MLII and MLIII mice exhibited normal renal/glomerular function we analyzed patient urine to determine possible alterations in the glomerular filtration barrier of MLII, MLIII alpha/beta and MLIII gamma patients in comparison to healthy controls. To this end, albuminuria and coomassie staining of creatinine-adapted urine were analyzed (Figure 13). The Coomassie staining of creatinine-adapted urine showed low levels of albumin loss in MLII patients, whereas the urine of MLIII alpha/beta and MLIII gamma did not show any loss of high or low molecular weight proteins (Figure 13 A). The quantification of absolute urinary albumin content in MLIII and MLII patients did not reveal significant albuminuria (Figure 13 B). However, calculating the albumin/creatinine ratio from these urines revealed the occurrence of microalbuminuria in MLII patients (Figure 13 C). Taken together these results suggest that glomerular cells are capable to compensate for severe lysosomal dysfunction in both mice and humans and are able to maintain glomerular function.

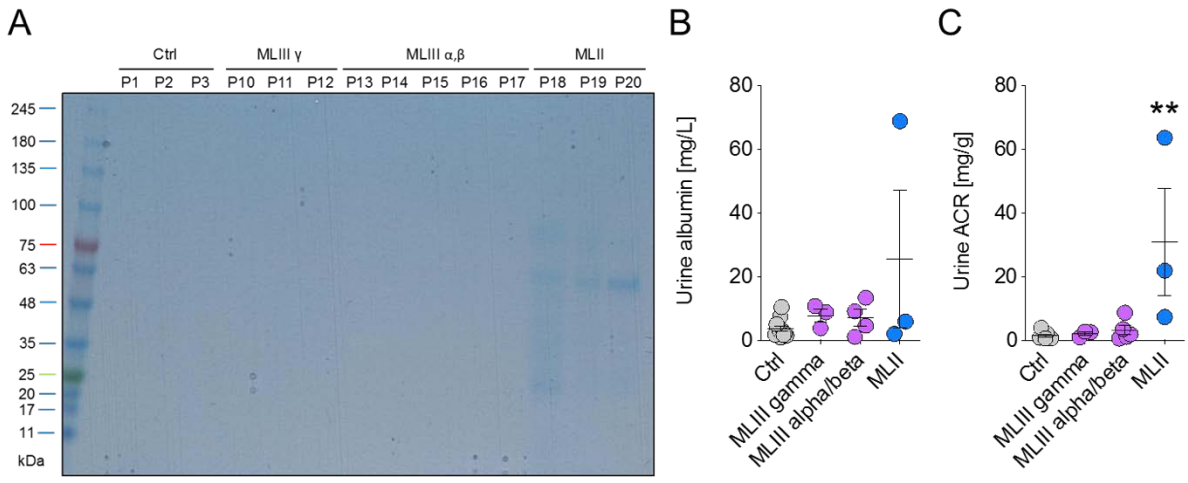

Figure 13: MLII patients exhibit microalbuminuria.

(A) Coomassie blue staining of patient urine adapted to creatinine to visualize low and high molecular weight proteinuria of a healthy control group, MLIIIγ, MLIIIα/β and MLII patients. (B) Urinary albumin content (mg/L) quantified by a human albumin ELISA. (C) The albumin creatinine ratio (ACR, mg/g) was determined by normalizing the urinary albumin content to the respective creatinine ratio. Statistical analysis: mean ± SEM, **p ≤ 0.01, Mann Whitney U test, n ≥ 3 per group.

4.2.4 Lysosomal dysfunction is differentially compensated for by the UPS in ML II and ML III mice

Since severe lysosomal dysfunction in glomerular cells was not associated with major functional changes of the glomerular filtration barrier the question arose, how glomerular cells of MLII and MLIII mice compensate for the proteotoxic stress of accumulating proteins and other non-degraded material. One explanation would be a compensatory upregulation of the UPS as a different protein degradation machinery. Therefore, Western blot analysis of proteasomal players in glomeruli derived from MLII and MLIII mice were performed. The Western blots revealed a significant upregulation of the proteasomal system in MLIII glomeruli in comparison to wildtype littermate controls (Figure 14 A), whereas MLII glomeruli showed no such upregulation of the UPS (Figure 14 B), which was surprising since the general phenotype of MLII mice is more severe than of MLIII mice. Glomeruli derived from MLIII mice showed increased levels of the standard proteasome (β5 subunit) as well as the stress-induced immunoproteasome (Lmp7 subunit) (Figure 14 A).

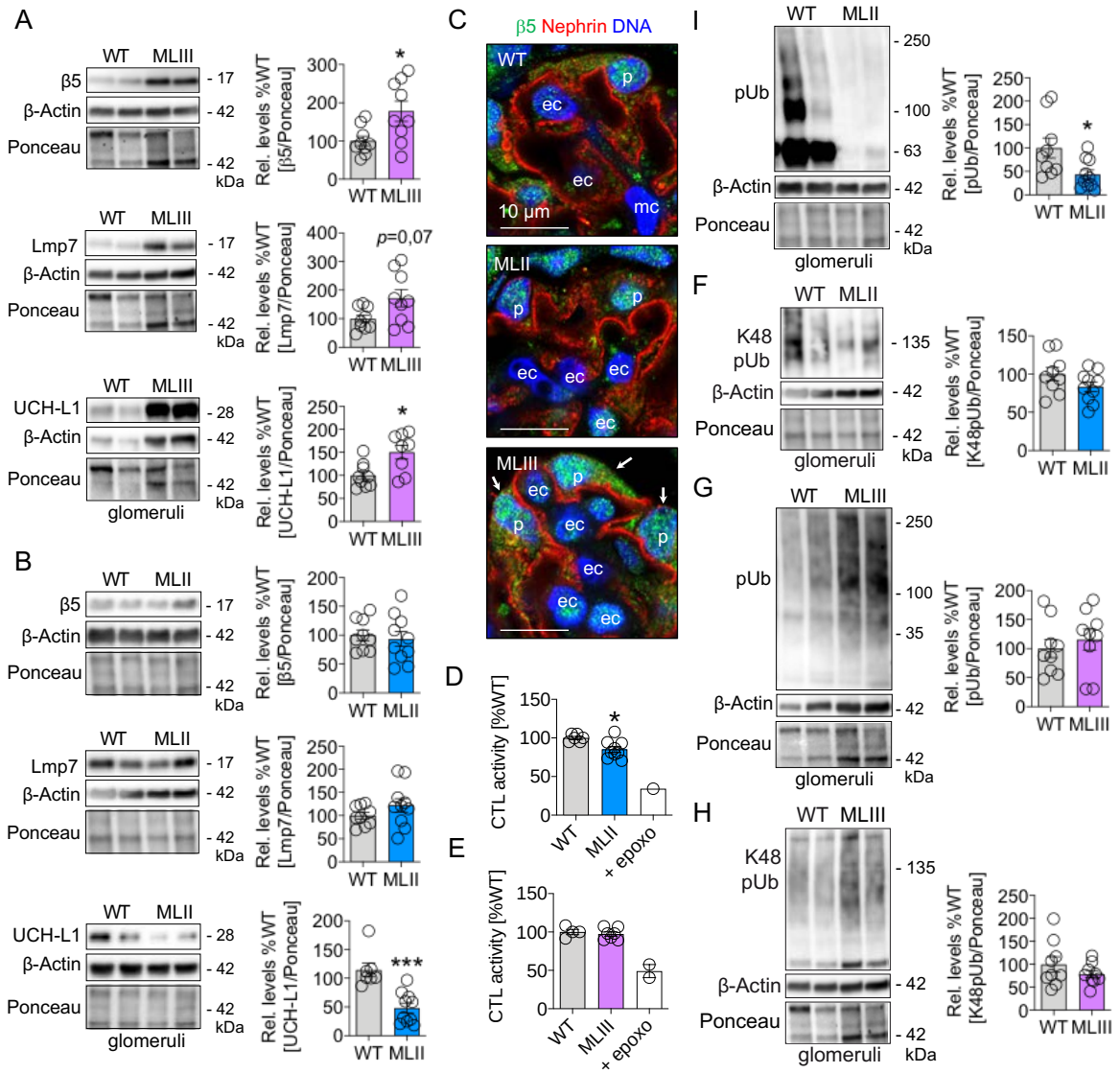

Figure 14: The proteasomal system is upregulated in glomerular cells of MLIII mice but not of MLII mice.

Western Blot analysis of isolated glomeruli from MLII (B, I, F) and MLIII (A, G, H) mice against the main proteolytic β5 subunit of the standard proteasome, the main proteolytic Lmp7 subunit of the immunoproteasome, the deubiquitinating enzyme UCH-L1, polyubiquitinated proteins and lysin 48 polyubiquitinated proteins. Determination of the main proteolytic activity of the proteasome, the chymotrypsin-like activity (CTL), in isolated glomeruli from MLII (D) and MLIII (E) mice. (C) Representative high-resolution confocal immunofluorescence images of the standard proteasome β5 subunit (green) in kidney sections from MLII, MLII and littermate control mice. Nephrin staining (red) represents the glomerular slit membrane, DNA is visualized in blue using Hoechst. Statistical analysis: mean ± SEM, *p ≤ 0.05, ***p ≤ 0.001, Mann Whitney U test, n ≥ 6 per group.

These findings were also confirmed by high-resolution confocal images of β5 staining that showed a pronounced β5 signal in MLIII podocytes but not MLII podocytes (Figure 14 C). To asses proteasomal activity, the chymotrypsin-like activity (encompasses the

proteolytic activity of the β5 and Lmp7 subunit) was measured in glomeruli derived from MLIII (Figure 14 E) and MLII (Figure 14 D) mice. The chymotrypsin-like activity in MLII mice was significantly reduced in comparison to wildtype littermate controls, whereas the chymotrypsin-like activity of MLIII mice was at the same level as the wildtype littermate controls. These results suggest that the elevated proteasome expression was sufficient to compensate for lysosomal impairment in MLIII glomeruli. We also assessed the levels of the deubiquitinating enzyme UCH-L1, which stabilizes the monoubiquitin pool and whose *de novo* expression in podocytes is an indicator for podocyte injury. UCH-L1 levels were elevated in MLIII glomeruli (Figure 14 A) but decreased in MLII glomeruli (Figure 14 B) in comparison to wildtype littermate controls. Since the proteasomal activity in MLII glomeruli was reduced and we could not show a compensatory upregulation of the proteasomal degradation system, we expected an accumulation of polyubiquitinated proteins in MLII mice. For this purpose, Western blot analysis of polyubiquitinated and K48-linked (the linkage targets for proteasomal degradation) proteins was performed.

However, both the polyubiquitin levels (Figure 14 I) and the K48-linked polyubiquitin levels were slightly reduced in MLII glomeruli (Figure 14 F) in comparison to wildtype littermate controls. On the other hand, in MLIII glomeruli the polyubiquitin levels were slightly increased (Figure 14 G) while the levels of K48-linked polyubiquitin levels remained unchanged (Figure 14 H) in comparison to wildtype littermate controls. Taken together, these results suggest that both MLII and MLIII mice do not accumulate protein up to proteotoxic levels in glomerular cells. MLIII mice upregulate the proteasomal degradation system to compensate for lysosomal dysfunction, the mechanism by which MLII mice overcome the proteostatic disbalance appears to be involve a different mechanism than a compensatory upregulation of the UPS.

4.2.5 Pathways regulating protein translation are differentially regulated in ML II and ML III mice

Since the lysosomal deficiency was not compensated for by the upregulation of the proteasomal degradation system in MLII mice, we investigated whether proteostasis (the balance of protein synthesis and protein degradation) was maintained through other mechanisms. We hypothesized that in MLII kidneys proteostasis was maintained

through a decrease of protein synthesis rather than the compensatory upregulation of the proteasomal degradation system in light of the decreased glomerular levels of polyubiquitinated proteins. The extent of protein translation is adapted to the cellular needs by two major pathways: the mammalian target of rapamycin complex 1 (mTORC1) pathway, and the integrated stress response (ISR). mTORC1 activity enhances protein translation through S6Kinase – S6 – 4E-BP1 pathway, whereas activation of the ISR results in translational repression. Central to this mechanism is the phosphorylation of eIF2α by the endoplasmic reticulum (ER) stress sensor PERK and/or by the cytoplasmic stress sensors PKR and/or GCN2, which results in the repression of general protein translation. Analysis of isolated glomeruli suggested that protein translation was repressed in MLII but not MLIII mice (Figure 15). Western blot analysis of the mTORC1 target S6 in MLII glomeruli (Figure 15 A) suggested a repression of the mTORC1 related translation activation. The nuclear translocation of the transcription factor TFEB (an inductor of lysosomal biogenesis activated in situations of decreased mTORC1 activity) in MLII and MLIII glomerular cells was in line with the decreased p-S6 expression and enhanced levels of lysosomal proteins in both mutants (Figure 15 B). Besides the repression of the mTORC1 pathway, MLII mice exhibited a strong induction of the integrated stress response in glomeruli. Transcript levels and phosphorylation of eIF2α was enhanced in MLII but not in MLIII glomeruli by qPCR (Figure 15 C), Western blot (Figure 15 D), and immunofluorescence (Figure 15 E). Phosphorylated eIF2α inhibits conventional protein biosynthesis and promotes the cap-independent translation of various stress proteins including the transcription factor ATF4. In turn, ATF4 decreases mTORC1 activity by inducing the transcription of 4E-BP1 and induces apoptosis in non-homeostatic untranslated protein response (UPR) by enhancing CHOP levels. In line, MLII glomerular cells and kidneys exhibited elevated ATF4 transcript levels and a marked nuclear translocation of ATF4 in glomerular cells of MLII mice (Figure 15 E). Interestingly, CHOP was transcriptionally elevated only in MLII glomeruli and repressed in MLII whole kidney lysate, suggesting that lysosomal dysfunction in tubulointerstitial cells of MLII kidneys does not result in pathologic UPR with cell death, explaining the absence of renal injury/apoptosis marker expression in MLII kidneys.

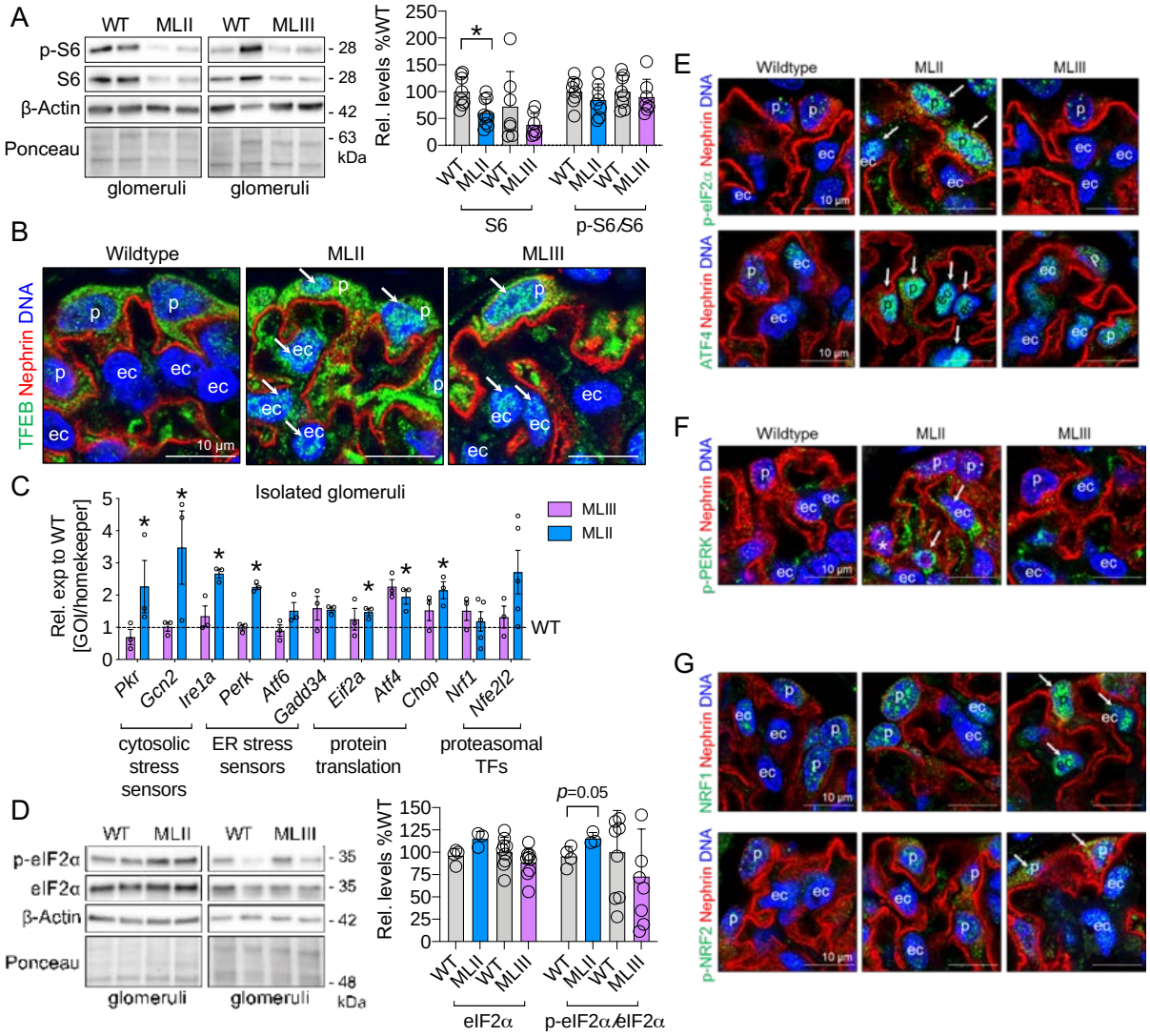

Figure 15: Glomerular cells of MLII but not MLIII mice activate the integrated stress response to alleviate proteostatic stress.

(A) Western Blots and densitometry against the mTORC1 target S6 and its phosphorylated form p-S6 in isolated glomeruli from MLII and MLIII mice in comparison to littermate controls. (B) Representative high-resolution confocal immunofluorescence images of the transcription factor TFEB, which translocates to the nucleus to initiate the transcription of lysosomal genes in the setting of decreased mTORC1 activity. White arrows indicate podocytes (p) and endothelial cells (ec) with nuclear TFEB signals. (C) Evaluation of the activation of the integrated stress response, a pathway to downregulate protein translation, by RT qPCR in MLII and MLIII glomeruli. Graph depicts the relative gene of interest (GOI) expression to the respective littermate controls (dashed line). GAPDH and 18S were utilized as homekeepers. (D) Western Blot against the eukaryotic translation initiation factor 2 alpha (eIF2α) and its activated (phosphorylated) form p-eIF2α. The graph depicts the densitometric quantification relative to littermate controls. Representative high-resolution confocal immunofluorescence images of (E) the activated p-eIF2α and its downstream target the transcription factor ATF4, (F) the activated ER stress sensor phospho-(p) PERK, and the transcription factors NRF1 and activated phospho-(p) NRF2, which induce the transcription of proteasome genes. Nephrin (red) visualizes the podocyte slit membrane and the DNA is visualized in blue using Hoechst.

White arrows indicate an enhanced signal for p-PERK in MLII endothelial cells (ec), for NRF1 and to a lesser extent for p-NRF2 in MLIII podocytes (p), of p-eIF2α in MLII podocytes and endothelial cells, and the ATF4 nuclear signal in MLII glomerular cells. Statistical analysis: mean ± SEM, *p ≤ 0.05, Mann Whitney U test, n ≥ 3 per group.

Phosphorylation of eIF2α is promoted by the eIF2α kinases and cytosolic stress receptors PKR and GCN2, whose transcript levels were enhanced in MLII glomeruli (Figure 15 C). Further, eIF2α phosphorylation is the consequence of the integrated stress response, as upon ER stress, the ER stress receptor PERK phosphorylates eIF2α. MLII glomeruli exhibited an activation of the integrated stress response at the transcriptional and protein level. The ER stress sensors IRE1α and PERK transcripts *Ire1a* and *Perk* were upregulated (Figure 15 C), and phospho-PERK expression was enhanced in glomeruli, especially in endothelial cells (Figure 15 F). Taken together, our data suggests that the integrated stress response pathway is responsible for eIF2α phosphorylation and for ATF4 induction in MLII kidneys. Based on our data, we propose that MLII glomeruli balance their proteostasis by repression of the mTORC1 pathway and by induction of the ISR. We validated this theory by assessing transcript levels and the nuclear translocation of the transcription factors Nrf1 and Nrf2 by high-resolution confocal microscopy in glomerular cells as well as their transcript levels *via* qPCR. In ML II mice Nrf2 transcript levels were elevated in comparison to wildtype littermates (Figure 15 C). Both Nrf1 and Nrf2 induce the transcription of UPS genes and were most prominently located in the nucleus of glomerular cells in MLIII and less in MLII mice (Figure 15 G). These results were in line with the strong upregulation of the proteasome system in MLIII but not MLII mice (Figure 14).

As summarized in Figure 16 our data suggests that in moderate lysosomal dysfunction glomerular cell proteostasis is mainly maintained 1) by upregulation of the UPS and 2) by suppression of mTORC1 signaling, whereas in severe lysosomal dysfunction glomerular proteostasis is mainly balanced by suppression of protein translation through 1) suppression of mTORC1 signaling and 2) through activation of the integrated stress response. UPS transcripts and proteins were downregulated as a result of the generally suppressed protein translation in MLII glomeruli.

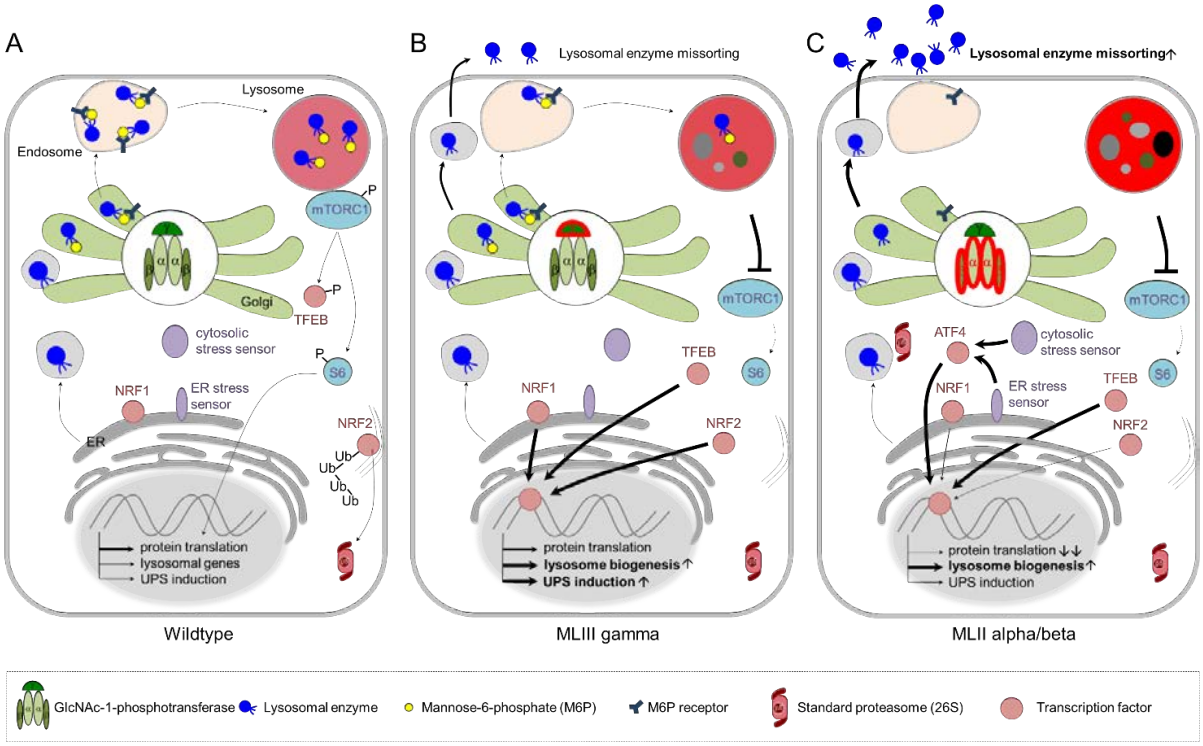

Figure 16: Proposed compensatory mechanisms activated in MLII and MLIII glomerular cells to maintain proteostasis.

(A) The Golgi-resident GlcNAc-1-phosphotransferase conjugates mannose-6-phosphate residues to lysosomal enzymes, which then results in proper sorting of lysosomal enzymes to lysosomes following binding to mannose-6-phosphate receptors. (B) In MLIIIγ glomerular cell proteostasis is maintained 1) by upregulation of the ubiquitin proteasome system (UPS) by Nrf1/Nrf2 activation and 2) by suppression of mTORC1 signaling resulting in decreased protein translation through the S6Kinase-S6 pathway. (C) In MLIIα/β glomerular cells, proteostasis is mainly maintained by suppression of protein translation by 1) suppression of mTORC1 signaling and 2) by activation of the integrated stress response by the endoplasmic reticulum (ER) stress sensors by cytosolic stress receptors. UPS transcripts and proteins are downregulated as a result of generally suppressed protein translation.

4.3 Differential effect of proteasomal inhibitors on the progression of experimental MN

4.3.1 Preventive Bortezomib treatment of experimental MN aggravates disease progression

Currently, the broad proteasome inhibitor bortezomib (Velcade®) is used clinically for the treatment of multiple myeloma (51) and is also under advisement for the treatment of membranous nephropathy in patients that don't respond to immunosuppressive treatment (29). In chapter 4.1 we have shown that broad proteasomal inhibition caused

albuminuria and subepithelial protein accumulation in the glomeruli of naïve Balb/c mice. Therefore, we investigated the effect of preventive treatment with bortezomib in experimental MN (Figure 17 and 18). Treatment with either vehicle or bortezomib was commenced in naïve Balb/c mice one day prior to induction of THSD7A associated membranous nephropathy (anti-THSD7A MN) (Figure 17 A), controls were treated with rabbit pre-immune (PI) serum. Disease progression was followed by determination of the urine albumin/creatinine ratio to assess the permeability of the glomerular filtration barrier for protein. Mice induced with PI serum maintained a consistent low amount of albumin/creatinine during the experiment progression, while an increase in albuminuria was observed after induction of anti-THSD7A MN (Figure 17 B). Interestingly, animals with anti-THSD7A MN treated with bortezomib exhibited significantly higher levels of albuminuria than vehicle control treated mice. To assess renal function and general health, serum BUN as well as the weight change over the disease course were determined. Both showed no notable differences between the groups (Figure 17 C). Since animals with anti-THSD7A MN exhibited higher amounts of protein loss after bortezomib treatment, we assessed podocyte loss and glomerular tuft swelling by staining for the podocyte marker p57 and by measuring the corresponding glomerular tuft area, under a light microscope (Figure 17 D). P57 staining revealed a decreased number of podocytes in healthy mice treated with bortezomib in comparison to vehicle treated mice, this effect was not noticeable in mice with anti-THSD7A MN treated with bortezomib. Animals with anti-THSD7A MN treated with bortezomib revealed an enlarged glomerular tuft area in comparison to healthy and diseased vehicle treated controls. Consequently, there was a decrease of calculated podocytes per tuft in mice after bortezomib treatment in both healthy and diseased mice in comparison to vehicle treated controls. Morphological assessment *via* PAS staining and light-microscopic evaluation of animals after induction of anti-THSD7A MN treated with bortezomib exhibited a decrease in podocyte structural integrity with swelling and vacuolization of the podocyte cytoplasm.

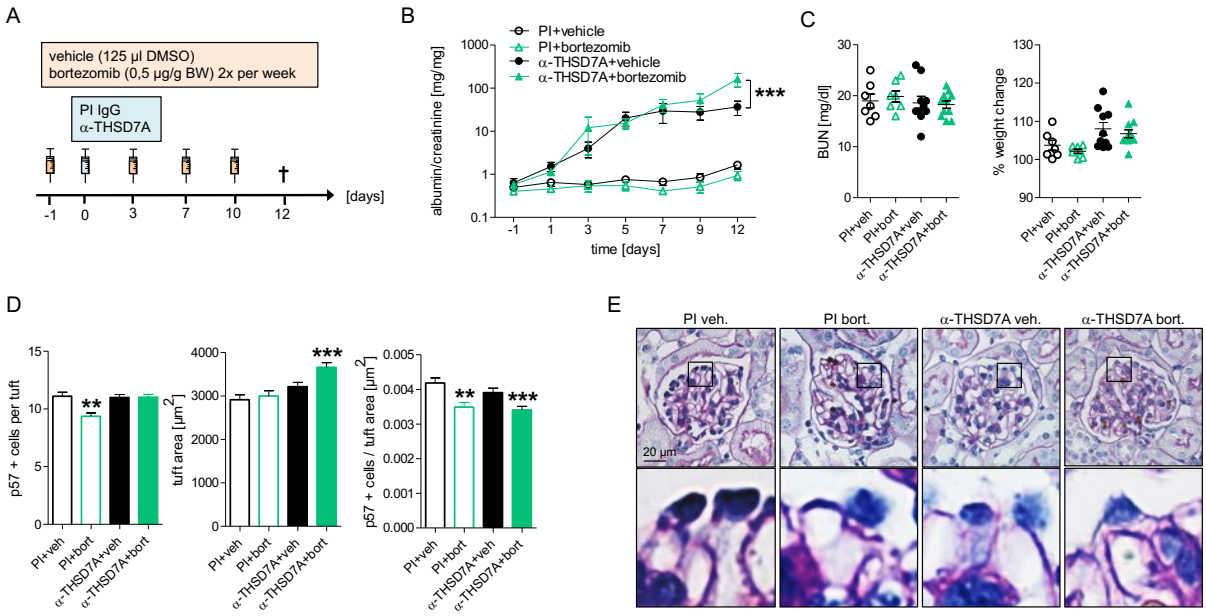

Figure 17: Proteasomal inhibition aggravates progression of THSD7A-associated MN.

(A) Experimental setup: Balb/c mice were treated with either vehicle or bortezomib in a preventive manner and continuously after induction of anti-THSD7A MN. (B) Albumin/creatinine ratio determines proteinuria during disease progression. (C) Assessment of serum BUN and the weight change to assess disease severity. (D) Podocyte loss and glomerular tuft swelling were quantified by staining for the podocyte protein p57 in paraffin embedded kidney sections. (E) Assessment of glomerular morphology by PAS staining. Statistical analysis: mean ± SEM, *p ≤ 0.05, **p ≤ 0.01***, p < 0.0001, 1 way ANOVA with Dunn's multiple comparison test, n ≥ 5 per group.

To assess whether the increase in glomerular tuft area was related to a glomerular accumulation of proteins, especially of THSD7A and the disease model autoantibody rbIgG, Western blots from isolated glomeruli were performed. For quantification of rbIgG deposition, glomeruli-number adapted lysates were separated in a soluble and insoluble fraction. Deposited proteins and immunoglobulins, which are usually found in the insoluble pellet were quantified by Western blot for rbIgG. Animals with anti-THSD7A MN showed significantly elevated levels of rbIgG in the insoluble pellet in comparison to the healthy controls. In corroboration to the elevated levels of albuminuria shown previously, the rbIgG accumulations were higher in THSD7A MN animals treated with bortezomib in comparison to the vehicle control treated THSD7A MN mice (Figure 18 A). High-resolution confocal evaluation of rbIgG accumulation in experimental MN showed a comparable granular-linear signal for rbIgG at the glomerular filtration barrier to vehicle treated THSD7A MN mice, corroborating the

subepithelial accumulation of immune complex, which is typical for MN. Interestingly, bortezomib treated THSD7A MN mice additionally exhibited a significant amount of intracellular aggregates of rbIgG, which were also present in vehicle treated THSD7A mice, however to a far lesser extent (Figure 18 B). We then evaluated the intracellular accumulation of lysin 48 polyubiquitinated proteins, the target proteins for proteasomal degradation, as we expected to see an enhanced accumulation in mice with preventive proteasomal inhibition. Significant differences were observed between vehicle treated preimmune and THSD7A gomeruli by Western blot from total glomerular lysates (Figure 18 C). Bortezomib treated THSD7A MN glomeruli depicted an increase of specific K48 polyubiquitinated proteins in glomerular lysates in comparison to vehicle treated THSD7A MN mice, which was not significant. High-resolution confocal microscopic evaluation of polyubiquitinated proteins revealed an aggravated accumulation of polyubiquitinated proteins in animals with THSD7A MN after the treatment with bortezomib (Figure 18 D). We next assessed, whether preventive bortezomib treatment resulted in an accumulation of the THSD7A protein, which represents the antigen against which the injected (and accumulating) rbIgG was directed. Western blot analyses from the insoluble glomerular fraction demonstrated significantly higher glomerular levels of THSD7A in bortezomib treated mice with anti-THSD7A MN in comparison to vehicle treated controls (Figure 18 E). High-resolution confocal microscopic evaluation of THSD7A and nephrin revealed a slight disruption of the THSD7A signal in PI mice treated with bortezomib in comparison to the vehicle treated controls (Figure 18 F), THSD7A MN led to the disruption of THSD7A and nephrin linearity, to podocyte foot process effacement and to intracellular podocyte THSD7A aggregates (Figure 18 F). The treatment with bortezomib in THSD7A MN aggravated disruption of THSD7A and nephrin linearity, with no linear THSD7A being present any more, whereas most of the THSD7A signal was in form of intracellular THSD7A aggregates in podocytes. Further, bortezomib treated THSD7A MN podocytes also showed severe foot process effacement.

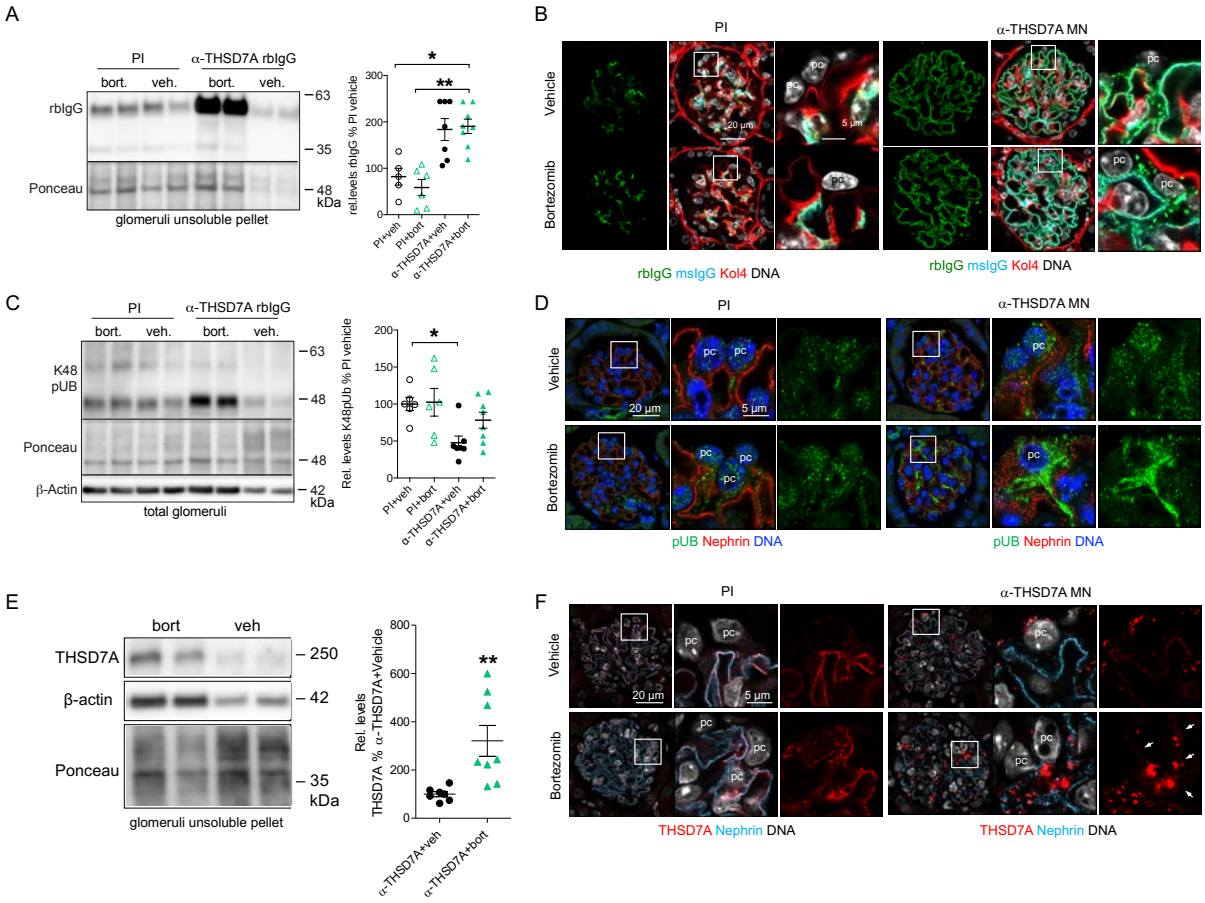

Figure 18: Proteasomal inhibition aggravates intra- and extracellular protein accumulation in THSD7A-associated MN.

Western blot against rbIgG in the unsoluble pellet from isolated glomeruli (A), lysin 48 (K48) polyubiquitinated proteins from isolated glomeruli, densitometric analysis depicted as percent of PI + Vehicle, (C) and against the MN associated antigen THSD7A from isolated glomeruli (E), depiction of densitometric analysis as percent of anti-THSD7A + vehicle. Representative high-resolution confocal immunofluorescence micrographs of (B) rbIgG. (green) and msIgG (blue) accumulation at the glomerular filtration barrier and in the subepithelial space following disease induction, collagen 4 (red) as a structural protein of the glomerular basement membrane, (D) polyubiquitinated (pUb) proteins (green), the proteins marked among other for degradation, with nephrin (red) staining to visualize the podocyte slit membrane and (F) the target antigen THSD7A (red) in THSD7A associated membranous nephropathy with nephrin in blue. DNA was visualized using Hoechst (B, F white; D blue). Statistical analysis: mean ± SEM, *p ≤ 0.05, **p ≤ 0.01***p < 0.0001, 1 way ANOVA with Dunn's multiple comparison test, n ≥ 5 per group.

In summary, preventive treatment of anti-THSD7A MN with the global proteasome inhibitor bortezomib aggravates disease progression and leads to increased protein accumulation in glomeruli, specifically of rbIgG and THSD7A and to a lesser extent of K48 polyubiquitinated proteins.

4.3.2 Preventive treatment of experimental MN with the immunoproteasome inhibitor ONX-0914 alleviates disease progression

One hallmark of MN is the upregulation of the immunoproteasome in podocytes early in the course of disease (33). Since broad proteasomal inhibition with epoxomicin or with bortezomib resulted in proteinuria and an aggravated disease course with enhanced glomerular protein accumulations, we wanted to assess if specific inhibition of the immunoproteasome with ONX-0914, which is currently being tested in a clinical trial, leads to a different result than broad proteasome inhibition. Therefore, Balb/c mice were treated with either vehicle or ONX-0914 prior to the induction of experimental anti-THSD7A MN, control animals were treated with pre-immune (PI) serum (Figure 19 A). As an indicator of disease severity, the urine albumin/creatinine ratio was measured during disease progression. Interestingly, mice with experimental MN treated with vehicle exhibited significantly higher levels of albuminuria during disease progression than mice treated with ONX-0914 (Figure 19 B). Possible podocyte loss and glomerular tuft swelling were assessed *via* p57 staining and measurement of glomerular tuft area under a light microscope. While mice with anti-THSD7A MN treated with vehicle show glomerular tuft swelling and therefore relative podocytopenia, THSD7A MN mice treated with ONX-0914 exhibited lower glomerular tuft sizes and increased amounts of podocytes per glomerular tuft area than PI vehicle treated controls and anti-THSD7A MN vehicle treated controls (Figure 19 C). Evaluation of the podocyte slit membrane via high-resolution confocal microscopy revealed podocyte foot process effacement in THSD7A MN in vehicle treated mice, while the treatment with ONX-0914 preserved podocyte foot process morphology (Figure 19 D). Further evaluation of immunoglobulin depositions showed granular-linear accumulation of rbIgG in mice with THSD7A MN with some rbIgG aggregates intracellularly, which were notably absent in ONX-0914 treated THSD7A MN mice (Figure 19 D). The accumulation of msIgG was also linear in THSD7A MN mice showing no difference between vehicle and ONX-0914 treatment (Figure 19 D).

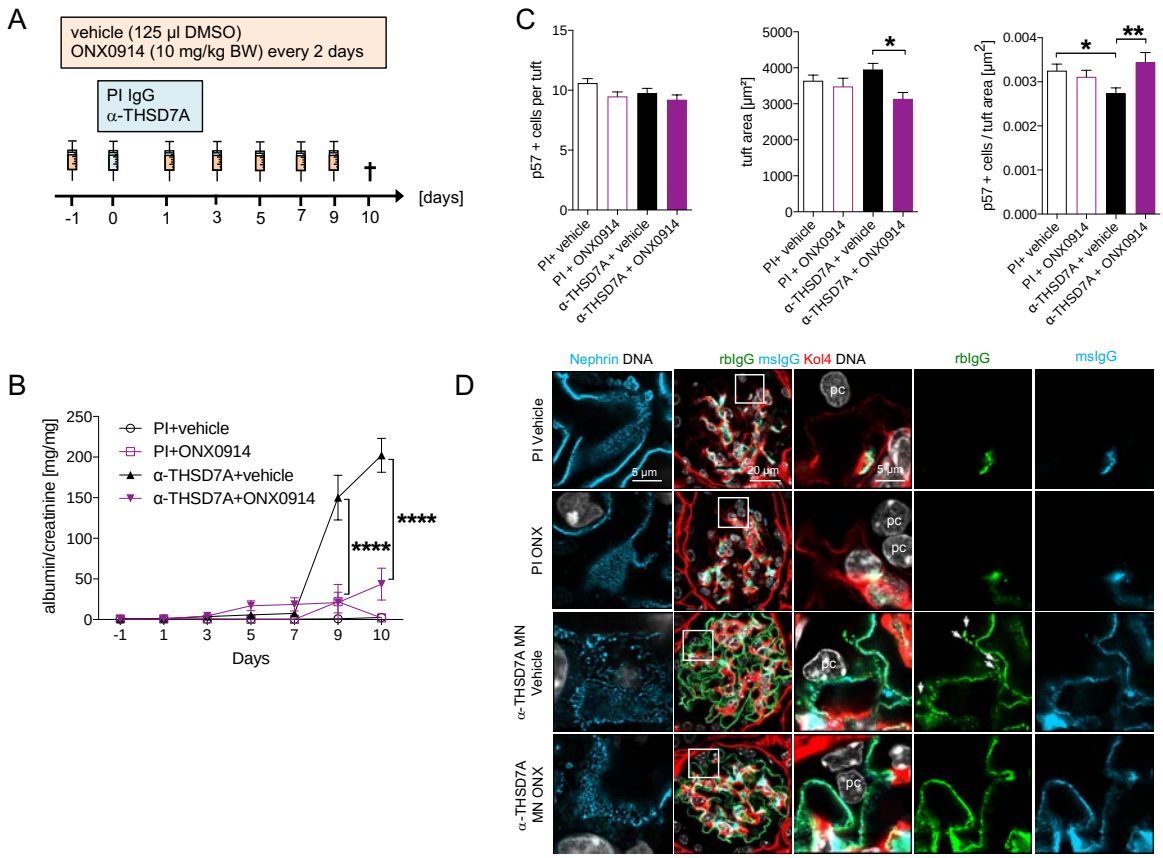

Figure 19: Preventive treatment of experimental THSD7A-associated MN with the immunoproteasome inhibitor ONX-0914 alleviates disease progression.

(A) Experimental setup: Balb/c mice were treated with either vehicle or ONX-0914 in a preventive manner in an experimental model of anti-THSD7A MN. (B) Albumin/creatinine ratio was measured to determine proteinuria development during disease progression. (C) Assessment of podocyte loss and glomerular tuft swelling by p57 staining of kidney sections embedded in paraffin. Representative high-resolution confocal micrographs of (D) nephrin (blue) to visualize the podocyte slit membrane as well as rbIgG (green) and msIgG (blue) with collagen 4 (red) representing the glomerular basement membrane to assess immunoglobulin accumulation and deposition. DNA (white) was stained *via* Hoechst Statistical analysis: mean ± SEM, *p ≤ 0.05, **p ≤ 0.01***, p < 0.0001, 1 way ANOVA with Dunn's multiple comparison test, n ≥ 5 per group.

Assessment of polyubiquitinated proteins showed lower levels of polyubiquitinated proteins in THSD7A MN mice treated with ONX-0914 in comparison to vehicle treated controls (Figure 20 A), while there was only a slight increase in the β5 subunit of the standard proteasome observed in these animals (Figure 20 B). These results suggest that the specific inhibition of the immunoproteasome has a therapeutic potential to alleviate the progression of MN, which could be the result of a cell-specific action on the resident glomerular cells and/or on the immune system. Further investigations will

aim at defining the impact of immunoproteasomal inhibition on the glomerular accumulation of antigen/antibody complexes in MN.

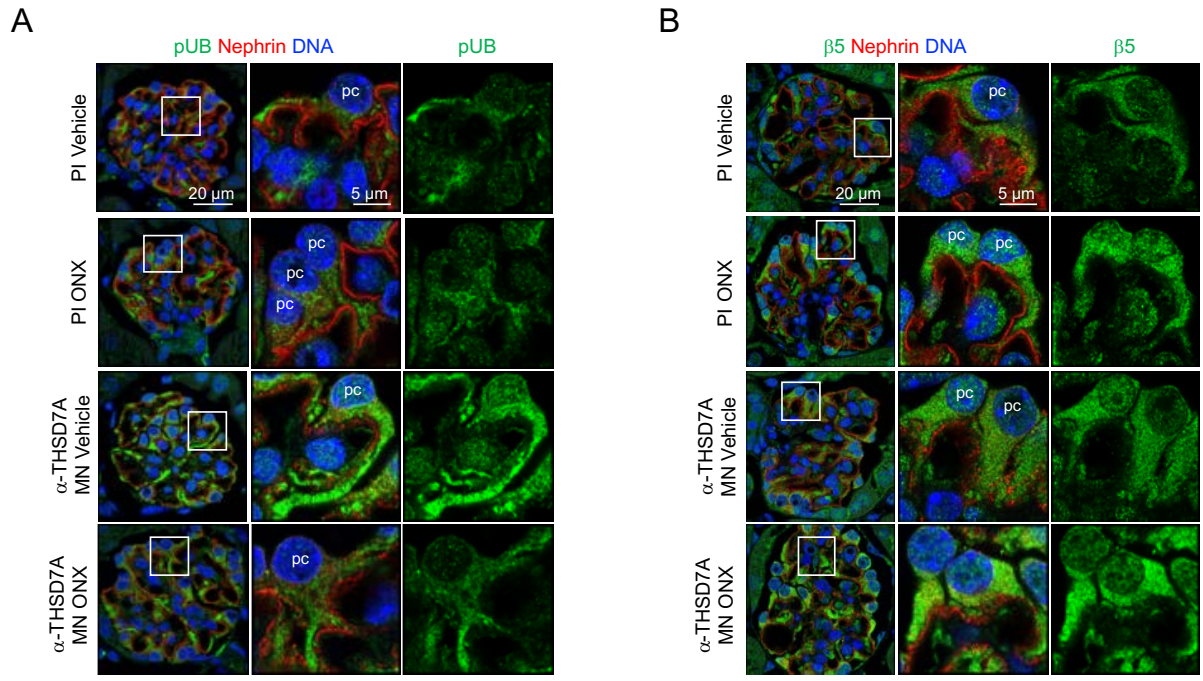

Figure 20: Treatment with ONX-0914 leads to lower levels of polyubiquitin accumulations.

Representative high-resolution confocal micrographs of proteins tagged for degradation, polyubiquitinated (pUb) proteins (green) (A), and the main proteolytic subunit of the standard proteasome β5 (green) (B). Nephrin (red) represents the podocyte slit membrane and DNA (blue) was stained *via* Hoechst.

4.4 Podocyte-specific Lmp7 knockouts are protected during experimental MN

4.4.1 Podocyte-specific Lmp7 knockouts show decreased glomerular Lmp7 levels

Since we observed a protective effect of the treatment with the immunoproteasome inhibitor ONX-0914 on the progression of experimental MN in mice, we decided to deepen our investigations to the role of the immunoproteasome during membranous nephropathy. First, we investigated the location and abundance of the immunoproteasome in patients with membranous nephropathy and in our experimental

mouse model of THSD7A-associated membranous nephropathy. High-resolution confocal images revealed the upregulation of the main proteolytic subunit of the immunoproteasome (Lmp7) in podocytes, and there specifically at the podocyte foot processes in patients with MN (Figure 21 A) and in the mouse model of THSD7A MN (Figure 21 B). The localization of the Lmp7 signal at podocyte foot processes was visualized by its close proximity and intercalating pattern to the slit membrane protein nephrin. The immunoproteasome is a more effective version of the standard proteasome with higher protein throughput and a different array of peptides generated, which are supposed to be more suitable for presentation to the immune system on MHC class I molecules. In order to investigate the effect of immunoproteasome function on proteostasis during membranous nephropathy, we wanted to specifically target the immunoproteasome in podocytes to take a possible effect on the immune system out of the equation.

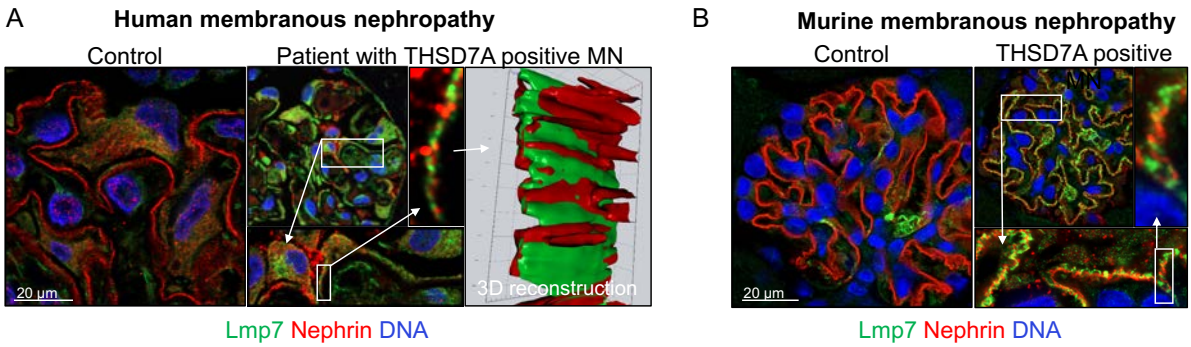

Figure 21: The i26S subunit LMP7 is upregulated in podocyte foot processes in membranous nephropathy.

Representative high-resolution confocal immunofluorescence images of the i26S subunit LMP7 (green) in (A) a healthy kidney biopsy and in a patient with THSD7A positive MN and (B) in a control mouse and in a mouse with THSD7A-associated MN. Nephrin (red) staining was used to depict the podocyte slit membrane and DNA is visualized in blue using Hoechst.

Therefore, we generated podocyte-specific Lmp7 knockout mice, termed Lmp7∆pod (Figure 22 A), with the cre/loxP system and the mice were characterized under naïve conditions. Under naïve conditions the podocyte-specific KO could not be shown by qPCR, Western blot and immunofluorescence. This is related to the fact that podocytes do not express visible amounts of Lmp7 under unchallenged naïve conditions. Further, glomerular endothelial cells highly express the immunoproteasome under naïve conditions, thereby precluding the detection of the podocyte-specific Lmp7 KO in the

qPCR and Western blot analysis performed in isolated glomeruli leading to the result that the podocyte-specific KO was not discernible in light of the endothelial Lmp7 expression (data not shown). We therefore induced a mild form of an experimental model of membranous nephropathy, the anti-podocyte nephritis (APN) to stress podocytes and to induce a Lmp7 expression in podocytes. Under these conditions, high-resolution confocal images of Lmp7 expression in glomeruli show the loss of Lmp7 in the podocytes of Lmp7Δpod mice, whereas the expression in glomerular endothelial cell remains intact (Figure 22 B).

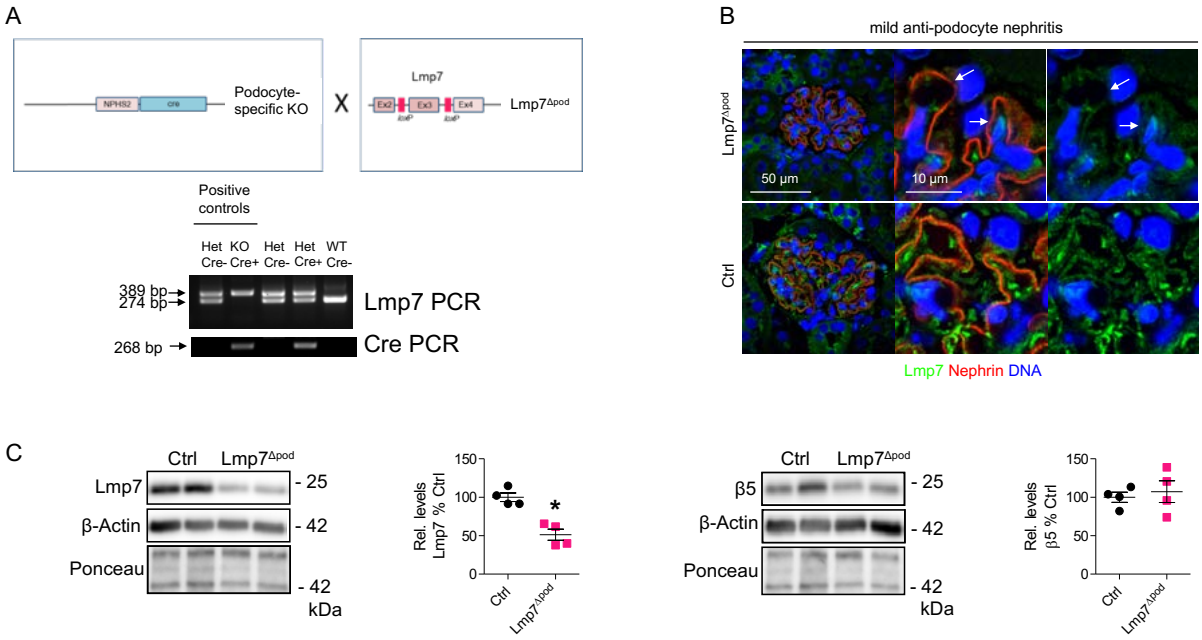

Figure 22: Characterization of podocyte-specific Lmp7 knock-out mice.

(A) Scheme of the generation of the Lmp7 podocyte-specific KO and representative depiction of a genotyping gel. (B) Representative high-resolution confocal immunofluorescence image of Lmp7 (green) in Lmp7Δpod and littermate controls after induction of a mild anti-podocyte nephritis (APN), a model of membranous nephropathy. Nephrin (red) visualizes the podocyte slit membrane and DNA is visualized in blue using Hoechst. Note the loss of linear LMP7 signal in LMP7Δpod mouse (arrows) (C) Representative Western blot against Lmp7 and β5 in Lmp7Δpod and littermate controls after mild APN induction. Statistical analysis: mean ± SEM, *p ≤ 0.05, ***p ≤ 0.001, Mann Whitney U test, n ≥ 4 per group.

Western blot analysis of glomeruli derived from these mice also showed a significant downregulation of Lmp7 in Lmp7Δpod mice in comparison to littermate controls,

whereas the levels of β5 (main proteolytic subunit of the standard proteasome) were unchanged in the Lmp7Δpod mice in comparison to littermate controls (Figure 22 C). These results were strong indicators that the generated mice exhibit a podocyte-specific Lmp7 knockout.

4.4.2 Lmp7Δpod mice are protected during anti-podocyte nephritis

We investigated the impact of podocyte-specific Lmp7 knockout on the disease progression in an experimental model of membranous nephropathy, the anti-podocyte nephritis (APN). The urine albumin/creatinine ratio was used as an indicator of disease progression (Figure 23 A). Lmp7Δpod mice developed significantly lower albuminuria during disease progression than the littermate controls. Assessment of glomerular morphology by PAS staining and light microscopic investigation corroborateed the attenuated course of APN in Lmp7Δpod as the glomerular morphology in Lmp7Δpod mice appeared normal, whereas control littermates exhibited glomerular capillary occlusion and a widened mesangial space (Figure 23 B). Further, podocyte in control littermates exhibited cytoplasmic swelling and vacuolization, which was absent in Lmp7Δpod podocytes after APN induction. Nephrin staining, to visualize the podocyte slit membrane, was evaluated by high-resolution confocal microscopy and showed destruction of the podocyte slit membrane in the control littermates, whereas the Lmp7Δpod glomeruli exhibited an even, meandering nephrin pattern suggesting that the podocyte slit membrane was mostly intact in these mice (Figure 23 C). Evaluation of podocyte loss and glomerular tuft swelling by p57 staining did not show noticeable differences between Lmp7Δpod and littermate controls (Figure 23 D). These results indicate that Lmp7Δpod mice are protected during APN, due to the lack of immunoproteasomes in podocytes.

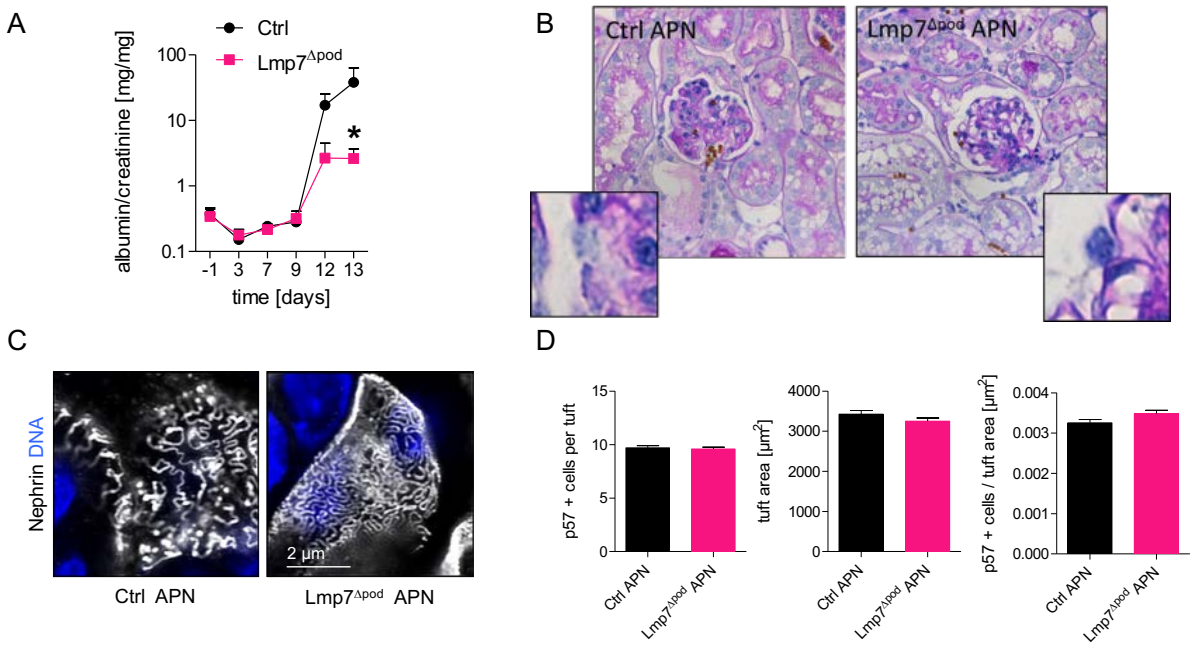

Figure 23: Lmp7Δpod mice are protected during APN.

(A) Assessment of proteinuria development during progression of a model of membranous nephropathy the anti-podocyte nephritis (APN) by determination of the albumin to creatinine ratio. (B) Representative PAS stainings to assess glomerular morphology in Lmp7Δpod and littermate controls after APN induction. (C) Representative high-resolution confocal immunofluorescence images of nephrin to visualize the podocyte slit membrane in Lmp7Δpod and littermate controls after APN induction, DNA is visualized in blue using Hoechst. Note the broadening of podocyte foot processes in the control APN mouse. (D) Assessment of podocyte loss and glomerular tuft swelling by p57 staining of kidney sections embedded in paraffin. Statistical analysis: mean ± SEM, *p ≤ 0.05, 2 way ANOVA with Bonferroni posttest, n ≥ 10 per group.

4.4.3 Protection of Lmp7Δpod due to the upregulation of the standard proteasomal degradation system

Lastly, we wanted to investigate a possible mechanism by which the Lmp7Δpod mice are protected during APN. Since abnormal protein accumulations are a hallmark of membranous nephropathy we hypothesized that a compensatory switch in the protein degradation machinery due to the lack of immunoproteasome in podocytes might be the reason for alleviated disease progression. Therefore, we investigated the proteasomal setup in podocytes and glomeruli of Lmp7Δpod mice. We measured the chymotrypsin-like activity (the main proteolytic activity of the standard and immunoproteasome) and the chymotrypsin-like activity in glomeruli derived from

Lmp7Δpod was significantly higher than in littermate controls (Figure 24 A). These results were corroborated by high-resolution confocal microscopy of immunofluorescence staining of polyubiquitinated (pUb) proteins in glomeruli. The Lmp7Δpod mice showed lower glomerular levels of pUb proteins than the littermate control animals, especially in podocytes (Figure 24 C). Western blots were performed to determine whether a change in proteasomal subtype setup in isolated glomeruli of Lmp7Δpod versus littermate control mice could explain the enhanced proteasomal activity in glomeruli from Lmp7Δpod mice. Indeed, the main proteolytic subunit of the standard proteasome, the β5 subunit, as well as Rpt5, a 19S proteasomal cap protein were significantly upregulated in glomeruli derived from Lmp7Δpod mice in comparison to wildtype littermates (Figure 23 B). Therefore, we conclude that Lmp7Δpod mice are protected during APN due to the compensatory upregulation of the standard proteasomal degradation system, which is able to remove proteins marked for degradation during membranous nephropathy.

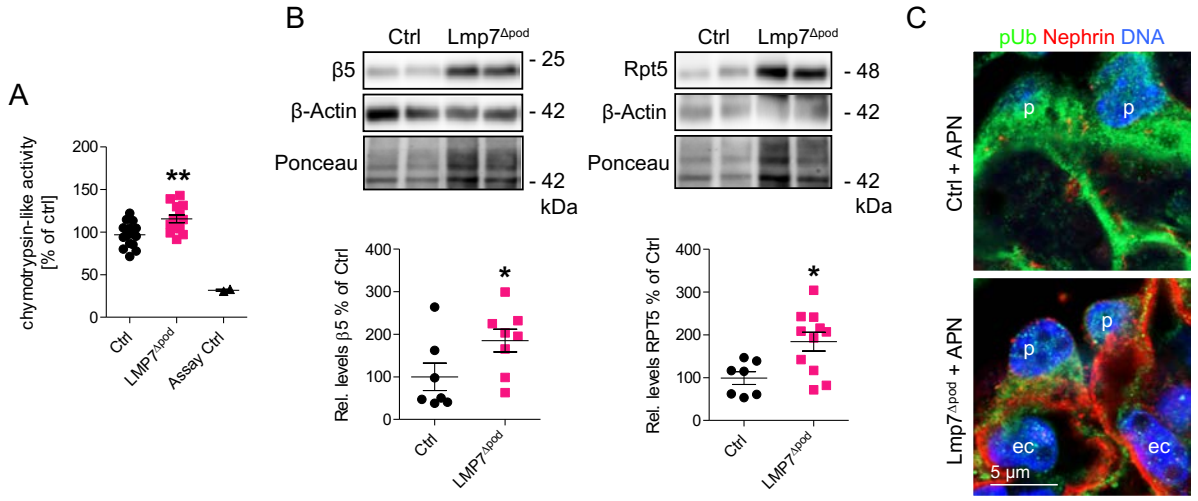

Figure 24: Protective effect in Lmp7Δpod during APN due to the upregulation of the 26S proteasome.

(A) Measurement of the main proteolytic activity (chymotrypsin-like) of the 26S and the i26S proteasome in isolated glomeruli of Lmp7Δpod and littermate controls after APN induction. Results are depicted as percent of littermate control mice. (B) Representative Western Blot against the 26S subunits β5 and Rpt5 in Lmp7Δpod and littermate controls after APN induction. Densitometric analysis depicted as percent of littermate controls. (C) Representative high-resolution confocal immunofluorescence images of the proteasome substrate pUb (green) in kidney sections from Lmp7Δpod and littermate control after APN induction. Nephrin (red) visualizes the podocyte slit membrane, DNA is visualized in blue using Hoechst. Statistical analysis: mean ± SEM, *p ≤ 0.05, **p ≤ 0.01, Mann Whitney U test, n ≥ 7 per group.

5. Discussion

5.1 Podocyte proteostasis depends on the proteasomal degradation machinery

Previously, it has been suggested that podocyte health depends on the interplay of the ubiquitin proteasome system (UPS) and the autophagosomal lysosomal system (ALS) (52) and that both regulate protein levels of podocyte associated proteins (53) (54). In a study by Björn Hartleben et al. mice with a podocyte-specific knockout of autophagy-related 5 (ATG5), a key regulator of autophagy, develop spontaneous proteinuria, which is enhanced after inhibition of the UPS with bortezomib (52). The authors conclude that autophagy is an important mechanism for podocyte homeostasis, and identify podocyte autophagy as a novel pharmaceutical target for glomerular disease (52). In depth study of this publication unearthed some contradictory data: First, mild albuminuria developed in podocyte-specific ATG5 knockout mice spontaneously at 8 month of age is at 0.164 mg/mg albumin/creatinine, which is arguably a low amount of albuminuria. Second, 6 month old podocyte-specific ATG5 knockout mice were treated with the proteasomal inhibitor bortezomib, which then lead to the development of proteinuria, with about 3 mg/mg albumin/creatinine 24 h post injection of the proteasomal inhibitor. The authors explained this bortezomib-related increase in proteinuria with a functional coupling of the two degradation systems (52). This publication led us to the conclusion that the role of the UPS and ALS for glomerular cells is largely unknown so far and required a precise dissection. We therefore aimed to unravel the impact and dependence of UPS and ALS degradation on glomerular cells by first evaluating the expression patterns of players from both degradation systems both histologically and biochemically in glomerular cells isolated from healthy wildtype mouse glomeruli. As a result of these investigations, we could demonstrate in section 4.1 that podocytes and endothelial cells mainly express players of the ubiquitin proteasome system, while mesangial cells mainly express players of the autophagy lysosomal degradation system. These results strongly implicate that glomerular cell proteostasis depends on very intricate regulation of the different degradation systems and that endothelial cell and podocyte proteostasis mainly depends on UPS regulation while mesangial cell proteostasis mainly depends on regulation through the ALS.

These findings could serve as an explanation for the observed albuminuria in podocyte-specific ATG5 knockout mice after treatment with bortezomib: Only when the proteasomal degradation system was impaired did the mice develop proteinuria, suggesting that podocyte health (as a vital part of the glomerular filtration barrier) depends on maintaining proteostasis through the UPS.

Our findings will pave the road to help shed light into understanding the contradicting published results of renal disease as a result of the impairment of either the proteasomal or the lysosomal degradation system. For one, studies have shown that patients with multiple myeloma that were treated with the proteasomal inhibitor bortezomib developed rare cases of nephrotoxic side effects, such as thrombotic microangiopathy and acute interstitial nephritis, while patients treated with the proteasomal inhibitor carfilzomib quite frequently suffer from nephrotoxic side effects with a 25 % occurrence of acute kidney injury in a phase 2 trial (55). On the other hand, treatment of a patient with nephrotic syndrome caused by idiopathic membranous nephropathy with bortezomib resolved the nephrotic syndrome (29). Regarding the autophagosomal lysosomal system, also contradicting findings have been published exhibiting the need for precise dissection of the patho-physiologic distribution and significance of this system. Thereby, patients with mutations in different lysosomal enzymes or proteins also exhibit involvement of glomerular cells. For example, action myoclonus-renal failure syndrome (AMRF), a lethal form of inherited progressive myoclonus epilepsy associated with renal failure, presents with a renal pathology of focal glomerulosclerosis with occasional glomerular collapse characterized by a mainly mesangial cell and podocyte involvement. Brain pathology shows unusual accumulations of storage material. As the underlying cause of AMRF, a mutation in the *SCARB2/Limp2* gene was identified which encodes a lysosomal membrane protein (56). As we have shown that mesangial cells mainly rely on the ALS to maintain proteostasis, the mesangial cell involvement as an effect in AMRF supports our findings. The podocyte involvement requires further investigations. As another example, Fabry disease is caused by the absence or deficiency of the lysosomal enzyme α-galactosidase A which leads to the accumulation of globotriaosylceramide and other glycosphingolipids in all glomerular cell types for the renal pathology (57). So far, we are unable to understand the mechanism for these observed accumulation patterns in Fabry disease. However, other lysosomal storage diseases such as Mucolipidosis type II alpha/beta, which presents with multi organ involvement exhibit

no overt renal phenotype, whereas in one report patients with Mucolipidosis type III (MLIII) alpha/beta have recently been described to present with focal segmental glomerulosclerosis. In this case it remained unclear if the renal involvement was caused by the MLIII alpha/beta or if it was present by pure coincidence (47). These different disease manifestations with or without renal involvement and the differential impact of different proteasomal inhibitors on renal pathology show that still very little is known about the dependence of glomerular cells on protein degradation systems and how UPS and ALS influence each other.

To investigate the functional significance of UPS or ALS impairment on renal / glomerular cell health, naïve wildtype mice were therefore treated with either the proteasomal inhibitor epoxomicin or with the lysosomal inhibitor leupeptin A. Epoxomicin served in the pharmaceutical industry as a scaffold for the generation of carfilzomib and shows high and irreversible selectivity for the proteasome (58). Leupeptin A, which reversibly inhibits enzymatic activity within lysosomes and therefore inhibits degradation of accumulated proteins within the lysosomal compartments. Leupeptin A treated mice exhibited accumulation of the lysosomal membrane protein Limp2 as well as lysosomal enzymes such as cathepsin D, which serve as an indicator for a successfully achieved pharmacologic lysosomal impairment. Interestingly, inhibition of lysosomal degradation caused ultrastructural alterations to mesangial cells, with electron dense lysosomal storage accumulations, while podocytes and endothelial cells exhibited normal morphological features. Otherwise, leupeptin A treated mice showed no signs of renal involvement, as proteinuria and serum BUN levels were unaltered. Epoxomicin treatment was also successful in our treatment approach, as the accumulation of polyubiquitinated proteins as well as of α-actinin 4 indicate a successful inhibition of the proteasomal system. In contrast to mice with lysosomal inhibition, mice treated with epoxomicin exhibited impairment of glomerular function at the clinical, morphological and biochemical level. Epoxomicin treated mice exhibited significant albuminuria, suggesting a leakiness of the glomerular filtration barrier which was validated by nephrin staining to visualize the podocyte slit membrane and by electron-microscopic evaluation, which showed podocyte foot process effacement, loss of endothelial fenestrations and focal splitting of the glomerular basement membrane. Besides the clinical and morphological alterations that develop with proteasomal impairment, glomeruli exhibit a pronounced accumulative phenotype to intracellular (ubiquitin) and extracellular (immunoglobulins)

proteins. Thereby our investigations were significant for distinct accumulation patterns of foreign rbIgG after inhibitor treatment. Under lysosomal inhibition rbIgG foremost accumulated in the mesangium, while under proteasomal inhibition rbIgG accumulated along the capillary loops in a predominantly subepithelial (between the glomerular basement membrane and the podocyte foot processes) localization. The reasons for this extracellular IgG deposition upon proteasomal inhibition require further investigations. Hypothetically, an altered glomerular perfusion could be one explanation, as proteasomal inhibition in the pig was shown to decrease GFR (59). Whether this is a side-effect of the decribed polyneuropathy secondary to long-term bortezomib treatment (60) is an open question, and whether this occurred in our short term treatment in mice needs to be further established. Another explanation could be that proteasomal inhibition affected the physiological role of FcRn on podocytes. FcRn, is an IgG and albumin transport receptor expressed in podocytes, which was suggested to function to internalize IgG from the GBM thereby actively maintaining the glomerular filtration barrier free of IgG (61). These results emphasize our findings that mesangial cells rely on the ALS to remove non-essential proteins, while endothelial cells and podocytes rely on the UPS to remove those proteins.

5.2 Mouse models of mucolipidosis type II and III show no renal involvement due to differential compensatory mechanisms

To further investigate glomerular cell involvement in the setting of lysosomal impairment we made use of murine models exhibiting varying degrees of lysosomal storage disorder in a disease termed Mucolipidosis. Mucolipidosis results from lysosomal enzyme missorting due to impaired M6P tagging by the Golgi resident GlcNAc-1-phophotransferase, encoded by the *GNPT* gene. We investigated renal and glomerular health and function in two mucolipidosis mouse models, whereby the MLIII model related to partial lysosomal enzyme missorting due *Gnptg* mutations and the MLII model related to severe lysosomal enzyme missorting due to *Gnptab* mutations. We further investigated if reported renal involvement in MLIII alpha/beta patients is a direct result of *GNPTAB* and/or *GNPTG* mutations. Even though the genetic cause of lysosomal storage disorders have been thoroughly investigated and even been understood, the mechanisms leading to the disruption of cell metabolic and signaling

pathways that are associated with these disease manifestations are less well understood. Even though lysosomal storage disorders vary significantly from each other it is a commonly accepted opinion that lysosomal storage disorders that store similar types of macromolecules such as sphingolipids, mucopolysaccherides or glycoproteins, exhibit similar biochemical, pathological and clinical phenotypes, which suggests that the nature and distribution of the stored material is the main lesion-defining factor (62). Ultrastructural analysis of MLII and MLIII kidneys showed that the electron density of the accumulated storage material in endothelial cells and podocytes differed from that in mesangial cells in our studies, which suggests that lysosomal dysfunction resulted in the accumulation of distinct types of macromolecules in a manner specific to the distinct glomerular cells. So far, the biochemical nature of the accumulated lysosomal storage material within glomerular cells of MLII or MLIII patients and mice has not been identified. In the brains of MLII mice electron-dense bodies were found to accumulate in the majority of cortical hippocampal and cerebral neurons, and numerous neurons exhibited swollen axons filled with heterogeneously appearing membrane-bound storage vacuoles ranging from electron-dense to electron-lucent structures. Further analysis of the storage material revealed a mixture of dense and multi-lamellar bodies, electron-lucent floccular bodies, zebra bodies and fingerprint-like storage material characteristic for the accumulation of lipofuscin, glycans or glycogen and gangliosides (49). It was found that both *Gnptab* and *Gnptg* genes are ubiquitously expressed in mouse tissue although the expression of *Gnptg* is constantly higher than that of *Gnptab*, which especially holds true for the expression in kidney tissue (48). Whether the different expression levels have functional consequences is not known so far. Our investigated MLIII (*Gnptg* mutation) and MLII (*Gnptab* mutation) mice showed similar lysosomal alterations in the extent and site of renal cells. Both mouse models showed especially abundant and enlarged Limp2-positive lysosomes, which were mostly found in renal tubulointerstitial cells, podocytes, endothelial cells, mesangial cells and juxtaglomerular cells. Surprisingly, Lamp2-positive lysosomes did not appear enlarged, even though they are most numerous present in proximal tubular cells in the mouse models as well as in healthy mice.

Not only does the biochemical nature of the abnormally stored material in lysosomes define and shape the characteristics of the clinical presentation of disease, but also the compensatory potential of the affected cell types with dealing with the storage stress may play a role. In kidney biopsies of patients with Mucolipidosis type III

alpha/beta and an autopsy report of a patient with renal involvement, alterations in foremost podocytes have been observed in these lysosomal storage disorders, podocytes are usually described there as having a foamy appearance most likely due to the accumulation of storage material (47). However, the foamy appearance of podocytes does not necessarily associate with reduced renal function, as the 45- year old patient whose autopsy was performed did not show any noticeable renal involvement (44). These findings in Mucolipidosis patients differ from patients with Fabry disease, where globotriaosylceramide accumulation due to low α-galactosidase A enzyme activity, occurs in multiple renal cell types, including podocytes, mesangial and interstitial cells, vascular endothelial and smooth muscle cells as well as the cells of the proximal and distal tubules and the loop of Henle (38). The MLII and MLIII mice analyzed during this thesis did not show a striking glomerular phenotype and we could not detect any significant signs of altered glomerular function, even though glomerular cells exhibited enlarged lysosomes with storage material. Despite observed focal glomerular basement alterations, overall podocyte foot processes and endothelial cell fenestrations appeared to be normal, which related to the absence of proteinuria. In line with the results derived from our Mucolipidosis mouse models, patients with MLII, MLIII alpha/beta and MLIII gamma did not exhibit gross protein loss to the urine. Only in MLII patients, microalbuminuria was observed. Therefore, we assume that the glomerular cell protein homeostasis was most likely not sufficiently perturbed by the lysosomal storage disorder to result in a disease promoting loss of glomerular filtration barrier integrity. It is however possible that the glomerular cell metabolism between humans and mice differs, as this has been shown for the glomerular lipid metabolism (63, 64). Possibly, this limits one-to-one comparisons of the mouse MLII and MLIII models with patients with MLII and MLIII. Species differences in glomerular lipid metabolism have, for example, hindered investigations of the pathogenesis of Fabry disease in mice. However, based on the fact that several lysosomal enzymes are missorted to the extracellular space in our MLII and MLIII mice, we are confident to conclude, that despite species differences in glomerular cell metabolism, the absence of significant glomerular function impairment in MLII and MLIII mice relates to the human situation. It remains yet unknown why in Fabry disease and not in MLII and MLIII patients, glomerular cell involvement is prominent and leads to Fabry nephropathy with podocyturia, proteinuria and reduced GFR (65).

It was long assumed that the autophagosomal/lysosomal and the ubiquitin proteasome system (UPS) operate independently from each other, but it has become clear that the two main degradation systems strongly cross react and thus compensate for the impairment of one another (32). In many cases, lysosomal storage disorders are accompanied by the appearance of ubiquitinated protein aggregates, this has been observed especially in small and motor neurons (62). Furthermore, podocyte-specific ATG5 knockout mice (ATG5 is essential for autophagosome formation) compensate autophagosome deficiency by upregulation of the UPS (52). As mentioned earlier, only upon UPS impairment in ATG5 podocyte-specific KO mice does ubiquitin accumulate and mild proteinuria occur (52). Therefore, we investigated the status of the UPS in glomeruli of MLII and MLIII mice. Due to their severe general mucolipidosis phenotype of MLII mice, the last assessable age was 40 weeks, whereas MLIII mice, which presented with a milder general phenotype, were assessed up to 90 weeks of age for the development of a renal phenotype. Surprisingly, only MLIII mice exhibited compensatory upregulation of the UPS. It is most likely that the extent of UPS upregulation was sufficient to preserve protein homeostasis during lysosomal dysfunction in MLIII glomerular cells, as glomerular ubiquitin levels and proteasomal activity were comparable to control littermates. In contrast, MLII mice did not upregulate the UPS in glomeruli. Moreover, the glomerular ubiquitin amounts were decreased on mRNA and protein level. Podocytes also only rarely exhibited ubiquitin aggregates. This led us to believe that there is a UPS independent compensatory mechanism that was activated to balance protein homeostasis during severe MLII, which prevented abnormal ubiquitin accumulations in the first place.

To evaluate not only the proteasome but other parts of the UPS, we investigated the expression levels of the deubiquitinating enzyme UCH-L1, which functions to stabilize cellular monoubiquitin levels (66) and whose *de novo* expression in podocytes is associated with podocyte injury (67). Only MLIII mice showed elevated levels of UCH-L1 in podocytes, which is in line with the induction of proteasome subunits to maintain protein homeostasis. In MLII glomeruli, UCH-L1 protein levels were reduced, while proteasome subunits were at comparable levels to littermate controls, suggesting a distinct involvement of UCH-L1 in these lysosomal storage disorders. In fact, the downregulation of UCH-L1, which we observed in MLII glomeruli, has already been shown in other lysosomal storage disorders. In fibroblasts of patients with syndrome of inappropriate antidiuresis secresion (SIAD), sialidosis, galactosialidosis, GM1-

gangliosidosis, Morquio syndrome type A and B and Gaucher disease a downregulation of UCH-L1 was observed (62). In these studies, it was also shown that the downregulation of UCH-L1 directly induced caspase-mediated apoptosis and it was suggested that UCH-L1 deficiency and impairment of the ubiquitin-dependent protein degradation pathway can contribute to increased cell death in lysosomal storage disorders (62). However, we could not detect any signs of apoptosis in MLII or MLIII glomeruli. Therefore, the involvement of UCH-L1 in mucolipidosis needs further investigations, as other studies have shown association of UCH-L1 and autophagosomal/lysosomal function. Thereby UCH-L1 directly interacts with Lamp2 and the expression of a hydrolase-deficient form of UCH-L1 inhibits chaperone-mediated autophagy (68). It has further been suggested that UCH-L1 destabilizes mTORC1 (69), a part of a signaling mechanism that helps sense the need for lysosomal degradation (70). mTORC1 forms a lysosome-to-nucleus axis which involves the transcription factor TFEB. In the absence of lysosomal stress, mTORC1 is recruited to the lysosomal surface, where it becomes activated and phosphorylates TFEB to prevent its translocation to the nucleus. Under lysosomal stress, mTORC1 detaches from the lysosome and remains in the cytosol in an inactive state and TFEB is no longer phosphorylated. When TFEB remains unphosphorylated, it translocates to the nucleus where it activates gene expression programs that enhance lysosomal function and autophagy. In our studies, MLII and, to a lesser extent, MLIII glomeruli showed signs of mTORC1 pathway repression in the form of decreased levels of total S6 and phosphorylated S6 in glomeruli, as well as in decreased levels of the mTORC1-related transcripts *Fasn*, *Vegfa* and *Hif1a*, and in increased levels of the lysosomal and autophagosomal proteins Lamp2, Limp2 and LC3. Interestingly, a decreased activation of the mTORC1 - S6Kinase - S6 - 4E-BP1 pathway represses protein synthesis, which was more pronounced in MLII glomeruli, with reduced levels of UPS-related transcripts and of ubiquitinated proteins, than in MLIII glomeruli. Also, we were able to demonstrate a repression of protein synthesis in MLII glomeruli through the activation of the integrated stress response (ISR), which we could not observe in MLIII glomeruli. It has been suggested that UCH-L1 can promote protein synthesis by bypassing mTORC1 and directly promoting the assembly of eIF4F, the target of 4E-BP1 (71). Therefore, in the setting of impaired mTORC1 signaling in MLII kidney, the reduced levels of UCH-L1 could represent a new pathway that decreases protein synthesis and therefore lessens proteotoxic stress.

These results suggest, that even though the levels of lysosomal dysfunction are comparable in MLII and MLIII kidneys, no impairment of glomerular function can be observed due to differential compensatory mechanisms, which balance protein homeostasis. MLII glomerular cells balance proteostasis by decreasing general protein synthesis by the upregulation of the integrated stress response, while MLIII glomerular cells balance proteostasis by the upregulation of the UPS and therefore enhancing their protein degradative capacity.

5.3 Proteasomal inhibitors have opposing effects on the progression of experimental membranous nephropathy

We have shown that under homeostatic conditions, the inhibition of the proteasome with epoxomicin is detrimental to podocyte health. Controversly, a patient was described who presented with nephrotic syndrome that was resistant to 6 month of high-dose oral prednisone and ramipril treatment. After receiving a single cycle (four doses) of the proteasomal inhibitor bortezomib the patient went into remission of the nephrotic syndrome and remained in remission after 1 year follow-up (29). The authors of the study deem it unlikely that the observed effect resulted from spontaneous remission, due to the fact that the patient did not respond to the 6 month high-dose glucocorticosteroid therapy prior to receiving bortezomib (29). This led us to investigate the effect of preventive treatment of experimental membranous nephropathy with bortezomib, which differs substantially from epoxomicin. Epoxomicin, a peptide structure with a epoxyketone pharmacophore with high selectivity for the proteasome, served as the scaffold for the generation of the synthetic tetrapeptide epoxyketone carfilzomib (58). Bortezomib on the other hand is a dipeptide boronic acid inhibitor (51), which is slightly less specific for the proteasome as it also inhibits other serine proteases (58). In line with our findings for the detrimental effect of epoxomicin application in naïve mice, preventive treatment with bortezomib in our model of experimental THSD7A-associated membranous nephropathy, led to elevated levels of albuminuria in comparison to vehicle treated controls. The bortezomib treated mice also exhibited abnormal protein accumulations consisting of large intracellular aggregates of THSD7A, rabbit IgG and msIgG within podocytes. This abnormal protein accumulation was also reflected by the swelling of glomerular tufts, which was enhanced upon bortezomib treatment. The adverse effects of proteasomal inhibition

on the progression of experimental MN are in line with our findings that podocyte proteostasis strongly depends on an intact UPS and that proteasomal impairment proves detrimental to podocyte health, especially under stress conditions (33, 72). Interestingly, very few renal side effects have been reported in patients with multiple myeloma in which bortezomib application has become a first line treatment. This could be related to the fact that it is difficult to distinguish between myeloma-related kidney disease and drug toxicity since myeloma itself frequently leads to kidney disease (55). In terms of nephrotoxicity associated with multiple myeloma under proteasomal treatment, cases of thrombotic microangiopathy have been reported (55), as disease condition characterized by the presence of endothelial cell injury and microvascular thrombi (73). To the best of our knowledge, no side effects of bortezomib involving podocytes, have been reported so far. Even though bortezomib has been shown to have an attenuating effect on MN progression in a patient with idiopathic membranous nephropathy, our results suggest that treatment of experimental MN with bortezomib aggravates disease progression due to the strong dependence of podocyte protein homeostasis on the standard proteasomal system. Which precise mechanisms relate to the ensuing enhanced protein aggregation and deposition in podocyte cytoplasm upon bortezomib application in experimental MN are unknown to date and require further investigations. They could however be the result of 1) altered compensatory mechanisms induced within resident cells to balance proteostasis following proteasome inhibition through bortezomib in the setting of MN, and / or 2) due to altered vesicular trafficking and thereby clearance of IgG from the glomerular filtration barrier (61) and podocytes, a process strongly orchestrated by the UPS. Further, the enhanced glomerular deposition of IgG measured in our experiments could again result from an altered glomerular filtration rate (GFR) (59) due to effects of proteasomal inhibitors such as bortezomib on the vasculature or / and on peripheral nerves resulting in polyneuropathy (60, 74). Polyneuropathy involving renal nerves would result in altered sympathetic renal innervation, and thus altered renal perfusion in turn decreasing GFR. However, the possibility remains that bortezomib treatment of human MN could have positive effects on disease progression that would outweigh the negative side effects, since bortezomib has been shown to enhance apoptosis of antigen secreting cells, such as plasma cells or memory B cells (75) and could therefore reduce the production of autoantibodies during MN.

Our group has demonstrated in previous work that during podocyte injury, such as membranous nephropathy, the β5i (Lmp7) subunit of the immunoproteasome is upregulated (33). The immunoproteasome is a specialized form of the standard proteasome, and while the standard proteasome is generally expressed in almost all mammalian cells, the immunoproteasome expression is generally lower under basal conditions (76). Upon interferon gamma exposure the immunoproteasome is upregulated, but it also responds to exposure to environmental stressors such as oxidative stress. The promotor region of the immunoproteasome exhibits binding sites for multiple transcription factors which enable cytokine dependent (Stat-1, IRF-1) and independent (CREB, NFκB) mechanisms of regulation (77). The immunoproteasome has been shown to exhibit an accelerated rate of degradation of polyubiquitylated proteins (35). We therefore assessed, whether targeting the proteasome system in a more subtype specific manner than was the case with bortezomib could confer an effect on MN disease progression. We hypothesized that upregulation of the immunoproteasome during early disease progression is detrimental to podocyte integrity, because podocyte structural proteins such as α-actinin 4 and podocin are degraded by the proteasome (33), and that the upregulation of the immunoproteasome at a late disease stage has a positive effect on disease progression because its enhanced proteolytic activity may be able to degrade the accumulated proteins more effectively. Therefore, we targeted the immunoproteasome pharmaceutically with the immunoproteasome inhibitor ONX-0914. Application of either vehicle or ONX-0914 to naïve Balb/c mice was commenced in a preventive manner prior to induction of THSD7A associated MN. To our surprise mice treated with ONX-0914 showed very low levels of albuminuria (the main indicator for disease severity) during disease progression in comparison to their vehicle treated controls. The less severe disease progression appreciated with the ONX-0914 treatment was also reflected in the measurement of the glomerular tuft area and the number of podocytes per glomerular tuft. While vehicle treated THSD7A MN mice showed a significant increase in their glomerular tuft area with slight podocytopenia in comparison to the pre-immune serum mice treated with vehicle, the glomerular tuft area as well as the number of podocytes per tuft of ONX-0914 treated THSD7A MN mice remained at comparable levels to the vehicle and ONX-0941 treated pre-immune mice. Interestingly, pharmaceutical targeting of the immunoproteasome with ONX-0941 proved to prevent intracellular aggregate formation of the MN antigen THSD7A and of the injected anti-THSD7A

rabbit IgG in podocytes, which was in stark contrast to bortezomib treatment in which nearly the opposite effects on intracellular protein aggregation and accumulation were observed.

Application of both inhibitors (bortezomib and ONX-0941) most likely affected proteasomal degradation in both immune and resident cells due to the systemic nature of application. However, one needs to take into consideration that the effects on resident renal cells and on immune cells are most likely to differ between both inhibitors. While both bortezomib and ONX-0914 have been described to enhance apoptosis in antibody secreting plasma cells (75, 78, 79) as well as reducing cytokine production, they differ in their effect on the nuclear factor (NF)-κB (75, 78). NF-κB is a transcription factor which regulates the expression of immune system components including pro-inflammatory cytokines, chemokines and major histocompatibility complexes (80). Bortezomib inhibits inducible NF-κB activity while enhancing constitutive NF-κB activity, therefore influencing the NF-κB pathway (75). ONX-0914 on the other hand, has not been shown to have an effect on the NF-κB pathway (78). Furthermore, bortezomib has been shown to reduce the antigen presenting function of dendritic cells, who present antigens in association with the major histocompatibility complex (MHC) II (75), while ONX-0914 inhibits presentation of Lmp7 specific MHC I antigens (81). Further analysis of the differential effects of these inhibitors on immune and resident cells are necessary to understand the systemic impact of these inhibitors.

To this point our experiments do not allow a dissection of the observed effects into cell (podocyte) specific effects and into effects on the immune response of ONX-0941. The association of the immunoproteasome with an immune response stems from the fact that the genes encoding for the Lmp2 and Lmp7 subunits of the immunoproteasome are located within the class II major histocompatibility complex (MHC) region, and these two subunits synthesized are assembled simultaneously into the proteasomal multi-subunit complex (82). Immunoproteasomes are suggested to exhibit altered peptidase activity and cleavage site preferences that result in more efficient liberation of MHC class I epitopes (35). Additionally, the increase in peptide supply achieved by immunoproteasomes has a positive effect on efficient MHC class I antigen presentation thereby triggering an effective early cytotoxic T cell response (35). Therefore, it is not surprising that immunoproteasome inhibitors are effective pharmaceuticals, targeting immune cells (83). Nonetheless, besides the undisputable

effects of immunoproteasome inhibitors on immune cell function and thereby on the immune reaction, we feel that the observed amelioration of MN after immunoproteasome inhibition is most likely attributable to podocyte-specific effects of ONX-0941 rather than to effects on the immune response due to the fact that 1) podocytes reside within an immune-privileged site and are so protected from cytotoxic T lymphocytes (84, 85), and 2) the involvement of the immune system on direct glomerular injury is thought to be minor, and 3) the amount of msIgG deposited within the glomeruli of ONX-0941 treated MN mice was comparable to vehicle treated mice, suggesting that the secondary immune reaction to the injected rabbit IgG was independent of the treatment. Further supporting the idea of podocyte-specific effects of ONX-0941 treatment are in the recent years published roles of the immunoproteasome in nonimmune cells, suggesting different, unknown roles of the immunoproteasome (76), which are distinct from its function in immune cells. For example, the immunoproteasome has been shown to act as a regulator of skeletal muscle differentiation, as well as a regulator of protein degradation of proteins associated with apoptosis (86). *PSMB8*, the gene encoding for the immunoproteasome subunit Lmp7 (β5i) is the essential component regulator not only of inflammation, but also of adipocyte differentiation, which indicates that the immunoproteasome has multiple functions in maintaining protein homeostasis in several cell types (87). Another interesting fact, which could point towards a podocyte-specific effect of the immunoproteasome targeting is our observation that in patients with membranous nephropathy as well as in murine THSD7A-associated membranous nephropathy the immunoproteasome is upregulated in a distinct cell domain, namely in podocyte foot processes, where the TSHD7A antigen resides and is targeted by the autoantibodies (88). This domain-specific localization of immunoproteasome expression in podocytes could reveal similar cell domain-specific functions as in neurons, where a cell domain-specific proteasomal degradation has entered the spotlight recently (89). In neurons, domain-specific proteasome expression and therefore degradation at the post-synaptic density has been established as a specific mode to modulate synaptic transmission (90). Specifically, a mammalian nervous system-specific membrane proteasome complex that directly and rapidly modulates neuronal function by degrading intracellular proteins into peptides and thereby stimulating neuronal signaling has been reported (91). Podocytes are thought to resemble neurons closely in morphology and in the expression of proteins (92). These thought similarities between podocytes and

neurons are of interest, if one speculates upon the function of the immunoproteasome in podocytes.

Our findings of the differential effects of the proteasomal inhibitors bortezomib and ONX-0941 on podocyte injury in membranous nephropathy need further investigations, in order to understand the intricate compensatory mechanism following proteasomal impairment.

5.4 Podocyte-specific immunoproteasome deficiency alleviates progression of immune-complex mediated membranous nephropathy

In order to be able to investigate the cell-specific role of the immunoproteasome in the development and progression of podocyte injury in MN without the confounding involvement or effect a pharmaceutical immunoproteasome targeting could/would have on the immune system, we generated a podocyte-specific immunoproteasome knockout mouse in which the Lmp7 subunit is knocked out with the help of the cre/lox system. Since the immunoproteasome expression is very low in podocytes and very prominent in glomerular endothelial cells under basal conditions the Lmp7 knockout could only be verified under stressed conditions, which result in an induction of immunoproteasome expression (33). Therefore, a mild-immune complex nephritis, the anti-podocyte nephritis (APN), was induced in the Lmp7∆pod mice, upon which LMP7 is upregulated (33). In this setting reduced Lmp7 protein levels could be appreciated, whereas the levels of the standard proteasome remained unchanged. To observe the effect of immunoproteasome loss on the progression of MN, APN was induced in Lmp7∆pod mice and in littermate controls. In line with the above-mentioned amelioration of THSD7A MN development through pharmacological inhibition of the immunoproteasome with ONX-0914 the progression of anti-podocyte nephritis was alleviated in Lmp7∆pod mice in comparison to littermate controls with little to no podocyte damage developing. Since podocyte-specific knockout of immunoproteasome basically rules out changes in immune response as the underlying mechanism of protection. we investigated for a mechanistic explanation of the observed effects. Interestingly, the chymotrypsin-like activity (which assesses and does not differentiate between the activity of the standard (β5) and the

immunoproteasome (β5i, Lmp7) was elevated in the Lmp7Δpod glomeruli in comparison to littermate control glomeruli. This finding suggests that the proteolytic activity of the standard proteasome is upregulated in a compensatory manner. This interpretation is strengthened by the fact that protein levels of the 20S core and 19S cap of the standard proteasome were also elevated in the Lmp7Δpod glomeruli in comparison to littermate controls.

To summarize, we show that podocyte-specific immunoproteasome knockout alleviates the progression of immune-complex mediated podocyte injury due to the compensatory upregulation of the standard proteasome. Further, we identify the immunoproteasome as a novel pharmaceutical target for the treatment of membranous nephropathy.

6. Literature

1. Farquhar MG, and Palade GE. Glomerular permeability. II. Ferritin transfer across the glomerular capillary wall in nephrotic rats. *J Exp Med.* 1961;114:699-716.
2. Farquhar MG, Wissig SL, and Palade GE. Glomerular permeability. I. Ferritin transfer across the normal glomerular capillary wall. *J Exp Med.* 1961;113:47-66.
3. Yu A, Chertow G, Luyckx V, Marsden P, Skorecki K, and Taal M. *Brenner and Rector's The Kidney, 2-Volume Set 11th Edition.* Elsevier Health Sciences; 2019.
4. Suh JH, and Miner JH. The glomerular basement membrane as a barrier to albumin. *Nat Rev Nephrol.* 2013;9(8):470-7.
5. Abrahamson DR. Structure and development of the glomerular capillary wall and basement membrane. *Am J Physiol.* 1987;253(5 Pt 2):F783-94.
6. Simons M, Hartleben B, and Huber TB. Podocyte polarity signalling. *Curr Opin Nephrol Hypertens.* 2009;18(4):324-30.
7. Lennon R, Randles MJ, and Humphries MJ. The importance of podocyte adhesion for a healthy glomerulus. *Front Endocrinol (Lausanne).* 2014;5:160.
8. Grahammer F, Wigge C, Schell C, Kretz O, Patrakka J, Schneider S, et al. A flexible, multilayered protein scaffold maintains the slit in between glomerular podocytes. *JCI Insight.* 2016;1(9).
9. Wieder N, and Greka A. Calcium, TRPC channels, and regulation of the actin cytoskeleton in podocytes: towards a future of targeted therapies. *Pediatr Nephrol.* 2016;31(7):1047-54.
10. Greka A, and Mundel P. Cell biology and pathology of podocytes. *Annu Rev Physiol.* 2012;74:299-323.
11. Asanuma K, Yanagida-Asanuma E, Faul C, Tomino Y, Kim K, and Mundel P. Synaptopodin orchestrates actin organization and cell motility via regulation of RhoA signalling. *Nat Cell Biol.* 2006;8(5):485-91.
12. Kerjaschki D, Sharkey DJ, and Farquhar MG. Identification and characterization of podocalyxin--the major sialoprotein of the renal glomerular epithelial cell. *J Cell Biol.* 1984;98(4):1591-6.
13. Nielsen JS, and McNagny KM. The role of podocalyxin in health and disease. *J Am Soc Nephrol.* 2009;20(8):1669-76.
14. Vaughan MR, and Quaggin SE. How do mesangial and endothelial cells form the glomerular tuft? *J Am Soc Nephrol.* 2008;19(1):24-33.
15. Floege J, Eitner F, and Alpers CE. A new look at platelet-derived growth factor in renal disease. *J Am Soc Nephrol.* 2008;19(1):12-23.
16. Barajas L. Cell-specific protein and gene expression in the juxtaglomerular apparatus. *Clin Exp Pharmacol Physiol.* 1997;24(7):520-6.
17. Drenckhahn D, Schnittler H, Nobiling R, and Kriz W. Ultrastructural organization of contractile proteins in rat glomerular mesangial cells. *Am J Pathol.* 1990;137(6):1343-51.
18. Kriz W, Elger M, Lemley K, and Sakai T. Structure of the glomerular mesangium: a biomechanical interpretation. *Kidney Int Suppl.* 1990;30:S2-9.

19. Hyink DP, Tucker DC, St John PL, Leardkamolkarn V, Accavitti MA, Abrass CK, et al. Endogenous origin of glomerular endothelial and mesangial cells in grafts of embryonic kidneys. *Am J Physiol.* 1996;270(5 Pt 2):F886-99.
20. Woolf AS, and Loughna S. Origin of glomerular capillaries: is the verdict in? *Exp Nephrol.* 1998;6(1):17-21.
21. Deen WM, Lazzara MJ, and Myers BD. Structural determinants of glomerular permeability. *Am J Physiol Renal Physiol.* 2001;281(4):F579-96.
22. Ryan GB, and Karnovsky MJ. Distribution of endogenous albumin in the rat glomerulus: role of hemodynamic factors in glomerular barrier function. *Kidney Int.* 1976;9(1):36-45.
23. Satchell SC, Tasman CH, Singh A, Ni L, Geelen J, von Ruhland CJ, et al. Conditionally immortalized human glomerular endothelial cells expressing fenestrations in response to VEGF. *Kidney Int.* 2006;69(9):1633-40.
24. Beck LH, Jr., Bonegio RG, Lambeau G, Beck DM, Powell DW, Cummins TD, et al. M-type phospholipase A2 receptor as target antigen in idiopathic membranous nephropathy. *N Engl J Med.* 2009;361(1):11-21.
25. Tomas NM, Beck LH, Jr., Meyer-Schwesinger C, Seitz-Polski B, Ma H, Zahner G, et al. Thrombospondin type-1 domain-containing 7A in idiopathic membranous nephropathy. *N Engl J Med.* 2014;371(24):2277-87.
26. Beck LH, Jr., and Salant DJ. Membranous nephropathy: recent travels and new roads ahead. *Kidney Int.* 2010;77(9):765-70.
27. Borza DB, Zhang JJ, Beck LH, Jr., Meyer-Schwesinger C, and Luo W. Mouse models of membranous nephropathy: the road less travelled by. *Am J Clin Exp Immunol.* 2013;2(2):135-45.
28. Couser WG. Primary Membranous Nephropathy. *Clin J Am Soc Nephrol.* 2017;12(6):983-97.
29. Hartono C, Chung M, Kuo SF, Seshan SV, and Muthukumar T. Bortezomib therapy for nephrotic syndrome due to idiopathic membranous nephropathy. *J Nephrol.* 2014;27(1):103-6.
30. Meyer-Schwesinger C, Dehde S, Klug P, Becker JU, Mathey S, Arefi K, et al. Nephrotic syndrome and subepithelial deposits in a mouse model of immune-mediated anti-podocyte glomerulonephritis. *J Immunol.* 2011;187(6):3218-29.
31. Tomas NM, Meyer-Schwesinger C, von Spiegel H, Kotb AM, Zahner G, Hoxha E, et al. A Heterologous Model of Thrombospondin Type 1 Domain-Containing 7A-Associated Membranous Nephropathy. *J Am Soc Nephrol.* 2017;28(11):3262-77.
32. Meyer-Schwesinger C. The ubiquitin-proteasome system in kidney physiology and disease. *Nat Rev Nephrol.* 2019;15(7):393-411.
33. Beeken M, Lindenmeyer MT, Blattner SM, Radon V, Oh J, Meyer TN, et al. Alterations in the ubiquitin proteasome system in persistent but not reversible proteinuric diseases. *J Am Soc Nephrol.* 2014;25(11):2511-25.
34. Huber EM, Basler M, Schwab R, Heinemeyer W, Kirk CJ, Groettrup M, et al. Immuno- and constitutive proteasome crystal structures reveal differences in substrate and inhibitor specificity. *Cell.* 2012;148(4):727-38.
35. Seifert U, Bialy LP, Ebstein F, Bech-Otschir D, Voigt A, Schroter F, et al. Immunoproteasomes preserve protein homeostasis upon interferon-induced oxidative stress. *Cell.* 2010;142(4):613-24.
36. Xu H, and Ren D. Lysosomal physiology. *Annu Rev Physiol.* 2015;77:57-80.
37. Luzio JP, Pryor PR, and Bright NA. Lysosomes: fusion and function. *Nat Rev Mol Cell Biol.* 2007;8(8):622-32.
38. Kantola IMJNDT. Renal involvement in Fabry disease. 2019.

39. Roth KS, Chan JC, Ghatak NR, Mamunes P, Miller WW, and O'Brien JS. Acid alpha-neuraminidase deficiency: a nephropathic phenotype? *Clin Genet.* 1988;34(3):185-94.
40. Sperl W, Gruber W, Quatacker J, Monnens L, Thoenes W, Fink FM, et al. Nephrosis in two siblings with infantile sialic acid storage disease. *Eur J Pediatr.* 1990;149(7):477-82.
41. Langman CB. Oh cystinosin: let me count the ways! *Kidney Int.* 2019;96(2):275-7.
42. Taylor J, Thorner P, Geary DF, Baumal R, and Balfe JW. Nephrotic syndrome and hypertension in two children with Hurler syndrome. *J Pediatr.* 1986;108(5 Pt 1):726-9.
43. Kobayashi H, Takahashi-Fujigasaki J, Fukuda T, Sakurai K, Shimada Y, Nomura K, et al. Pathology of the first autopsy case diagnosed as mucolipidosis type III alpha/beta suggesting autophagic dysfunction. *Mol Genet Metab.* 2011;102(2):170-5.
44. Kerr DA, Memoli VA, Cathey SS, and Harris BT. Mucolipidosis type III alpha/beta: the first characterization of this rare disease by autopsy. *Arch Pathol Lab Med.* 2011;135(4):503-10.
45. Velho RV, Harms FL, Danyukova T, Ludwig NF, Friez MJ, Cathey SS, et al. The lysosomal storage disorders mucolipidosis type II, type III alpha/beta, and type III gamma: Update on GNPTAB and GNPTG mutations. *Hum Mutat.* 2019;40(7):842-64.
46. Kollmann K, Pohl S, Marschner K, Encarnacao M, Sakwa I, Tiede S, et al. Mannose phosphorylation in health and disease. *Eur J Cell Biol.* 2010;89(1):117-23.
47. Tuysuz B, Ercan-Sencicek AG, Canpolat N, Koparir A, Yilmaz S, Kilicaslan I, et al. Renal involvement in patients with mucolipidosis IIIalpha/beta: Causal relation or co-occurrence? *Am J Med Genet A.* 2016;170A(5):1187-95.
48. Di Lorenzo G, Velho RV, Winter D, Thelen M, Ahmadi S, Schweizer M, et al. Lysosomal Proteome and Secretome Analysis Identifies Missorted Enzymes and Their Nondegraded Substrates in Mucolipidosis III Mouse Cells. *Mol Cell Proteomics.* 2018;17(8):1612-26.
49. Kollmann K, Damme M, Markmann S, Morelle W, Schweizer M, Hermans-Borgmeyer I, et al. Lysosomal dysfunction causes neurodegeneration in mucolipidosis II 'knock-in' mice. *Brain.* 2012;135(Pt 9):2661-75.
50. Moeller MJ, Sanden SK, Soofi A, Wiggins RC, and Holzman LB. Podocyte-specific expression of cre recombinase in transgenic mice. *Genesis.* 2003;35(1):39-42.
51. Adams J, and Kauffman M. Development of the proteasome inhibitor Velcade™(Bortezomib). *Cancer investigation.* 2004;22(2):304-11.
52. Hartleben B, Godel M, Meyer-Schwesinger C, Liu S, Ulrich T, Kobler S, et al. Autophagy influences glomerular disease susceptibility and maintains podocyte homeostasis in aging mice. *J Clin Invest.* 2010;120(4):1084-96.
53. Guhr SS, Sachs M, Wegner A, Becker JU, Meyer TN, Kietzmann L, et al. The expression of podocyte-specific proteins in parietal epithelial cells is regulated by protein degradation. *Kidney Int.* 2013;84(3):532-44.
54. Tossidou I, Teng B, Drobot L, Meyer-Schwesinger C, Worthmann K, Haller H, et al. CIN85/RukL is a novel binding partner of nephrin and podocin and mediates slit diaphragm turnover in podocytes. *J Biol Chem.* 2010;285(33):25285-95.

55. Wanchoo R, Abudayyeh A, Doshi M, Edeani A, Glezerman IG, Monga D, et al. Renal Toxicities of Novel Agents Used for Treatment of Multiple Myeloma. *Clin J Am Soc Nephro.* 2017;12(1):176-89.
56. Berkovic SF, Dibbens LM, Oshlack A, Silver JD, Katerelos M, Vears DF, et al. Array-based gene discovery with three unrelated subjects shows SCARB2/LIMP-2 deficiency causes myoclonus epilepsy and glomerulosclerosis. *Am J Hum Genet.* 2008;82(3):673-84.
57. Basic-Jukic N, Kes P, Coric M, and Basic-Kes V. Renal complications of Fabry disease. *Curr Pharm Des.* 2013;19(33):6046-50.
58. Kim KB, and Crews CM. From epoxomicin to carfilzomib: chemistry, biology, and medical outcomes. *Nat Prod Rep.* 2013;30(5):600-4.
59. Chade AR, Herrmann J, Zhu X, Krier JD, Lerman A, and Lerman LO. Effects of proteasome inhibition on the kidney in experimental hypercholesterolemia. *J Am Soc Nephrol.* 2005;16(4):1005-12.
60. Bilinska M, Usnarska-Zubkiewicz L, and Pokryszko-Dragan A. Bortezomib-induced painful neuropathy in patients with multiple myeloma. *Contemp Oncol (Pozn).* 2013;17(5):421-6.
61. Akilesh S, Huber TB, Wu H, Wang G, Hartleben B, Kopp JB, et al. Podocytes use FcRn to clear IgG from the glomerular basement membrane. *Proc Natl Acad Sci U S A.* 2008;105(3):967-72.
62. Bifsha P, Landry K, Ashmarina L, Durand S, Seyrantepe V, Trudel S, et al. Altered gene expression in cells from patients with lysosomal storage disorders suggests impairment of the ubiquitin pathway. *Cell Death Differ.* 2007;14(3):511-23.
63. Abe A, Gregory S, Lee L, Killen PD, Brady RO, Kulkarni A, et al. Reduction of globotriaosylceramide in Fabry disease mice by substrate deprivation. *J Clin Invest.* 2000;105(11):1563-71.
64. Mattocks M, Bagovich M, De Rosa M, Bond S, Binnington B, Rasaiah VI, et al. Treatment of neutral glycosphingolipid lysosomal storage diseases via inhibition of the ABC drug transporter, MDR1. Cyclosporin A can lower serum and liver globotriaosyl ceramide levels in the Fabry mouse model. *FEBS J.* 2006;273(9):2064-75.
65. Fall B, Scott CR, Mauer M, Shankland S, Pippin J, Jefferson JA, et al. Urinary Podocyte Loss Is Increased in Patients with Fabry Disease and Correlates with Clinical Severity of Fabry Nephropathy. *PLoS One.* 2016;11(12):e0168346.
66. Osaka H, Wang YL, Takada K, Takizawa S, Setsuie R, Li H, et al. Ubiquitin carboxy-terminal hydrolase L1 binds to and stabilizes monoubiquitin in neuron. *Hum Mol Genet.* 2003;12(16):1945-58.
67. Meyer-Schwesinger C, Meyer TN, Munster S, Klug P, Saleem M, Helmchen U, et al. A new role for the neuronal ubiquitin C-terminal hydrolase-L1 (UCH-L1) in podocyte process formation and podocyte injury in human glomerulopathies. *J Pathol.* 2009;217(3):452-64.
68. Kabuta T, Furuta A, Aoki S, Furuta K, and Wada K. Aberrant interaction between Parkinson disease-associated mutant UCH-L1 and the lysosomal receptor for chaperone-mediated autophagy. *J Biol Chem.* 2008;283(35):23731-8.
69. Hussain S, Feldman AL, Das C, Ziesmer SC, Ansell SM, and Galardy PJ. Ubiquitin hydrolase UCH-L1 destabilizes mTOR complex 1 by antagonizing DDB1-CUL4-mediated ubiquitination of raptor. *Mol Cell Biol.* 2013;33(6):1188-97.

70. Settembre C, Zoncu R, Medina DL, Vetrini F, Erdin S, Erdin S, et al. A lysosome-to-nucleus signalling mechanism senses and regulates the lysosome via mTOR and TFEB. *EMBO J.* 2012;31(5):1095-108.
71. Hussain S, Bedekovics T, Liu Q, Hu W, Jeon H, Johnson SH, et al. UCH-L1 bypasses mTOR to promote protein biosynthesis and is required for MYC-driven lymphomagenesis in mice. *Blood.* 2018;132(24):2564-74.
72. Meyer-Schwesinger C, Meyer TN, Sievert H, Hoxha E, Sachs M, Klupp EM, et al. Ubiquitin C-terminal hydrolase-l1 activity induces polyubiquitin accumulation in podocytes and increases proteinuria in rat membranous nephropathy. *Am J Pathol.* 2011;178(5):2044-57.
73. Brocklebank V, Wood KM, and Kavanagh D. Thrombotic Microangiopathy and the Kidney. *Clin J Am Soc Nephro.* 2018;13(2):300-17.
74. Meregalli C. An Overview of Bortezomib-Induced Neurotoxicity. *Toxics.* 2015;3(3):294-303.
75. Pellom ST, Jr., Dudimah DF, Thounaojam MC, Sayers TJ, and Shanker A. Modulatory effects of bortezomib on host immune cell functions. *Immunotherapy.* 2015;7(9):1011-22.
76. Kimura H, Caturegli P, Takahashi M, and Suzuki K. New Insights into the Function of the Immunoproteasome in Immune and Nonimmune Cells. *J Immunol Res.* 2015.
77. Ferrington DA, and Gregerson DS. Immunoproteasomes: structure, function, and antigen presentation. *Prog Mol Biol Transl Sci.* 2012;109:75-112.
78. Schmidt C, Berger T, Groettrup M, and Basler M. Immunoproteasome Inhibition Impairs T and B Cell Activation by Restraining ERK Signaling and Proteostasis. *Frontiers in Immunology.* 2018;9(2386).
79. Li J, Koerner J, Basler M, Brunner T, Kirk CJ, and Groettrup M. Immunoproteasome inhibition induces plasma cell apoptosis and preserves kidney allografts by activating the unfolded protein response and suppressing plasma cell survival factors. *Kidney Int.* 2019;95(3):611-23.
80. Moynagh PN. The NF-κB pathway. *Journal of cell science.* 2005;118(20):4589-92.
81. Muchamuel T, Basler M, Aujay MA, Suzuki E, Kalim KW, Lauer C, et al. A selective inhibitor of the immunoproteasome subunit LMP7 blocks cytokine production and attenuates progression of experimental arthritis. *Nat Med.* 2009;15(7):781-7.
82. Aki M, Shimbara N, Takashina M, Akiyama K, Kagawa S, Tamura T, et al. Interferon-gamma induces different subunit organizations and functional diversity of proteasomes. *J Biochem.* 1994;115(2):257-69.
83. Li J, Basler M, Alvarez G, Brunner T, Kirk CJ, and Groettrup M. Immunoproteasome inhibition prevents chronic antibody-mediated allograft rejection in renal transplantation. *Kidney Int.* 2018;93(3):670-80.
84. Heymann F, Meyer-Schwesinger C, Hamilton-Williams EE, Hammerich L, Panzer U, Kaden S, et al. Kidney dendritic cell activation is required for progression of renal disease in a mouse model of glomerular injury. *J Clin Invest.* 2009;119(5):1286-97.
85. Kurts C, and Meyer-Schwesinger C. Protecting the kidney against autoimmunity and inflammation. *Nat Rev Nephrol.* 2019;15(2):66-8.
86. Cui Z, Hwang SM, and Gomes AV. Identification of the immunoproteasome as a novel regulator of skeletal muscle differentiation. *Mol Cell Biol.* 2014;34(1):96-109.

87. Kitamura A, Maekawa Y, Uehara H, Izumi K, Kawachi I, Nishizawa M, et al. A mutation in the immunoproteasome subunit PSMB8 causes autoinflammation and lipodystrophy in humans. *J Clin Invest.* 2011;121(10):4150-60.
88. Herwig J, Skuza S, Sachs W, Sachs M, Failla AV, Rune G, et al. Thrombospondin Type 1 Domain-Containing 7A Localizes to the Slit Diaphragm and Stabilizes Membrane Dynamics of Fully Differentiated Podocytes. *J Am Soc Nephrol.* 2019;30(5):824-39.
89. Frampton JP, Guo C, and Pierchala BA. Expression of axonal protein degradation machinery in sympathetic neurons is regulated by nerve growth factor. *J Neurosci Res.* 2012;90(8):1533-46.
90. Bingol B, Wang CF, Arnott D, Cheng D, Peng J, and Sheng M. Autophosphorylated CaMKIIalpha acts as a scaffold to recruit proteasomes to dendritic spines. *Cell.* 2010;140(4):567-78.
91. Ramachandran KV, and Margolis SS. A mammalian nervous-system-specific plasma membrane proteasome complex that modulates neuronal function. *Nat Struct Mol Biol.* 2017;24(4):419-30.
92. Rastaldi MP, Armelloni S, Berra S, Calvaresi N, Corbelli A, Giardino LA, et al. Glomerular podocytes contain neuron-like functional synaptic vesicles. *The FASEB journal.* 2006;20(7):976-8.

7. Appendix

7.1 Hazard Statements

H201 Explosive; mass explosion hazard

H225 Highly flammable liquid and vapor

H226 Flammable liquid and vapour

H227 Combustible liquid

H228 Flammable solid

H271 May cause fire or explosion; strong oxidiser

H272 May intensify fire; oxidizer

H290 May be corrosive to metals

H301 Toxic if swallowed

H301+H311+H331 Toxic if swallowed, in contact with skin or if inhaled

H301+H331 Toxic if swallowed or if inhaled

H302 Harmful if swallowed

H302+H332 Harmful if swallowed or if inhaled

H303 May be harmful if swallowed

H304 May be fatal if swallowed and enters airways

H310 Fatal in contact with skin

H311 Toxic in contact with skin

H312 Harmful in contact with skin

H312+H332 Harmful in contact with skin or if inhaled

H314 Causes severe skin burns and eye damage

H315 Causes skin irritation

H317 May cause an allergic skin reaction

H318 Causes serious eye damage.

H319 Causes serious eye irritation

H331 Toxic if inhaled

H332 Harmful if inhaled

H334 May cause allergy or asthma symptoms or breathing difficulties if inhaled

H335 May cause respiratory irritation

H336 May cause drowsiness or dizziness

H341 Suspected of causing genetic defects

H350 May cause cancer

H351 Suspected of causing cancer

H360 May damage fertility or the unborn child

H360D May damage the unborn child

H360Df May damage the unborn child. Suspected of damaging fertility

H361dSuspected of damaging the unborn child

H370 Causes damage to organs

H372 Causes damage to organs (Liver, Kidney) through prolonged or repeated exposure

H373 May cause damage to organs through prolonged or repeated exposure

H400 Very toxic to aquatic life

H410 Very toxic to aquatic life with long lasting effects

H412 Harmful to aquatic life with long lasting effects

7.2 Precautionary statements

P201 Obtain special instructions before use

P202 Do not handle until all safety precautions have been read and understood

P210 Keep away from heat

P221 Take any precaution to avoid mixing with combustibles

P233 Keep container tightly closed

P240 Ground and bond container and receiving equipment

P241 Use explosion-proof [electrical/ventilating/lighting/…] equipment

P260 Do not breathe dusts or mists

P261 Avoid breathing dust/fume/gas/mist/vapours/spray

P262 Do not get in eyes, on skin, or on clothing

P264 Wash thoroughly after handling

P271 Use only outdoors or in a well-ventilated area

P272 Contaminated work clothing should not be allowed out of the workplace

P273 Avoid release to the environment

P280 Wear eye protection/face protection

P283 Wear fire/flame resistant/retardant clothing

P284 Wear respiratory protection

P301+P310 IF SWALLOWED: Immediately call a POISON CENTER or doctor/physician

P301+P312+P330 IF SWALLOWED: Call a POISON CENTER/doctor if you feel unwell. Rinse mouth

P301+P330+P331 IF SWALLOWED: Rinse mouth. Do NOT induce vomiting

P302+P352 IF ON SKIN: Wash with plenty of soap and water

P303+P361+P353 IF ON SKIN (or hair): Remove/Take off immediately all contaminated clothing. Rinse skin with water/shower

P304+P340 IF INHALED: Remove person to fresh air and keep comfortable for breathing

P305+P351+P338 IF IN EYES: Rinse cautiously with water for several minutes. Remove contact lenses, if present and easy to do. Continue rinsing

P305+P351+P338+P310 IF IN EYES: Rinse cautiously with water for several minutes. Remove contact lenses, if present and easy to do. Continue rinsing. Immediately call a POISON CENTER/doctor

P306+P360 IF ON CLOTHING: Rinse immediately contaminated clothing and skin with plenty of water before removing clothes.

P308+P310 IF exposed or concerned: immediately call a POISON CENTER or doctor/ physician

P308+P313 IF exposed or concerned: Get medical advice/ attention

P310 Immediately call a POISON CENTER or doctor

P312 Call a POISON CENTER or doctor/physician if you feel unwell

P331 Do NOT induce vomiting

P337+P313 If eye irritation persists: Get medical advice/attention

P361 Remove/take off immediately all contaminated clothing

P370+P378 In case of fire: Use sand, carbon dioxide or powder extinguisher for extinction

P371+P380+P375 In case of major fire and large quantities: Evacuate area. Fight fire remotely due to the risk of explosion

P390 Absorb spillage to prevent material damage

P403+P233 Store in a well-ventilated place. Keep container tightly closed

P403+P235 Store in a well-ventilated place. Keep cool

P405 Store locked up

P501 Dispose of contents/container to industrial combustion plant

8. Acknowledgements

I want to express my gratitude to Prof. Catherine Meyer-Schwesinger, who gave me the opportunity to conduct the work for my doctoral thesis in her lab and under her supervision. Without her expertise, motivation and enthusiasm this work would not have been possible. I could not have imagined a better PI for my thesis work.
I would also like to thank Prof. Wolfram Brune for taking on the responsibility of being my second reviewer.
I want to thank all the people who have contributed to the process, especially Dr. Sandra Pohl for providing the Mucolipidosis mice and lending her expertise on lysosomal degradation. I want to thank Dr. Oliver Kretz for kindly conducting the electron microscopic analyses.
Special thanks belongs to all the members of the Meyer-Schwesinger lab, especially Favian Hatje, who developed the technique of isolating the glomerular cell types, and Stephanie Zielinski, a lab technician who helped with all the histologic stainings. But foremost I want to thank my mom Marlies Sachs, who as a lab technician has helped with my experimental work and has always supported me on my way as my parent.
Therefore, I want to thank my parents and my brother for providing me with encouragement and support all my life, without them I wouldn't be where I am today.
Lastly, I want to thank my husband for his support and patience, especially when times at work were stressful, I could always count on him.

9. Eidestattliche Versicherung

Hiermit versichere ich an Eides statt, die vorliegende Dissertation selbst verfasst und keine anderen als die angegebenen Hilfsmittel benutzt zu haben. Die eingereichte schriftliche Fassung entspricht der auf dem elektronischen Speichermedium. Ich versichere, dass diese Dissertation nicht in einem früheren Promotionsverfahren eingereicht wurde.

Ort, Datum Unterschrift